DEPARTMENT OF CIVIL ENGINEERING
COLLEGE OF ENGINEERING AND TECHNOLOGY
OLD DOMINION UNIVERSITY
NORFOLK, VIRGINIA 23529

POLYMER INFILTRATION STUDIES

By

Joseph M. Marchello, Principal Investigator

Progress Report
For the period 16 September to 31 December 1991

Prepared for
National Aeronautics and Space Administration
Langley Research Center
Hampton, Virginia 23665

Under
Research Grant NAG-1-1067
Robert M. Baucom, Technical Monitor
MD-Polymeric Materials Branch

January 1992

Kathleen J Ganas

Kathleen J. Ganas
Word Processing Supervisor

/kjg

Encl: Prog. Report, 3 copies

cc: Dr. Marchello, 5 copies
NASA Sci. & Techn. Info. Facility, 2 copies
Dr. Chang, 1 copy
Dean Cross, letter
Mr. R. Siebels, Grants Officer, 1 copy
ODURF File (104043), 1 copy

P.O. Box 6369 • 800 West 46th Street • Norfolk, Virginia 23508-0369
Phone 804/683-4293 • FAX 804 683-5290
An Affirmative Action/Equal Opportunity Employer

DEPARTMENT OF CIVIL ENGINEERING
COLLEGE OF ENGINEERING AND TECHNOLOGY
OLD DOMINION UNIVERSITY
NORFOLK, VIRGINIA 23529

POLYMER INFILTRATION STUDIES

POLYMER INFILTRATION STUDIES

SUMMARY

Progress has been made in several areas during the reporting period on the preparation of carbon fiber composites using advanced polymer resins. The results are set forth in recent reports, patents and publications, and will be presented in forthcoming national and international meetings.

Current and ongoing research activities reported herein include:

- LaRC Powder Towpreg Process
- Weaving, Braiding and Stitching Dry Powder Prepreg
- Advanced Tow Placement
- Customized ATP Towpreg

Research during the period ahead will be directed toward preparation of towpreg for textile preform weaving and braiding and for automated tow placement. Studies of multi-tow powder prepregging will be initiated in conjunction with continued development of prepregging technology and the various aspects of composite part fabrication.

CONTENTS

I. Introduction

Polymer infiltration studies during the period have focused on ways of preparing composite materials from advanced polymer resins and carbon fibers. This effort is comprised of an integrated approach to the process of composite part fabrication.

The goal of these investigations is to produce advanced composite materials for automated part fabrication utilizing textile and robotics technology in the manufacture of subsonic and supersonic aircraft. The objective is achieved through research investigations at NASA Langley Research Center and by stimulating technology transfer between contract researchers and the aircraft industry.

The sections of this report cover literature reviews, status report on individual projects, current and planned research, and publications and scheduled technical presentations.

II. TEXTILE TECHNOLOGY: WEAVING, BRAIDING, AND STITCHING

M. K. Hugh, J. M. Marchello and N. J. Johnston, PMB
R. J. Cano, M. B. Dow and H. B. Dexter, AMB

OBJECTIVE: To develop powder-coated towpreg technology as a viable alternative to RTM for fabrication of textile composites.

WEAVING STUDY

TOWPREG WEAVING CONDITIONS

Rewinders	-	Cross Wind Pattern, 2"D Cores
		Parallel Wind, 2"D Cores
Loom	-	Iwer 1200 Loom
		Actual speed of 40 ppm
Weave Pattern	-	Eight Harness Satin

TENSION PROPERTIES OF 8HS FABRIC MADE FROM LARC™-TPI POWDER COATED TOWPREG

Tow Bundle Size	Max. Stress (ksi)	Modulus (msi)	Vf (%)
6k	95.9 ± 5.5	7.93 ± .16	44
12k	67.3 ± 7.0	7.77 ± .38	57

WEAVING PARAMETERS

Towpreg Characteristics

- Yarn Shape
- Amount of Twist
- Flexibility
- Degree of Damage

Weaving Characteristics

- Eyelets
- Turns and Bends
- Tensioning
- Heddles

Final Parts

- Optimal Resin Content
- Bulk Factor

WOVEN TOWPREG CURE CYCLE

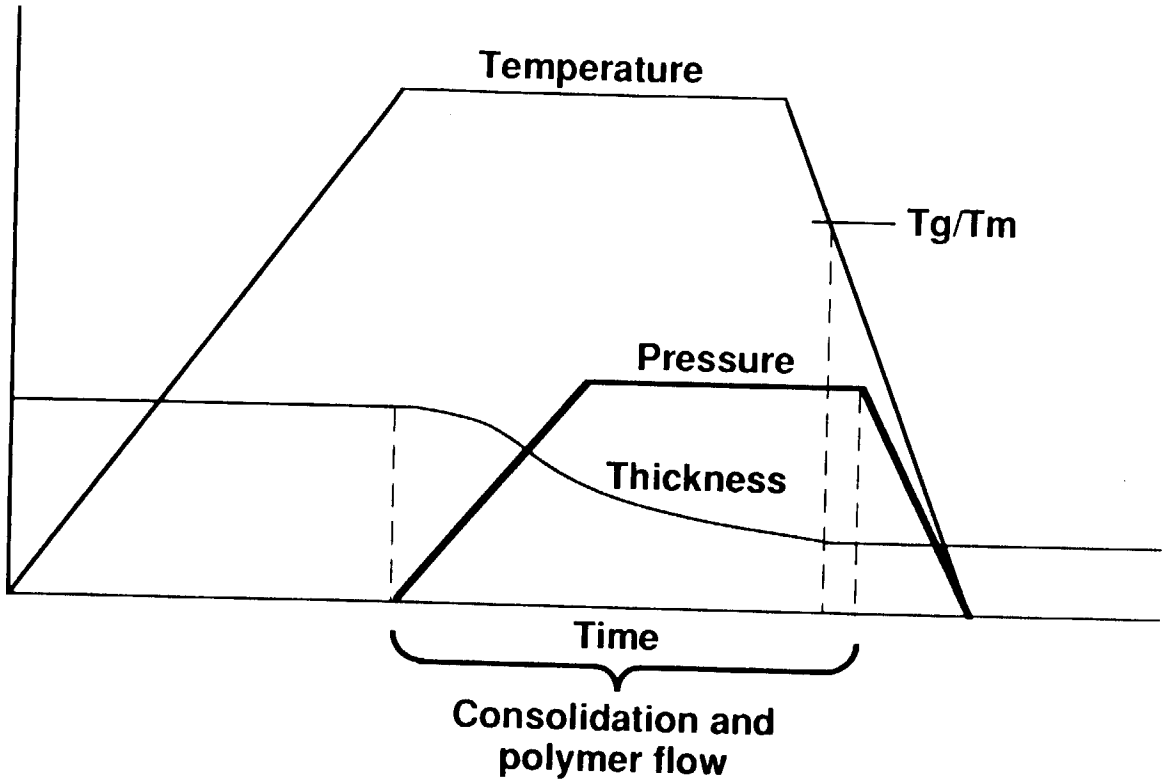

- Vacuum is used to eliminate air voids.
- Pressure ramp allows time for fiber movement into a compact arrangement with minimum fiber crimping and breakage.
- Pressure ramp also provides time for resin flow and adhesion.
- Holding temperature above Tg or Tm anneals the composite relieving fiber elastic stresses.
- Cooling below Tg or Tm stops consolidation before thickness curve flattens and avoids resin squeeze out and resulting dry spots.

CONCLUSIONS FROM WEAVING STUDIES

- From the present study, towpreg that has a high flexural rigidity (>10,000 mg-cm) is preferred for weaving.

- A shaped or compacted tow will allow the towpreg to pass easily through the heddles and reed. A circular-type cross-section is preferred.

- Yarn preparation and weaving damages towpreg creating broken, loose fibers on the surface of the yarn. Towpreg shaping and compacting will reduce the damage, as will using a 12k yarn bundle.

BRAIDING AND STITCHING

Future Plan

JUSTIFICATION

- Automated part fabrication processes.
- Braiding produces structures with $\pm \theta$.
- Stitching produces orthogonal, 3-D reinforcement that prevents delamination and improves the out-of-plane properties.

Braiding Issues

- Loose fibers on surface of yarn
- Tow-to-tow abrasion
- Braiding carriers and bobbins

Stitching Issues

- Determining appropriate flexibility of the yarn
- Aids in wet-out problems that arise with a tightly stitched preform

ACT [PMB - AMB] TEXTILE PREFORM STUDIES

Epoxy Powder-Coated Towpreg

- Establish weaving and braiding protocals

  BASF, PMB - prepreggers
  TTI - weavers
  Fiber Innovations - weavers and braiders
  Albany International
  Atlantic Research } braiders

  - Develop cure cycles and consolidate flat panels
  - Obtain engineering property data

- Develop tooling concepts
  - Non-autoclave
  - Soft tooling
  - Cure cycle modifications

- Fabricate a stringer panel component from powder-coated towpreg

III. RIBBONIZING

December 18, 1991

Memorandum:

To: J.M. Marchello

From: D.A. Sandusky

Subject: Ribbonizing, and LaRC-TPI-1500 Progress

The purpose of this memorandum is to share with you the information and design ideas accumulated since my arrival in October. Your comments, particularly in regard to missing information and misinterpretations, would be appreciated.

Since early October, 1991 I have had opportunity to study background information on similar technologies to ribbonizing, from which several design ideas have emerged. The notion of ribbonizing seems fairly straight forward. Coat a fiber bundle with polymer then flatten it out and form a continuous ribbon. It seemed reasonable to assume that processing could be achieved with slight alterations of existing Calendering or pultrusion technologies so they became the basis of design considerations.

The primary function of any ribbonizing device is of course to flatten and smooth. With composite materials intended for prepreg use, much higher expectations should be realized. For example, uniform cross-section integrity along the ribbon length, a fair degree of fiber wet-out, and minimal fiber damage from the processing, should be essential requirements. Knowing that this type of technology was fairly well understood, it was reasonable to propose an attempt to design and build experimental ribbonizing equipment.

Advanced Tow Placement, (ATP) processing currently has a lap-gap industrial standard tolerance of approximately 0.03" between individual ribbons. The gaps are primarily the result of variation of ribbon cross-section along its length. The ATP machinery can certainly control ribbon placement more precisely but the ribbon material has too much variation. Here is the justification for tighter tolerances and forming interlocking or overlapping shapes to ease the ill-effects of ribbon width variation. With a shape such as a "flattened" isosceles triangle the process becomes more robust and forgiving. Several other shapes have been proposed, (Figure 1), such as diamonds, ovals, "house-shapes", and various interlocking shapes.

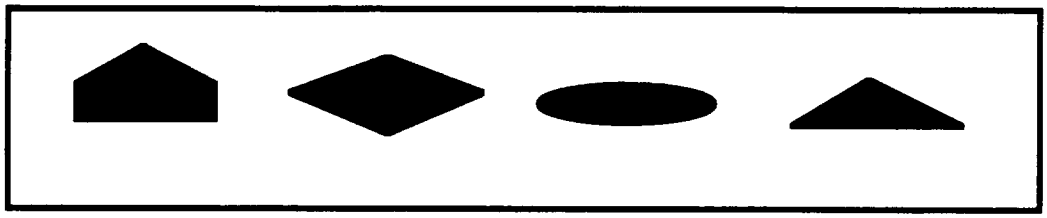

Figure 1. Various cross-sectional shapes.

An attempt at "proof of concept" has been planned and is currently being constructed. Two existing processes have been selected as candidates for what was coined "towpreg architecture". Calendering, (or nip-rolling), and Pultrusion were chosen as the bases upon which experimental apparatus were designed. Roller Ribbonizing and Die Ribbonizing are the new terms which will be referred to from this point forward which are specific variations of Calendering and Pultrusion manufacturing methods.

I. Roller Ribbonizing

A Roller Ribbonizer was designed in October, constructed, and is in the initial stages of assembly. Experiments are planned to begin in January 1992. It is very much an experimental apparatus in the sense that as many orientations as possible were "designed-in" form the beginning. All attempts were made to keep it simple.

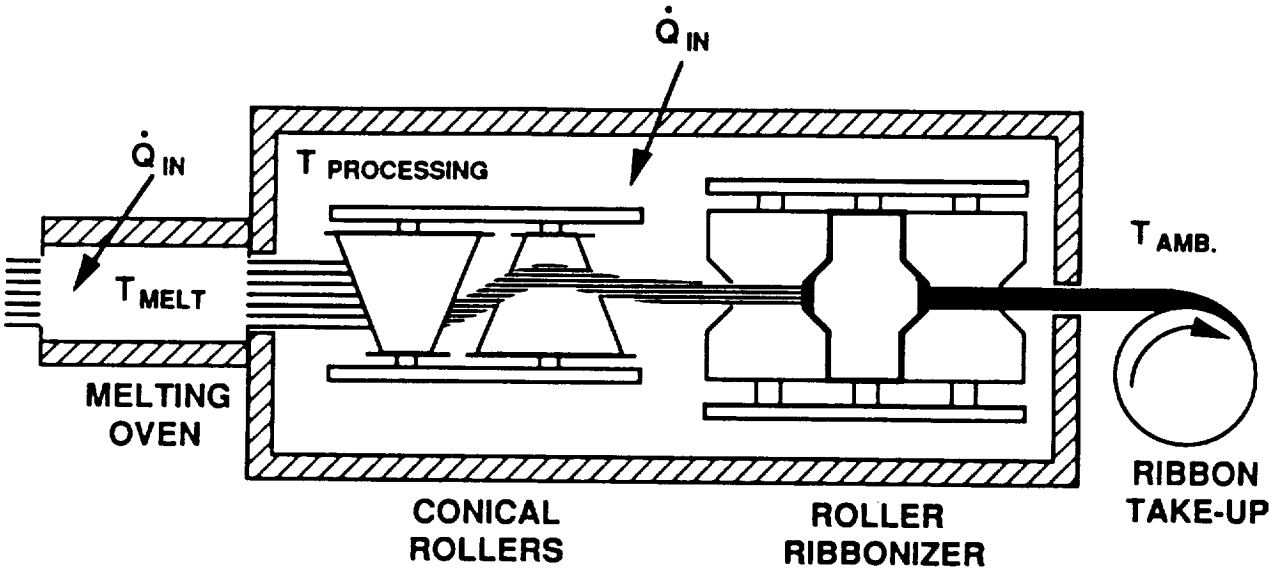

Figure 2. Roller Ribbonizer Schematic.

Dry, clean carbon fiber tow is powder coated with a matrix polymer. The powder is fused onto the fiber bundle in the melting oven, (Figure 2), and soon thereafter passed over two opposing conical rollers which are intended to assist initial debulking and contain any "loose hairs" to the "sticky" surface of the coated tow bundle. At this point the bundle passes thru the first set of spring-loaded nip-rollers and assumes a nominal shape then passes over a carrier wheel to a second spring loaded nip, (stronger spring and smaller X-sec.), and immediately exits to a temperature below T_g. Thermal history of the resulting prepreg and evaluation of its cross-sectional integrity will be considered.

The underlying principal of Roller Ribbonizing is appropriately simple. When debulking a powder coated towpreg bundle, a process should try to avoid any axial components of force, (Figure 3), since they are a significant cause of fiber damage. A fundamental review of Statics reveals the most effective way to accomplish a contact point with only normal force vectors is a free rolling wheel. In effect this Rolling Ribbonizer is a "normal die" and can be treated as such if the coefficient of friction between the wheel and its shaft is effectively negligible.

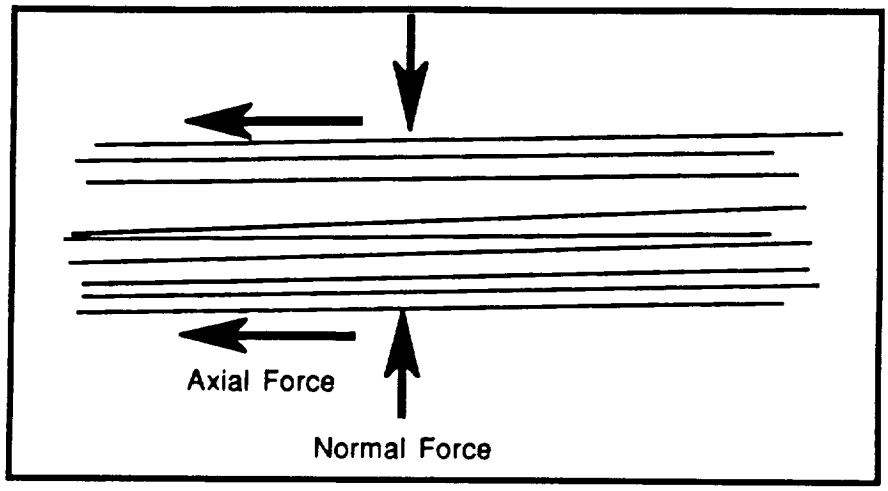

Figure 3. Forces acting of fibers.

If operated at the proper temperature and speed, significant improvements in ribbon size and shape control may be realized. Since there is such a short pressure nip residence time, there will be difficulties with some highly viscous polymers. It is fairly likely that this process will prove useful for many low viscosity epoxy resin systems.

The Die Ribbonizer is in the stages of design and development. Pultrusion of thermoset composites is a very well understood manufacturing method. Generally speaking, pultrusion is slow and unforgiving by nature, but it is consistent. It will exert high axial components of force on the fiber bundle surfaces closest to the die walls in addition to normal consolidation forces. There are many benefits of this proven technology. It is simple. Very few moving parts means that it is less likely to break down and is simple to control.

The use of ultra-sonic vibrations to augment flow within the pultrusion die has been proven to effectively increase pulling rates while maintaining quality parts. The ultrasonic waves may be causing the particles of polymer to resonate and fuse, or may be increasing the melt shear rate and having a favorable effect on viscosity and other polymer flow properties.

II. LaRC-TPI-1500 Progress

Since the middle of November, 1991. I have been involved with developing a method of cure cycle selection for MTC LaRC-TPI-1500 /CF (T-800) UD hot-melt prepreg. Three batches have arrived from MTC, each a different blend of the high flow grade (HFG) and medium flow grade (MFG), specifically 10/0 (HFG/MFG), 7/3, & 5/5. Fortunately there are extensive memos and publications regarding the various properties of LaRC-TPI-1500. It would have been fairly straight forward to "eye-ball" a processing cycle from all that material but not necessarily correct. The prepreg material will have distinct properties.

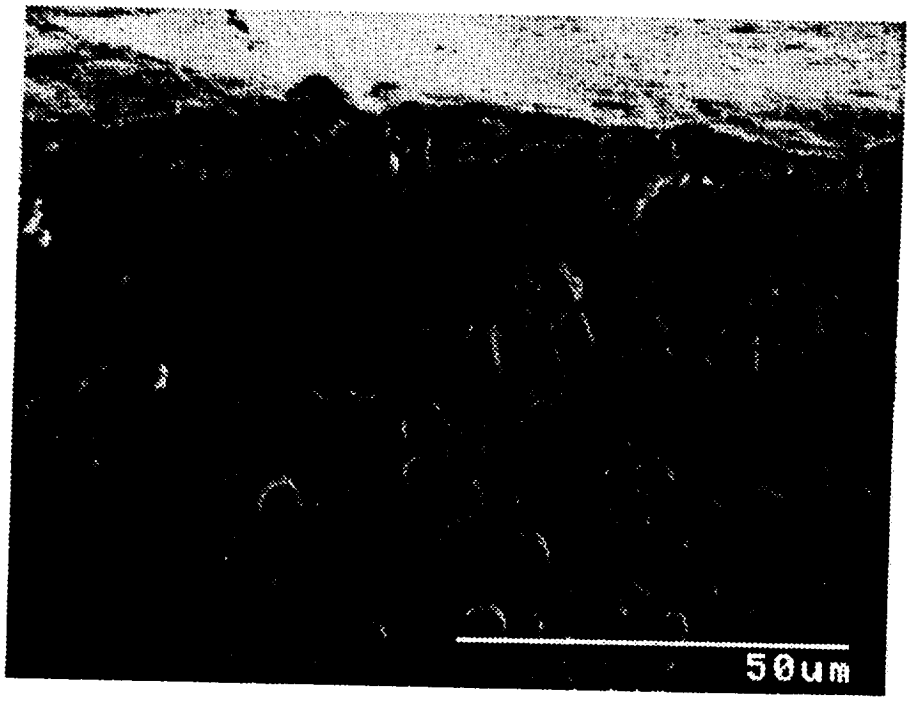

Figure 5. SEM photo of prepreg.

To methodize the cure cycle selection from an engineering point of view seemed to be appropriate. It seems fitting that the place to start was by physical evaluation of the prepreg. Simple things like prepreg wet-out, surface characteristics, thermal history, crystallinity, and fiber volume fraction, should all be known before any attempt to process. An effective way to get a feel for what you're working with is photo-image analysis or SEM photography, (Figure 5), of the surface and cross-section of the prepreg.

The shape of the die can be modeled after previously developed processing cycles, (Figure 4), which rely on three primary variables: Temperature, Pressure, and Debulking as a function of time. The level of ultrasonic augmentation will likely promote aggressive expectations of processing speed.

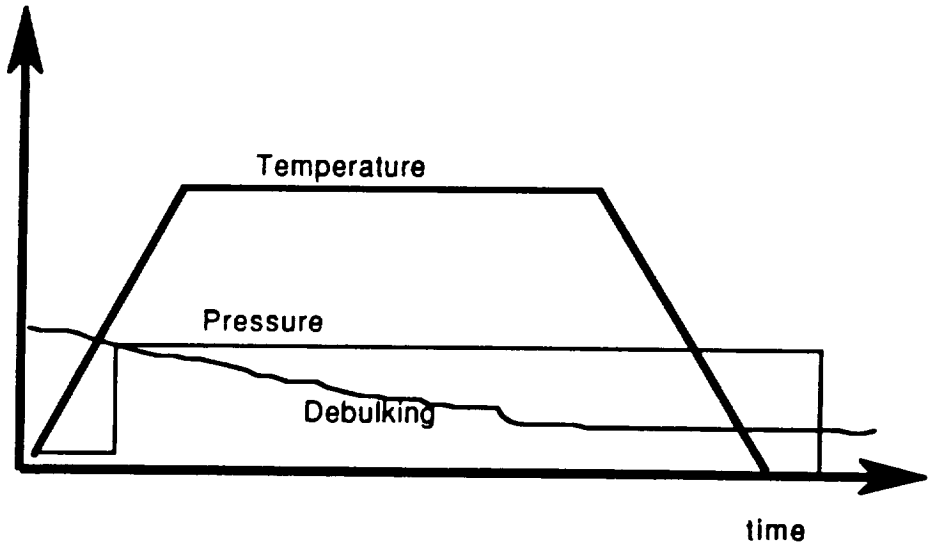

Figure 4. Process cycle schematic.

It is premature to compare these two experimental methods in anything more than general terms but Die Ribbonizing will likely perform better than the Roller method in applications where multiple tows are necessary. For instance, if there were an application for ribbons shaped like the silhouette of a house, (isosceles triangle atop a wide based rectangle), at least eight (8), 12K tows would be necessary to produce a piece with a 1/8" wide base. Logically, the more complex shapes will need more working area. For the simpler shapes, (ovals, rectangles, and triangles), three, two, and even single 12K tows may be sufficient and the Roller Ribbonizer may be used.

Over the next few months I look forward to experimenting with, and developing this idea into practical useful tool for production of customized ribbon.

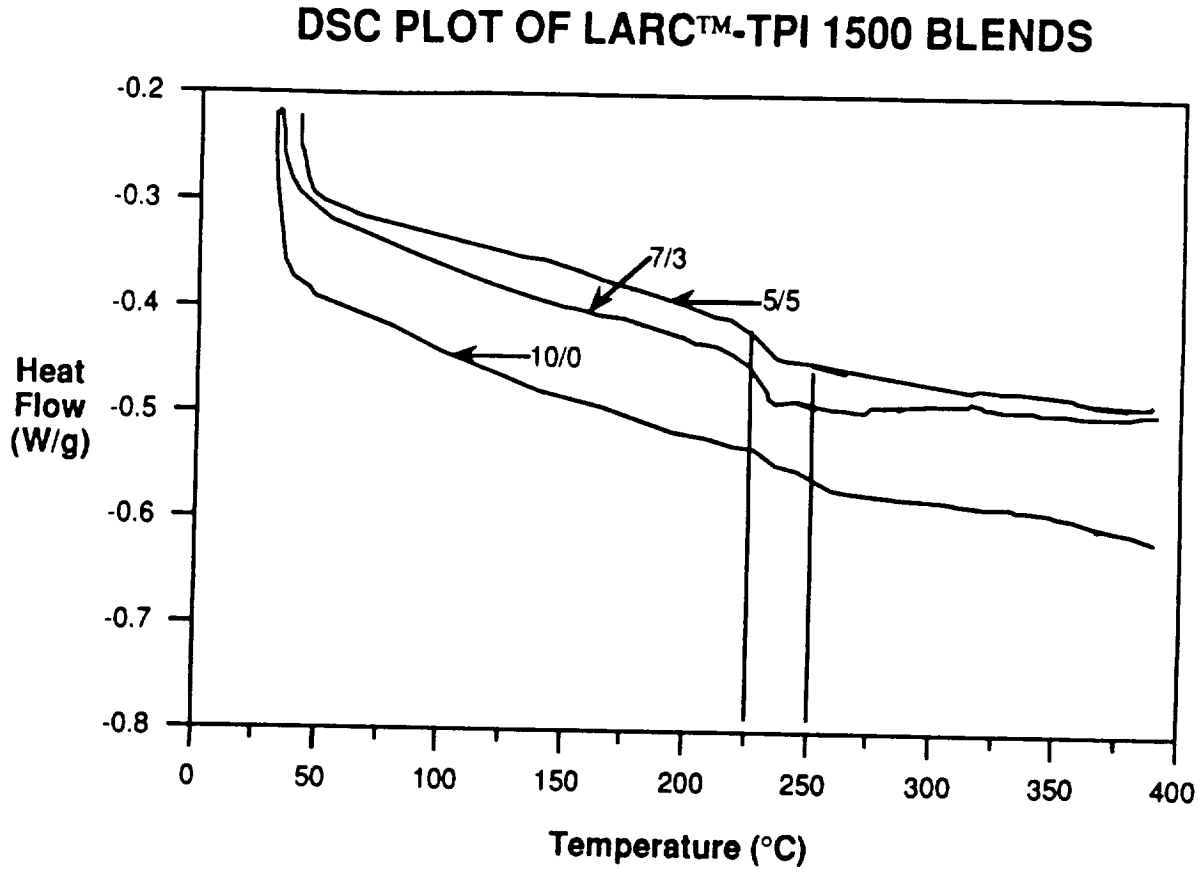

Figure 6. DSC plots of prepregs

One of the primary variables of most processing cycles is temperature. Generally speaking, one wants to process above Tg but below the polymers degradation temperature. A good way to find these temperature values for the prepreg, is by DSC, (for lower limit temperature), and TGA, (upper limit temperature). Even with an amorphous material like LaRC-TPI-1500 the DSC, (Figure 6), provided a noticeable Tg. The TGA should be understood to hold a composite, not a neat resin. When the TGA is completed, the carbon fibers will still be in tact whereas most all of the polymer is gone. This is important to keep in mind when reading the results of a TGA. Depending on the weight fraction of polymer to carbon fiber, a TGA indicated weight loss of 5% of the composite, could actually mean 10% weight loss of polymer. When performed properly, these two tests should provide a processing temperature window.

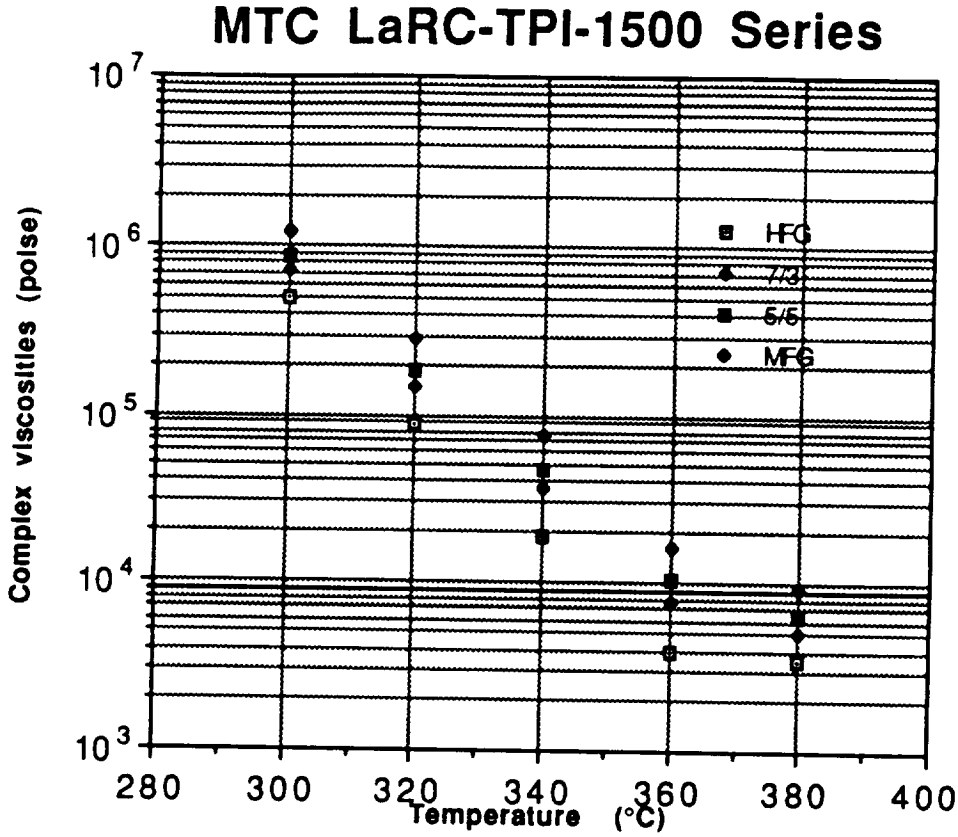

Figure 7. Viscosity at 1 rad/s sheer rate.

Another significant processing parameter is polymer viscosity. A rheometric study of the neat resin, can provide viscosity as a function of temperature, (Figure7). For this particular application, Dr. T.H. Hou had previously done a parametric study of both HFG and MFG viscosities as a function of temperature and sheer rate. From Hou's data, a reasonable approximation of 1 rad/sec for the sheer rate in a closed mold, was chosen and viscosity values at different temperatures were plotted. Since the prepregs were a weighted blends of 10/0, 7/3, & 5/5 linear interpolations were made within the newtonian region of the viscosity profile and are plotted.

With this plot, a researcher could choose a favorable viscosity, (assuming it coincided within the previously determined temperature window), for the type of flow necessary to make a quality part. In the case of these three blends, choose one viscosity for all three blends and process at the associated temperature from the x-axis of the plot.

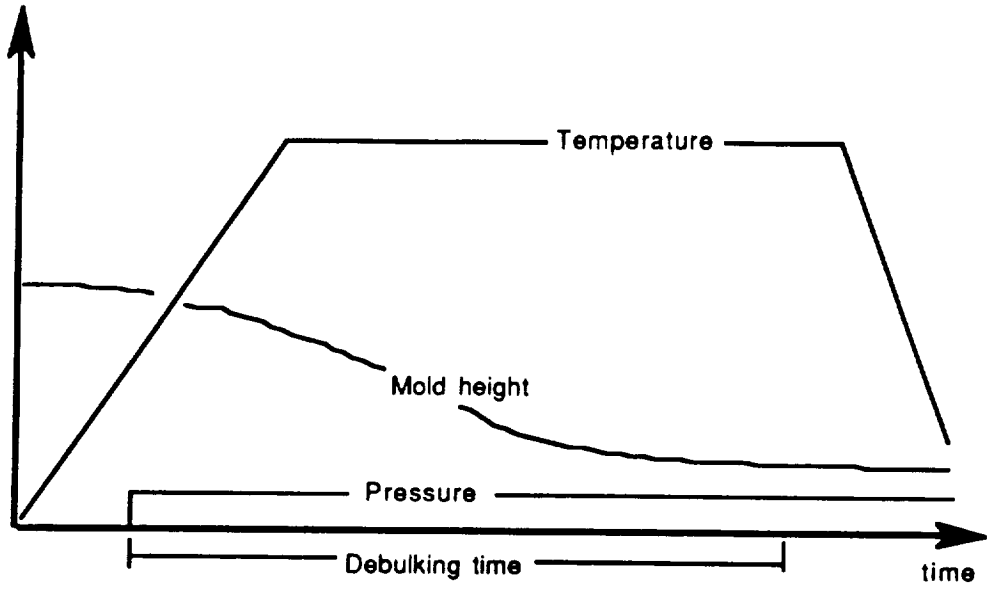

Figure 8. PPP Plastograph

One way of determining a "ball park" figure for the pressure/time relationship is to use the parallel plate plastometer, (PPP) which provides debulking as a function of temperature pressure and time. The PPP, (Fiugure 8), provides a historical plot of the gap between platens during an isobaric heating to the previously selected temperature, and held until debulking levels off. This time value will change with the amount of applied pressure This test should be repeated for several different pressures to get a feel for its effect.

The pressure is difficult to calculate for several reasons. The complexity of the flow necessary for lamination plays a significant role. Obviously, a well wet-out prepreg should require very little applied pressure to laminate because the flow necessary for consolidation is simply enough flow to promote ply-ply adhesion. With a poorly wet-out prepreg, a much more complex flow problem arises with trapped air encapsulated within the fiber bundles. No amount of pressure will eliminate all of the trapped air inside a fiber bundle once it is encapsulated by a highly viscous polymer. This happens to be the case with this MTC LaRC-TPI-1500 hotmelt prepreg.

Generally speaking, if a researcher follows these described examinations of the prepreg, there should be enough information to intelligently select a cure cycle for the material.

United States Patent [19]

Baucom et al.

[11] **Patent Number: 5,057,338**

[45] **Date of Patent: Oct. 15, 1991**

[54] **PROCESS FOR APPLICATION OF POWDER PARTICLES TO FILAMENTARY MATERIALS**

[75] Inventors: **Robert M. Baucom**, Newport News; **John J. Snoha; Joseph M. Marchello**, both of Hampton, all of Va.

[73] Assignee: **The United States of America as represented by the Administrator of the National Aeronautics and Space Administration**, Washington, D.C.

[21] Appl. No.: **524,109**

[22] Filed: **May 16, 1990**

[51] **Int. Cl.**[5] **B05D 1/24**

[52] **U.S. Cl.** **427/185**; 427/195; 427/375; 118/DIG. 5; 156/166; 156/283

[58] **Field of Search** 427/189, 195, 375; 118/DIG. 5; 156/166, 283; 264/136, 133, 134

[56] **References Cited**

U.S. PATENT DOCUMENTS

3,742,106	6/1973	Price	264/134
3,862,287	1/1975	Davis	264/134
4,243,699	1/1981	Gibson	427/183
4,614,678	9/1986	Ganga	264/136
4,799,985	1/1989	McMahon et al	156/166

Primary Examiner—Shrive Beck
Assistant Examiner—Benjamin L. Utech
Attorney, Agent, or Firm—George F. Helfrich

[57] **ABSTRACT**

This invention is a process for the uniform application of polymer powder particles to a filamentary material in a continuous manner to form a uniform composite prepreg material. A tow of the filamentary material is fed under carefully controlled tension into a spreading unit, where it is spread pneumatically into an even band. The spread filamentary tow is then coated with polymer particles from a fluidized bed, after which the coated filamentary tow is fused before take-up on a package for subsequent utilization. This process produces a composite prepreg uniformly without imposing severe stress on the filamentary material, and without requiring long, high temperature residence times for the polymer.

2 Claims, 1 Drawing Sheet

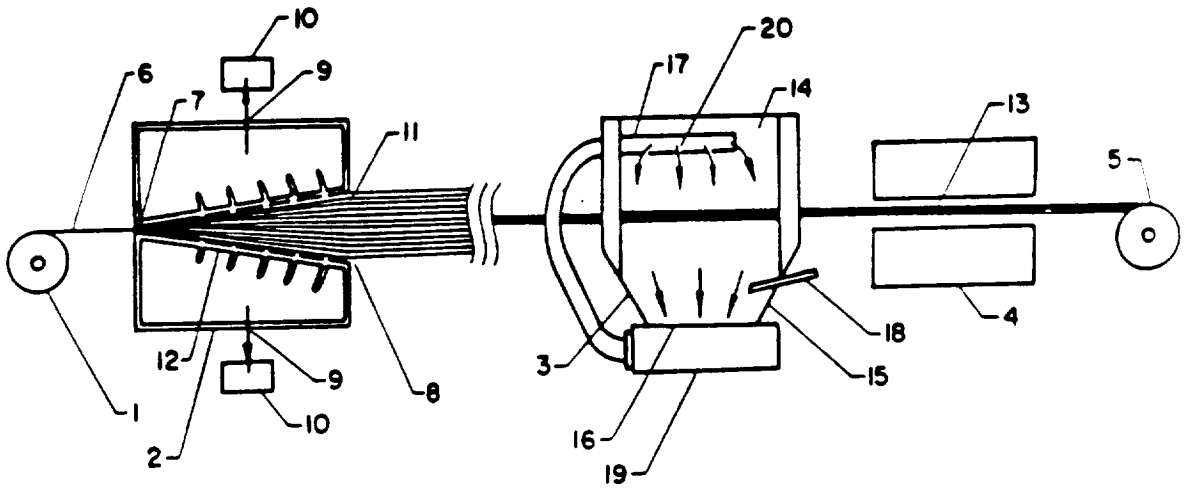

PROCESS FOR APPLICATION OF POWDER PARTICLES TO FILAMENTARY MATERIALS

ORIGIN OF THE INVENTION

The invention described herein was jointly made in the performance of work under a NASA Contract and an employee of the United States Government. In accordance with 35 U.S.C. 202, the contractor elected not to retain title.

BACKGROUND OF THE INVENTION

1. Field of the Invention

The present invention relates generally to the application of powder particles to filamentary materials. It relates in particular to the uniform application of polymer powder particles to spread continuous fiber tows in a fluidized bed unit.

2. Description of Related Art

Thermoplastic composites offer the potential of more attractive mechanical properties at elevated temperatures than do other materials. The primary concern in achieving this potential has been the difficulty experienced in combining thermoplastics with continuous fiber tows to produce a composite prepreg material.

Many previous attempts to apply polymer matrices to filamentary materials have been attempted including: slurry coating, coating from solvent base matrices, film coating and calendaring. The general disadvantage of most prior art methods for producing composite prepreg materials is the non-uniform distribution of the polymer materials throughout the filamentary materials and the difficulty in removal of some species of carrier materials in the polymer matrix in subsequent processing steps. In particular, the high viscosity of polymer melts and the limited solubility of polymer in volatile solvents have ruled out conventional hot melt and solution prepregging methods. This in turn has led to efforts to develop other combining methods such as emulsion, slurry and dry powder. See, e.g., Babu Varughese and John Muzzy, "Combining LARC-TPI and Powder with Carbon Fiber by Electrostatic Fluidized Bed Coating," 21st International SAMPE Technical Conference, Atlantic City, September 1989. The dry powder prepreg processes presently under development contact the tow with powder and either encase, bind, or sinter the powder to the fibers. See especially, J. L. Throne, R. M. Baucom, and J. M. Marchello, "Recent Developments in Dry Powder Prepregging on Carbon Fiber Tow," FiberTex Conference, Clemson University, October 1989; and K. Friedreich, T. Gogera and S. Fakirove, *Composite Science and Technology*, Vol. 33, pp. 97-120, 1988. Because of the tendency for movement of powder encased with the tow in an extruded tube, and for binder failure with powder loss during weaving, sintering appears to be the preferred method for attaching the powder. The dry processes spread the tow and contact it with powder suspended in air or nitrogen. Investigators at Georgia Institute of Technology and the University of Akron utilize electrostatic force to collect the particles on the tow.

It is accordingly the primary object of the present invention to provide a method for the uniform application of polymer powder particles to filamentary materials in a continuous manner to form a uniform composite prepreg material.

SUMMARY OF THE INVENTION

This primary object, as well as its attending advantages and benefits, are attained by the provision of a process having the following sequential steps:

(1) Feeding filamentary material: In order to provide precise filament tow tension control, externally pressurized air bearing rolls are utilized to provide frictionless filament feed spool rotation. A bulk carbon faced brake is utilized to provide accurate tow tension on the feed spool during processing.

(2) Spreading the filamentary material: Spreading of the filamentary material is effected by introducing a tow bundle into a slot tunnel which is composed of upper and lower plates separated by divergent bars which have holes perpendicular to the fiber tow feed direction. Vacuum pressure is applied to a plenum chamber which surrounds the slot tunnel. This vacuum, in turn, is drawn through the aforementioned holes in the bars on either side of the slot tunnel. The flow of the air lateral to the filament feed direction has the effect of uniformly spreading the fiber tow into an even band. The spread of the tow into a band is controlled by the level of vacuum in the slot tunnel and the tow tension applied at the feed roll station.

(3) Coating the spread filamentary material: The spread fiber tow is then directed into a powder circulation chamber which operates by establishing a recirculating cloud of air borne powder particles. Provisions are made to add additional powder material as it is plated out on the fiber tow.

(4) Fusing the coated filamentary material: Heat is applied to the coated filamentary material to fuse the polymer powder onto the fibers. A standard laboratory horizontal tube furnace is conveniently employed.

(5) Taking up the fused coated filamentary material: The fused coated fiber tow is collected on a take-up spool, e.g., a standard traveling/rotating take-up spool mechanism.

BRIEF DESCRIPTION OF THE DRAWING

For a more complete understanding of the present invention, including its primary object and attending advantages and benefits, reference should be made to the Description of the Preferred Embodiments, which is set forth in detail below. This detailed description should be read together with the accompanying drawing, wherein the sole FIGURE is a schematic representing the combination of procedural steps which is the present invention.

DESCRIPTION OF THE PREFERRED EMBODIMENTS

In the specific examples which follow, the following materials and equipment were utilized:

A. Starting Materials. Unsized Hercules AS-4 carbon fibers in three and 12K tows were used with LARC-TPI2000 polyimide powder obtained from Mitsui Toatsu Chemicals, Inc., 200 Park Avenue, New York, N.Y. 10166. The powder had an average particle size of 19 microns (7.4×10^{-4} in.).

B. Prepreg System. Referring to the drawing, the experimental set-up was comprised in sequence of: a tow feed spool with tow tension brake 1; a pneumatic tow spreader 2; a fluidized bed coating unit 3; a horizontal tube furnace 4; and a take-up spool 5.

Particularly, tube furnace 4 was an electric oven with a 5.0 cm (2.0 in.) diameter and 37.5 cm (15.0 in.) long

ends of a cylinder and applying nitrogen pressure to the cylinder. The small nitrogen flow out through the bearings served to keep resin from entering and greatly reduced maintenance requirements.

THEORETICAL CONSIDERATIONS

1. Tow Spreader. In the pneumatic spreader tow fibers are subject to the tow tension, F_t, and the air drag, F_w, toward the wall. Under these forces a fiber would move at an angle, ϕ, given by

$$\text{Tan } \phi = F_w/F_t \quad (1)$$

Tow tension is set by the brake on the feed spool. Air drag on the fiber results from flow in the spreader chamber.

The air drag on a fiber can be determined from data correlations for flow passed through a cylinder. The pressure difference between the air in the spreader and the surrounding vacuum manifold is primarily due to the flow resistance of the small holes in the spreader section walls. For subsonic flow through these holes the air velocity, U_o, may be obtained from the orifice equation:

$$U_o = C_o(2g_c\Delta P/\rho)^{\frac{1}{2}} \quad (2)$$

Where C_o is the orifice coefficient, g_c the gravitational constant, ρ the air density and ΔP the pressure drop. The coefficient is constant, $C_o = 0.61$, in the flow range of interest.

In the spreader chamber, the air flow toward the walls, U_w, is related to flow through the holes by the area ratio

$$U_w = U_o(A_o/A_w) \quad (3)$$

The air drag for flow passed a cylinder is (7)

$$F_w = (C_D\rho U_w^2 D_f L/g_c \quad (4)$$

Where C_D is the drag coefficient, D_f the diameter and L the length of the fiber. Substituting equations (2) and (3) into (4) gives

$$F_w = (C_D D_f L C_o^2 A_o^2/A_w^2)\Delta P \quad (5)$$

with the exception of C_D all the terms in the bracket are constant. In the lower flow ranges the drag coefficient is a function of Reynolds number of U_w and may be expressed in terms of ΔP through equations (2) and (3). therefore,

$$F_w = f(\Delta P) \quad (6)$$

and from equation (1) the fiber angle, ϕ, would be

$$\phi = \tan^{-1}[f(\Delta P)/F_t] \quad (7)$$

For a given tension, F_t, the angle can be set by the pressure difference drawn on the chamber. Conversely, for a given ΔP, the angle may be adjusted by changing the tow brake setting for the tension.

The above analysis has dealt with the air drag on a single isolated fiber. The tow is comprised of thousands of fibers and air flow passed through a fiber is influenced by the surrounding fibers. While the exact flow conditions are unknown, the general form of equation (7) also would apply for a multi-fiber system. This suggests that the tow spread angle may be correlated as a function of tension and pressure drop.

2. Fluidized Bed. The expanded fiber tow behaves like a fibrous filter. Particle collection is by momentum impaction, inception owing to van der Waals forces, Brownian diffusion and in some cases electrostatic force. Theoretical analysis (8) indicate that the collection efficiency of a single fiber, η_o, is a function of the parameter, Ψ,

$$\Psi = D_p^2 U\rho_p/18\mu D_f \quad (8)$$

Where D_p is the particle diameter, U, the gas velocity, ρ_p, the particle density, μ, the gas viscosity and D_f, the fiber diameter.

The collection efficiency of a fiber when other fibers are nearby is given by the relationship (9):

$$\eta_i = \eta_o[1 + 1.0R_e^{\frac{1}{2}}(1 - \epsilon_f)] \quad (9)$$

Where R_e is the Reynolds number for flow passed through the fiber and ϵ_f, is the void fraction of the fiber mat.

The fiber-particle collision cross-section is $[D_p + D_f]L$. For a particle cloud density, n, and gas velocity, U, the rate at which particles arrive at the fiber surface is $nU[D_p + D_f]L$. With an average collection efficiency, η_i, the rate of deposition on the N fibers in the tow is

$$dM/dt = n\eta_i U[D_p + D_f]LN \quad (10)$$

and

$$dM/dt = PW_tU_t \quad (11)$$

Where P is the weight percent prepreg, W_t, the tow weight per unit length and U_t, the linear tow rate. Combining equation (10) and (11)

$$P = \{\eta_i U[D_p + D_f]L\ N/W_t\}nU_t \quad (12)$$

For a given type of flow bundle, chamber dimensions and recirculation level, and resin powder the term {} is constant. This is the transport operating equation for fluidized bed units. For a given system the prepreg level is directly proportional to the resin cloud density, n, and inversely proportional to the tow rate, U_t.

EXAMPLES

1. Prepreg Operation. The fluidized bed powder prepreg system of the present invention was operated over a range of conditions to confirm design theory and operating correlations and to provide the basis for scale up.

A series of test runs were made at tow speeds from 0.87 to 4.2 cm/sec (0.34 to 1.65 in./sec) and oven temperatures from 260° to 300° C. (500° to 572° F.). Runs were started with initial amounts of resin charge in the chamber ranging from 50 to 150 grams (1.8 to 5.3 oz.). Samples were cut at regular intervals from the tow leaving the electric oven and weighed to determine the resin level in the prepreg. From these test runs the operating conditions were established for longer steady rate operation of the system.

A typical LARC-TPI run to produce a 30.5 m (100 ft.) continuous sample would start with 75 grams (2.6 oz.) of resin in the chamber, an oven temperature of 280° C. (536° F.) a tow rate of 4.2 cm/sec (1.7 in./sec)

$$P = 195n/U_t \quad (13)$$

This is the theoretical relation between weight percent prepreg, resin cloud density and tow speed.

Resin cloud samples were not taken, but initial cloud densities for four runs serve to demonstrate the viability of equations (12) and (13). Table 2 presents data from a series of runs that began with different initial amounts of resin placed in the chamber. The cloud density was calculated assuming that 80 percent of the charge is fluidized by the circulation fan into the 5.6 liter chamber volume. This information was used to calculate the prepreg level predicted by equation (13). Comparison of the data with the predictions suggests that equations (12) and (13) can serve as a basis for design and operating data correlation.

TABLE 2

PREPREG DATA
TOW SPEED OF 4.2 CM/SEC

Initial Resin Charge, Grams	Cloud Density, g/cc	Prepreg wt % Data	Prepreg wt % Equation (10)
140	0.0200	46	49
100	0.0140	41	41
50	0.0071	28	26
75	0.0107	34	34

What is claimed is:

1. A process for the uniform application of polymer powder particles to a filamentary material in a continuous manner to form a uniform composite prepreg material, which process comprises the following combination of sequential procedural steps:

continuously feeding a tow of the filamentary material under controlled tension into a spreading unit,

spreading the moving filamentary tow into an even band by a controlled cross-flow of air providing lateral force on the moving filamentary tow,

coating the spread filamentary tow with polymer particles from a fluidized bed, which acts in cooperation with a bubbling bed resin feeder providing a constant, recirculating resin mass flow to the fluidized bed for steady-state operation,

fusing the coated filamentary tow, and taking up the fused, coated filamentary tow on a package for subsequent utilization.

2. The process of claim 1 wherein the fluidized bed provides a cloud of polymer powder particles which contacts the moving, spread filamentary tow.

* * * * *

WEAVING TOWPREG MADE FROM DRY POWDER PREPREGGING PROCESS

Maylene K. Hugh, Joseph M. Marchello, ODU / NASA Langley
Janice Maiden, Textile Technologies, Inc.
Norman J. Johnston, NASA Langley

A study was conducted to establish the parameters for weaving 3k, 6k, and 12k carbon fiber impregnated with LARC™-TPI dry powder. The resulting eight-harness satin broad goods were fabricated into test specimens to determine mechanical properties.

Previous studies for weaving the dry powdered tows dealt with tow flexibility and adhesion of powder particles to carbon fiber. Manipulation of the thermal treatment step in the prepregging process enabled successful control over these two variables. Abrasion and fiber damage during weaving were unresolved matters. In this investigation, tow bundle twisting was used to reduce the separation of filaments, tow-to-tow abrasion, and fiber loss.

Optimal weaving protocol was established and mechanical property data were obtained for the consolidated woven material. Utilization of appropriate textile techniques for composites processing is an important factor for automating the production of quality composite parts from powdered towpreg.

WEAVING TOWPREG MADE FROM DRY POWDER PREPREGGING PROCESS

Maylene K. Hugh and Joseph M. Marchello, Old Dominion University
and NASA Langley Research Center

Janice Maiden, Textile Technologies, Inc.

Norman J. Johnston, NASA Langley Research Center

Overview

- Dry Powder Prepregging Process
- Weaving Studies
- Processing
- Mechanical Properties
- Conclusions

CHALLENGES/BARRIERS IN CURRENT PREPREG TECHNOLOGY

Toughened epoxy prepreg and towpreg

- Short out-times
- High scrap losses
- Refrigeration
- Expensive

Thermoplastic Matrices

- Difficult to hot-melt or solution coat
- Expensive

Solution Prepregging

- Handling solvents

Commingled Yarns

- Expensive

RTM Matrices

- Environmental Stability

IMPORTANT FEATURES OF THE POWDER COATING PROCESS

- VERSATILE: THERMOPLASTICS AND THERMOSETS
- OPERATES AT ROOM TEMPERATURE
- NO SOLVENTS INVOLVED
- MANAGEABLE EXPOSURE TO TOXIC MATERIALS
- PREPREG REQUIRES NO SIGNIFICANT REFRIGERATION: REDUCES WASTE/SPOILAGE
- PREPREG CAN BE WOVEN, FILAMENT WOUND, PULTRUDED, THERMOFORMED
- VIABLE ALTERNATIVE TO RTM PROCESSING OF TEXTILE PREFORM COMPOSITES

DRY POWDER TOWPREG SYSTEMS

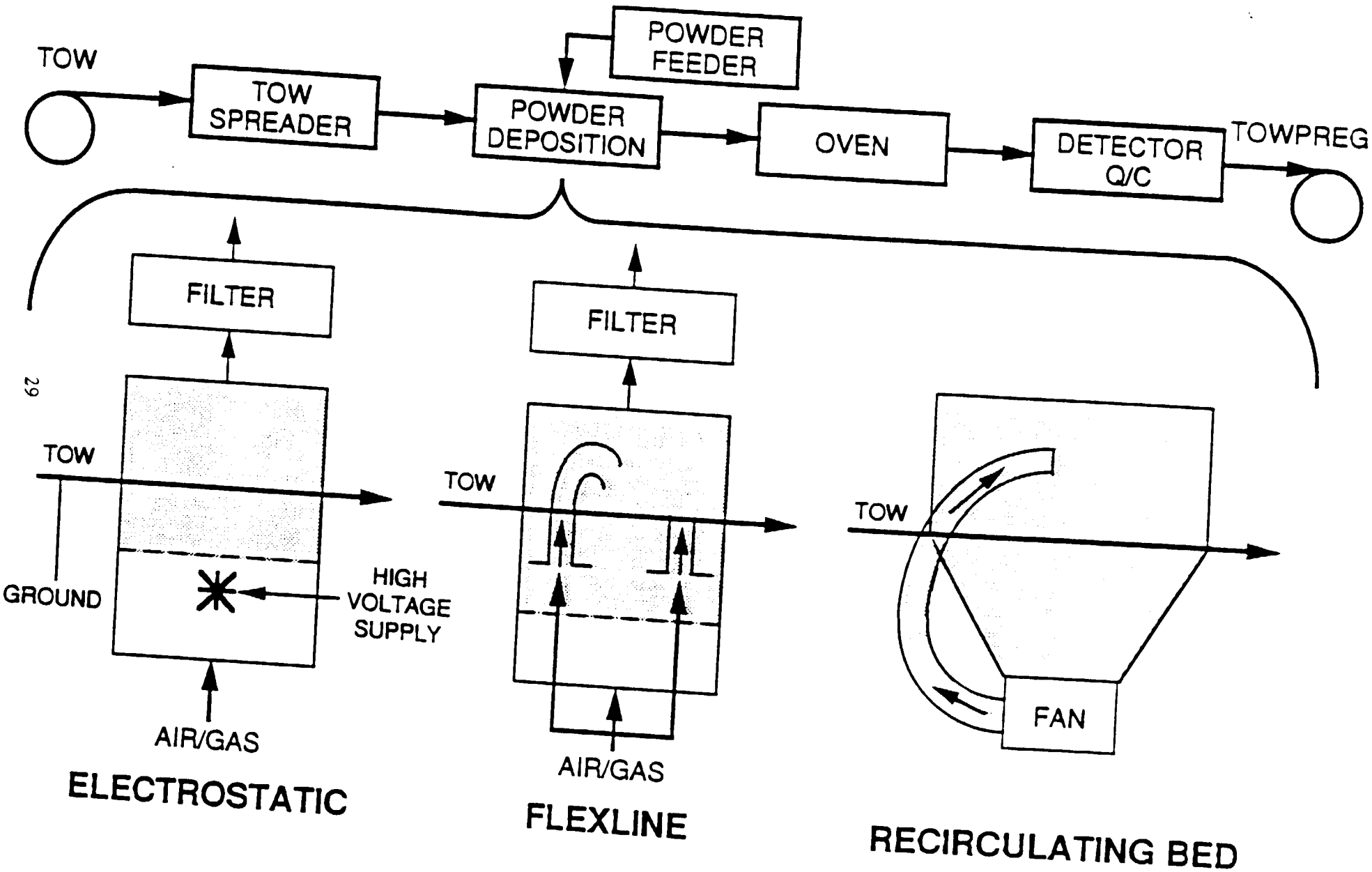

Advanced Polymer Powder Prepreg Facility
ACT/HSR Research Support

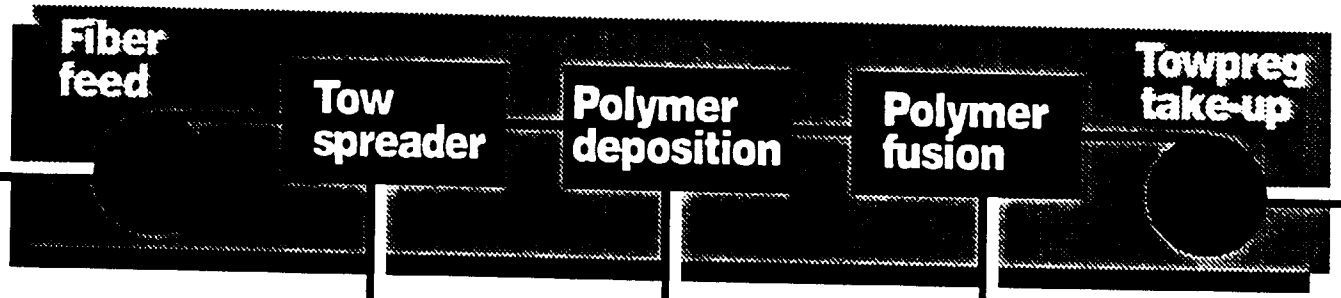

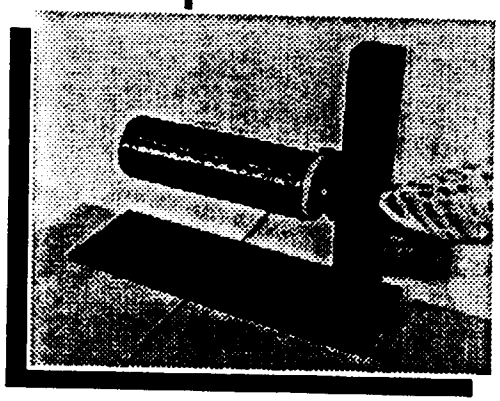

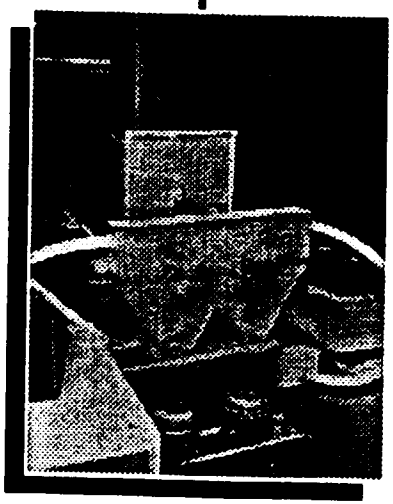

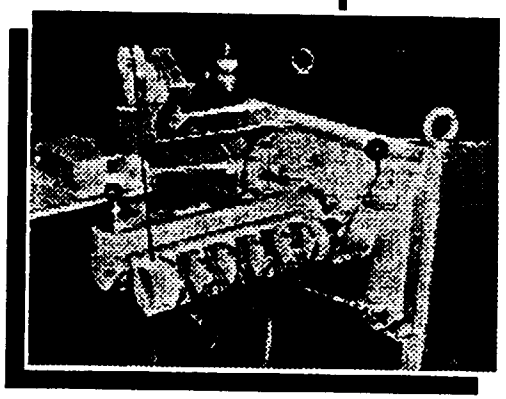

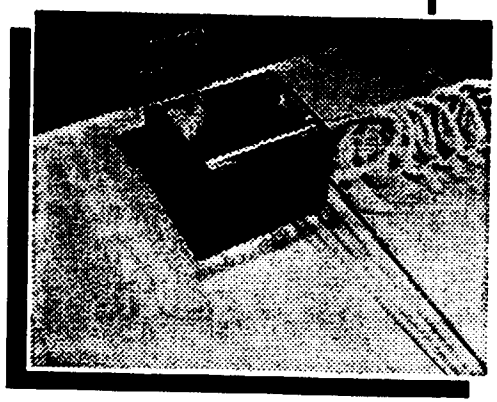

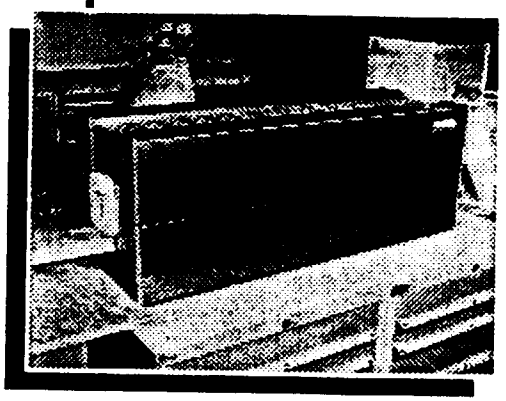

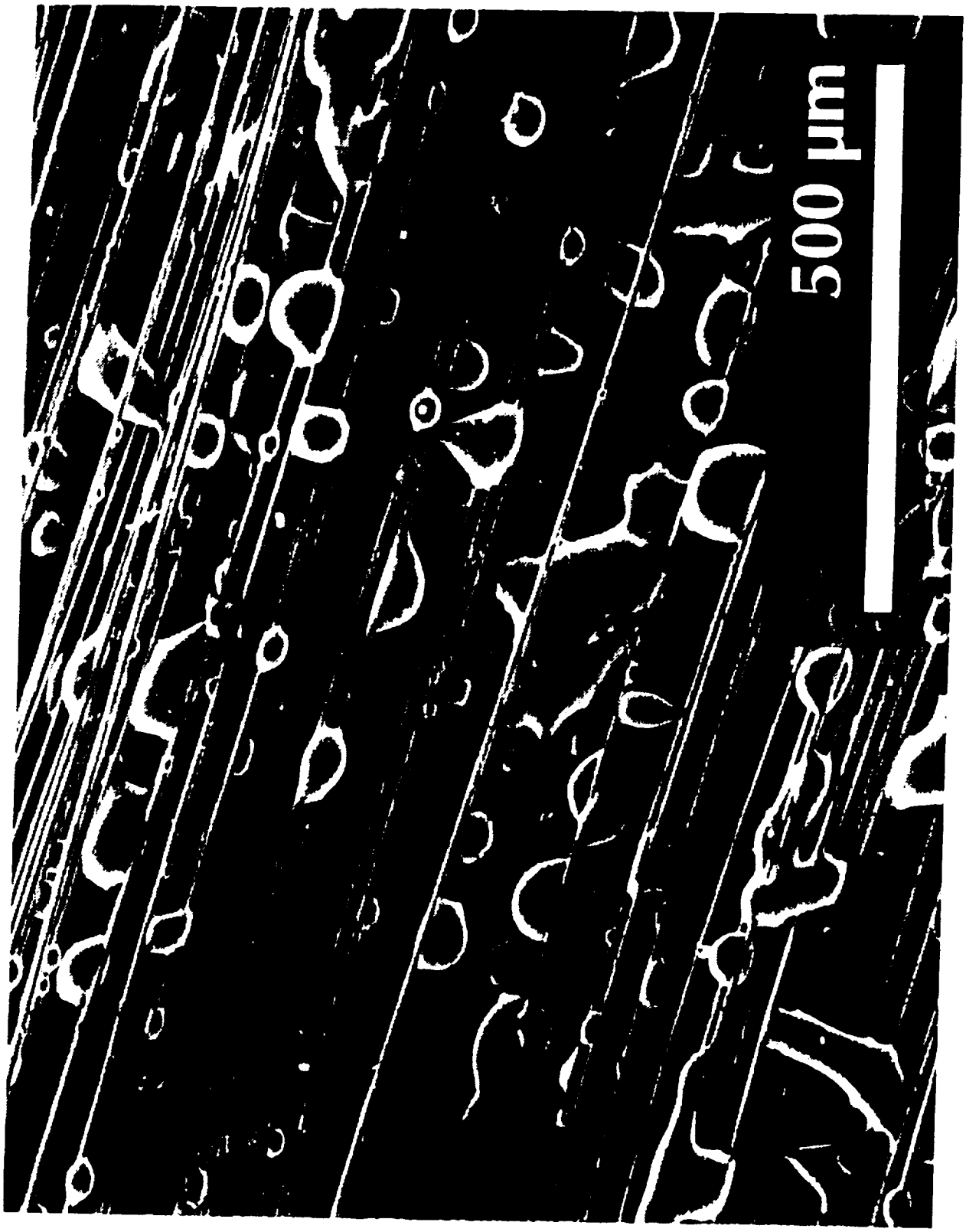

POWDER-COATED TOWPREG TECHNOLOGY FOR TEXTILE COMPOSITES

OBJECTIVE: Develop powder-coated towpreg technology as a viable alternative to RTM for fabrication of textile composites.

APPROACH:

1. Verify weave capability of powder-coated towpreg by systematically fabricating and evaluating flat composite panels of increasing complexity.

2. Verify braid capability of powder-coated towpreg by fabricating and evaluating braided flat composite panels.

3. Fabricate and evaluate single- and three-stringer panels from powder-coated towpreg.

4. Conduct engineering studies to determine the important physical properties and processing characteristics of powder-coated towpreg.

5. Conduct detailed compaction/consolidation studies to determine the proper fabrication procedures for preforms made from powder-coated towpreg.

Towpreg Weaving Conditions

Rewinders	-	Server Machine, Cross Wind Pattern, 2"D Cores
	-	Ruff Winder Machine, Parallel Wind, 2"D Cores
Loom	-	Iwer 1200 Loom, Capable Speeds of 100 ppm
		Actual speed of 40 ppm
Weave Pattern	-	Eight Harness Satin, Balanced Fabric 12k - 8 x 8 ppi 6k - 10 x 10 ppi 3k - 20 x 20 ppi

WEAVING PARAMETERS

Towpreg Characteristics

- Yarn Shape
- Amount of Twist
- Flexibility
- Degree of Damage

Weaving Characteristics

- Eyelets
- Turns and Bends
- Tensioning
- Heddles and Reed

Final Parts

- Optimal Resin Content
- Bulk Factor

TOWPREG 8HS FABRIC ANALYSIS

Material	Weave Count (ppi)	Weight (g/m)	Thickness (in)
Celion 6k / LARC™-TPI No Twist	10.2 x 9.8	478.36	.067
Celion 6k / LARC™-TPI Twisted Tow	10.2 x 9.8	483.74	.071
Celion 6k / LARC™-TPI No Twist	10.1 x 10.0	448.21	.077
Celion 6k / LARC™-TPI Twisted Tow	10.2 x 9.3	499.37	.103
AS-4 12k / LARC™-TPI Twisted Tow	8.2 x 8.2	810.5	.126
Celion 3k / LARC™-TPI Twisted Tow	20 x 20	TBD	TBD

WOVEN TOWPREG CURE CYCLE

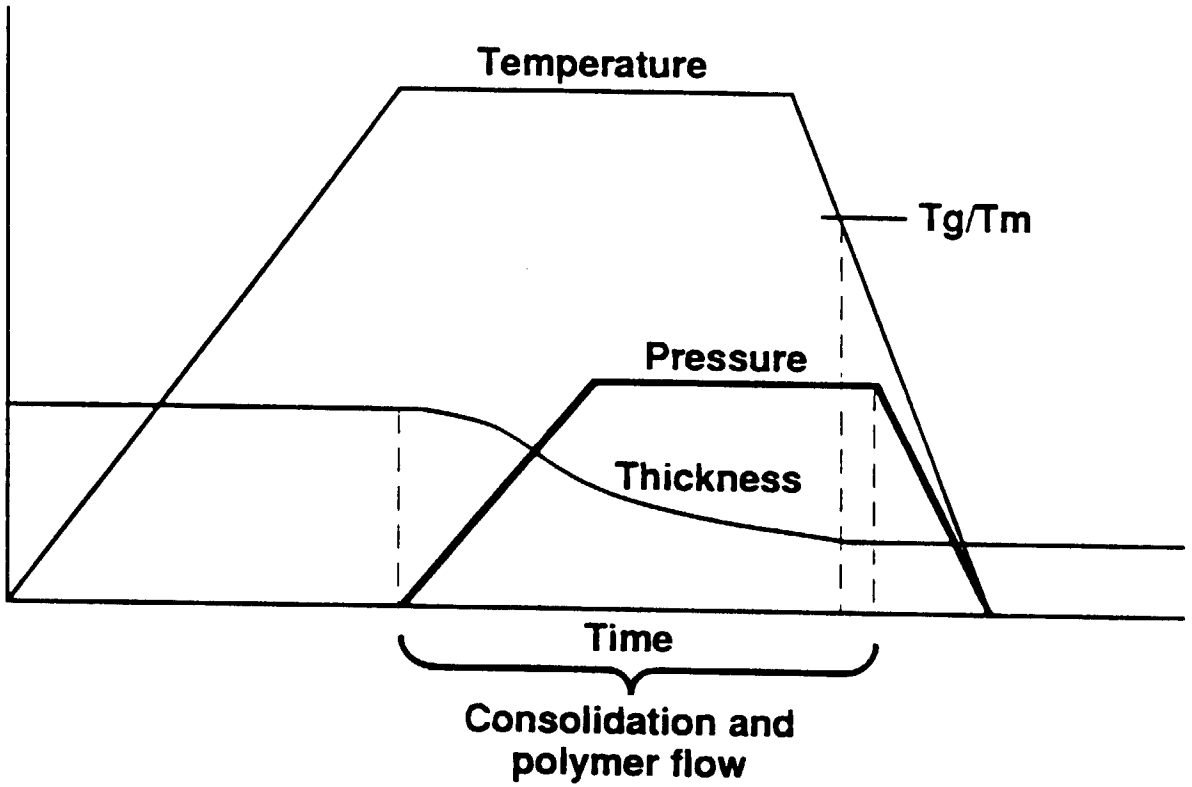

- Vacuum is used to eliminate air voids.
- Pressure ramp allows time for fiber movement into a compact arrangement with minimum fiber crimping and breakage.
- Pressure ramp also provides time for resin flow and adhesion.
- Holding temperature above Tg or Tm anneals the composite relieving fiber elastic stresses.
- Cooling below Tg or Tm stops consolidation before thickness curve flattens and avoids resin squeeze out and resulting dry spots.

Tension Properties of 8HS Fabric Made From LARC™-TPI Powder Coated Towpreg

Tow Bundle Size	Max. Stress (ksi)	Modulus (msi)	Poisson's Ratio	V_f (%)
6k	95.9 ± 5.5	7.93 ± .16	.0524 ± .0161	53
12k	67.3 ± 7.0	7.77 ± .38	.0559 ± .0061	47

Conclusions

- Twisting the towpreg before weaving allows the towpreg to pass easily through the heddles by keeping a round cross-section and by constraining the loose filaments.
- Towpreg that has a high flexural rigidity (>10,000 mg-cm) is preferred for weaving.
- 12k tow bundles are preferred over 6k and 3k tow bundles since less damage is imparted to larger tow bundles.

Conclusions

- Twisting the towpreg before weaving allows the towpreg to pass easily through the heddles by keeping a round cross-section and by constraining the loose filaments.
- Towpreg that has a high flexural rigidity (>10,000 mg-cm) is preferred for weaving.
- 12k tow bundles are preferred over 6k and 3k tow bundles since less damage is imparted to larger tow bundles.
- The effects of tow bundles on mechanical properties is still an open issue.

V. ATP ROBOT HEAD

November 27, 1991

Memorandum

To: N.J. Johnston, R.M. Baucom, D. Sandusky and M.K. Hugh

From: J.M. Marchello

Subject: ATP Robot Head

In conjunction with our studies of towpreg ribbonizing and on-the-fly consolidation, we need to consider the design and operation of the ATP robot head. The following summarizes my observations during visits to McAir, Hercules, and Cincinnati Milicron, and what I have picked up from literature references.

Advanced tow placement, ATP, utilizes robotic technology to position the tow laying robot head on the tool/part surface, and to move it over the surface in a controlled manner, as an array of towpreg ribbons are laid down. Spools of towpreg ribbon are held in a creel on the robot and fed to the head. The robot computer software system governs the ribbon placement process.

ATP robot heads are capable of in-process compaction, individual tow cut/stop/start, resin tack control, differential tow payout, and tow tensioning. During tow placement, for each tow ribbon:

> The ribbon passes first between two wheels, one spring loaded and the other driven by a small electric motor. This system can provide brake/drive tension of up to 15 pounds (6.8 kg). As the robot head moves, towpreg ribbon is paid out from the creel spools at a tension level established by the brake/drive motors. During straight laydown runs, all tows are subjected to about 1 pound (0.454 kg) of tension. During turns, braking pressure, and correspondingly tow tension, is increased differentially on the inner tow ribbons to slow tow payout. For a 24 tow head, wrinkle free turns with radii as small as 5 inches (12.2 cm) are possible.
>
> A knife tow cutter/clamp system is used to achieve tow ribbon drop/add capability. In this way the number of adjacent tows being laid may be decreased or increased to accomodate changes in tool/part geometry. When a tow is dropped, the cut tow is held

(clamped) by its tension brake. To add, or restart, the tow ribbon, the brake/drive wheel is driven (negative braking) to push the stiff towpreg ribbon forward onto the tool/part surface. To join the towpreg array ribbon tape, the pushed ribbon must be picked up by the roller. That is, the pushed tape must not twist or move out of line and must stay close to its neighbor with minimum gap. The tow push distance may be several inches.

With thermoset towpreg, a tack control system decreases or increases the "B" stage prepreg material tack at critical points along the cut/clamp/restart operation in the robot head. To achieve this the tow ribbon is passed over heated and cooled surfaces. When a thermoset tow is dropped, the cut, hot, clamped tow may gel and stick to the heater/cooler/clamp/cutter surfaces if not restarted in a few minutes. This requires shutdown and cleaning of the robot head mechanism. Thermoplastic towpreg does not require this system. Not having to handle tacky towpreg eiminates the tow heating and cooling system inside the robot head.

As the tape of adjacent towpreg ribbons are laid on the tool/part surface, it is heated and then compacted by a pressure roller. The hot gas, or infrared heater, and the roller are attached to the robot head and follow along behind as the head moves. The pneumatic pressure controlled, elastometric, compliant roller can conform to convex or concave surfaces, having cross band radii as small as 6 inches (15.2 cm) , and apply even pressure across the width of the roller.

The following figures illustrate the robot head internal mechanisms, under the hood operations, for thermoplastic towpreg ribbons. Also shown are the changes that might be made in converting from rectangular to triangular towpreg. The changes deal with use of grooved brake/drive wheels and an alternating up/down tape array. Not shown are the heating and cooling surfaces used with thermostet towpreg.

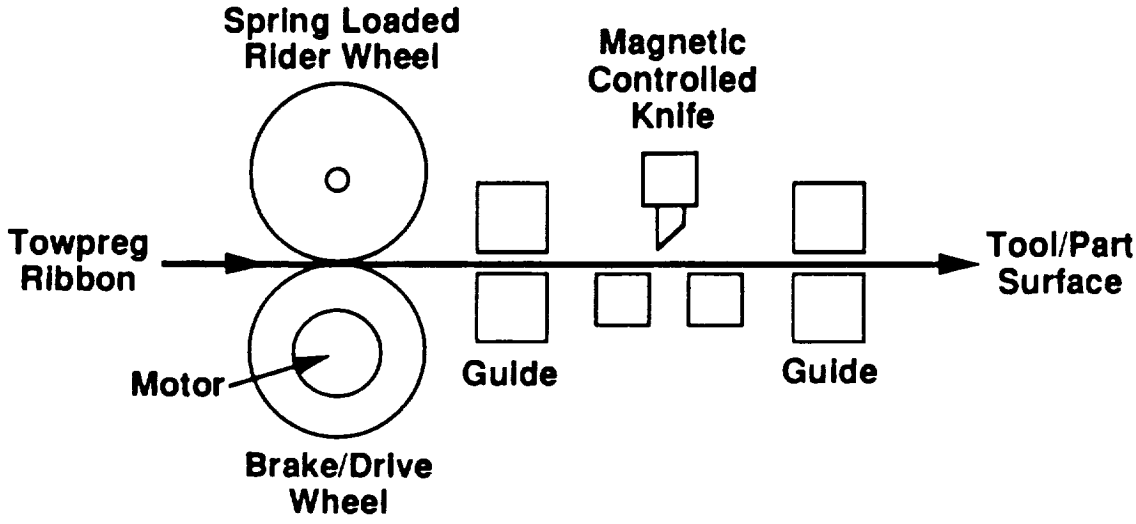

CROSS SECTION VIEW

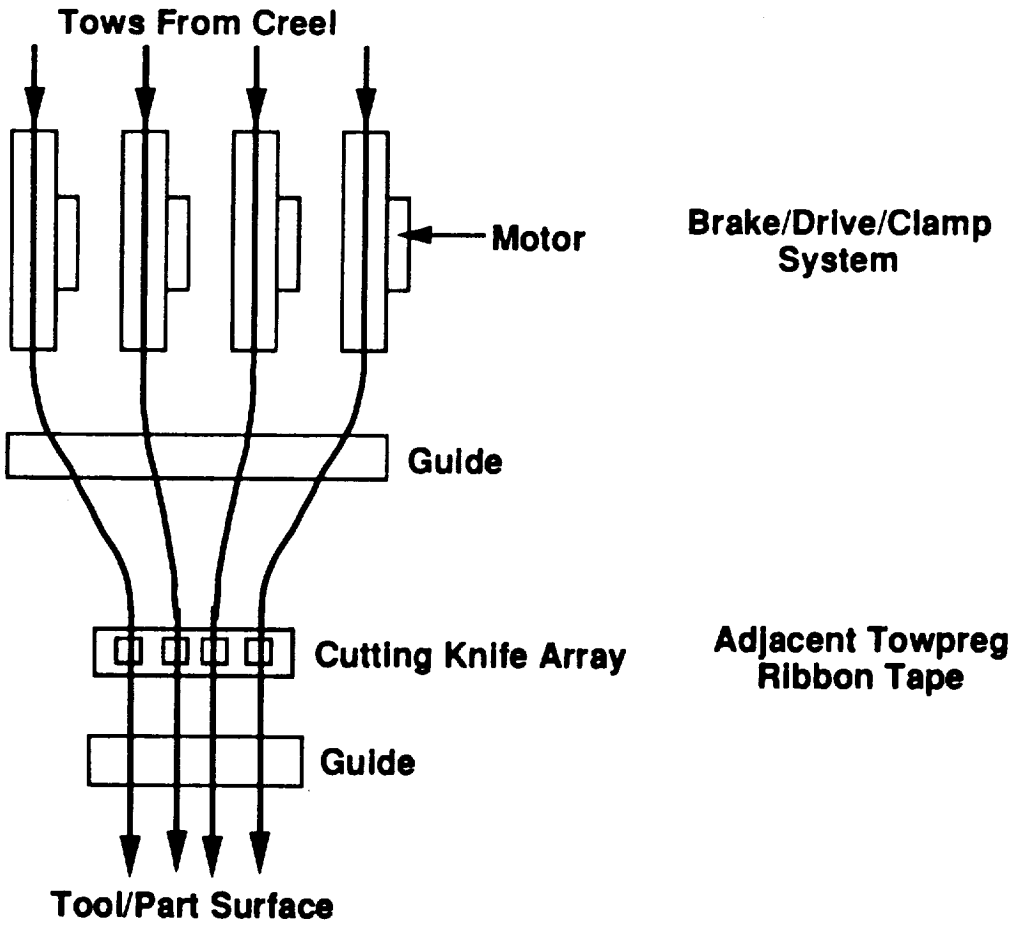

TOP VIEW

SCHEMATIC VIEWS OF ROBOT HEAD ATP TOWPREG RIBBON CONTROL MECHANISMS

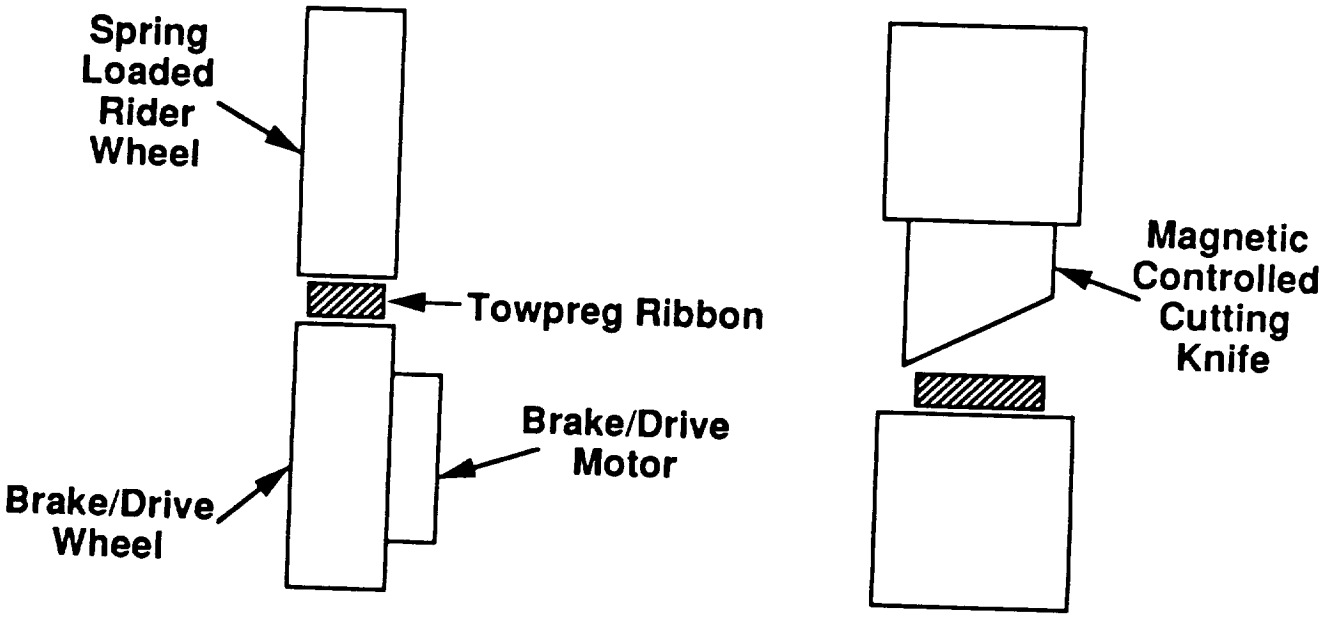

Rectangular Towpreg

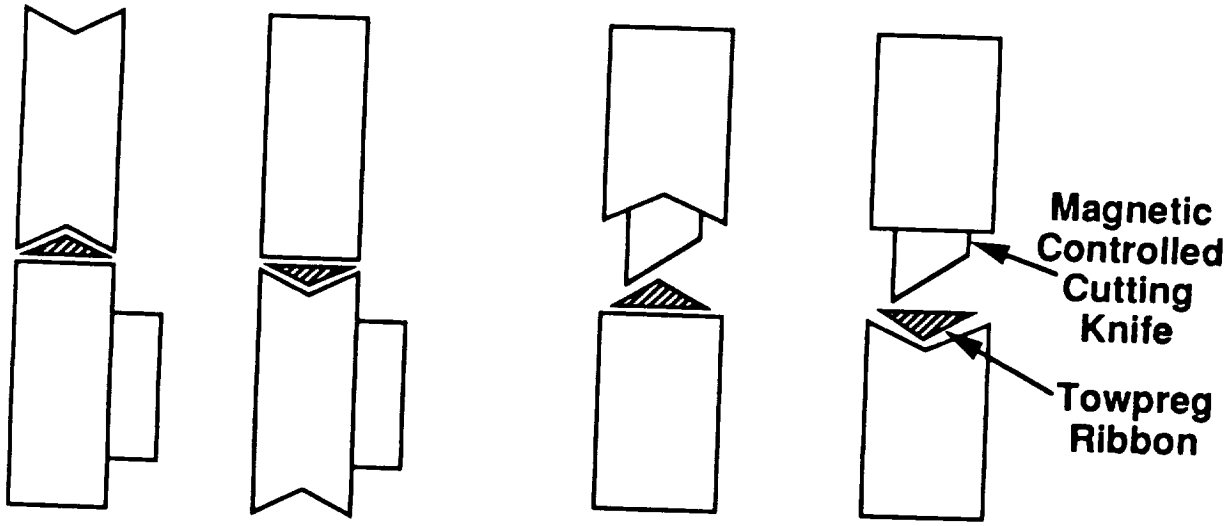

Up/Down Adjacent Triangular Towpreg

Front View of ATP Robot Head Mechanisms

VI. ADVANCED TOW PLACEMENT REVIEW

November 13, 1991

MEMORANDUM

To: N.J. Johnston, R.M. Baucom, T.L. St Clair, J.A. Hinkley, J. Nelson, T.H. Hou, D. Sandusky, and M.K. Hugh

From: J.M. Marchello

Subject: Advanced Tow Placement

During the past few months, in an effort to obtain background information for our study of advanced tow placement, I have reviewed literature on calendering, pultrusion, tape laying and tow placement. This study also draws on the review of consolidation presented in my August 27 memorandum.

The objective of this review was to learn about ways to prepare towpreg ribbon for tow placement, to identify potential improvements in the tape laying robot head, and to explore ways of carrying out "on the fly consolidation" during automated tow placement.

The purpose of this memorandum is to share with you the information I have and my observations. Your comments, particularly in regard to missing information and misinterpretations, would be appreciated.

JMM
11/13/91

ON ADVANCED TOW PLACEMENT

I. INTRODUCTION

Advanced tow placement, ATP, utilizes robotic technology to position the tow laying robot head on the tool surface and move it over the surface in a controlled manner as the towpreg ribbons are laid down. Laser, infra-red, or hot gas heating and roller pressure are used to attach and partially, or fully, consolidate the material as it is laid down. If consolidation is not achieved "on the fly", the part is placed in an autoclave to complete the consolidation.

The mechanisms of resin flow, fiber movement, and consolidation, that occur during ATP are similar to those of the more established technologies of calendering, pultrusion, and tape laying. Therefore, these processes were reviewed as a means of understanding ATP and perhaps contributing to its theoretical background, and of obtaining information for devising experiments that may provide needed information with which to improve ATP equipment and process operation.

II CALENDERING

The process of calendering, or pressing between rollers, was developed over 100 years ago by the rubber industry. It is widely used for tire-fabric coating, for production of floor tiles, and for coating paper and fabric with various thermoplastic materials (PVC, asphalt, polyethylene, cellulose acetate, etc.).

One of the first theoretical studies of calendering was made in 1950 by Gaskell (1) who modelled through the thickness resin flow for both Newtonian and non-Newtonian fluids to predict shear stress and pressure gradient as functions of the roller nip gap, roller speed, and resin viscosity. In his 1974 patent, Ancher (2) draws upon the theory to describe apparatus for impregnating fiber webs with molten polymeric materials, see following figures. Figure 2a illustrates the hydrostatic pressure profile showing a peak of 100 atmospheres just in front of the roller nip area.

In the 1974 patent, Ancher observes that it is extremely important to avoid formation of air bubbles in the composites because they become voids in the final composite. Voids cause serious reduction in the mechanical properties of the composite by acting as stress risers. "Thus the embodiment of the process shown in fig 3, when applied to high strength filament warp, can be operated to maximize the air rejection ability of the roll nip. This is done by operating with the minimum nip opening commenserate with the thickness of the filaments and by having a fairly large amount of fluid surface at points 26 and 28 exposed to the atmosphere". Interestingly, in his earlier (1972) patent, Ancher (3) describes the air bubble circulating flow in the resin buldge and discusses using a flow obstruction to reduce air entrapment, see fig 3 and item 26 of fig 7 and discussion in the following page.

In a recent review of calendering Tseng (4), addresses current processing concerns dealing with temperature and pressure variation along the roller length. Calender rolls are relatively long and are constrained at their ends by bearings. During processing, the relative pressure produced by the polymeric flow can bend or deflect the rolls and cause a non-uniform gap, known as the bending crown. Obviously this effects the flatness and uniformity of the sheet. Another important observation is that sheet speeds range up to as high 2 meters per second, which means pressure is applied for

about 0.01 seconds.

In their progress report a few months ago, Foster-Miller, Inc. (5) developed a theoretical approach to high shear prepregging. As shown in the following pages, their die process is essentially calendering with through the thickness flow, fig 15. The model is applied to LARC-TPI and indicates that pressures of 1,000 psi, and flow times of up to 20 seconds, are required for impregnation. They conclude that to achieve through the thickness impregnation in one second requires resin viscosity less than 10 PaS.

Essientially the same theoretical analysis was used by Seo and Lee (6) to model resin impregnation in thermoplastic composites. Their through-the-bundle press experiments to validify the model used PEEK 150P, see following pages. Viscosities ranged from 300 to 800 Pa-sec and impregnation times were from 10 to 30 minutes depending upon temperature and pressure.

In closing this section, it seems appropriate to comment that powder coated tow requires less resin flow for consolidation, since resin particles are already distributed within the fiber tow bundle. It would be interesting to repeat Seo and Lee's experiment using powder towpreg. Also, the Foster-miller die might be capable of handling high viscosity resins in one second if powdered towpreg were used.

Fig. 1

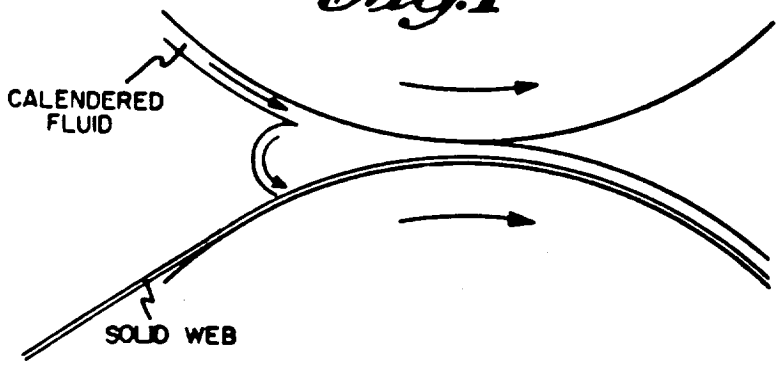

Fig. 2a

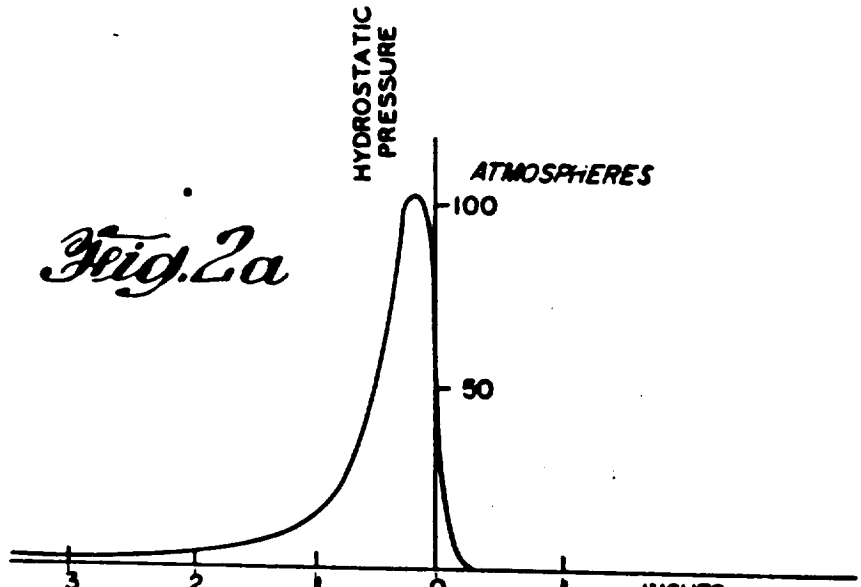

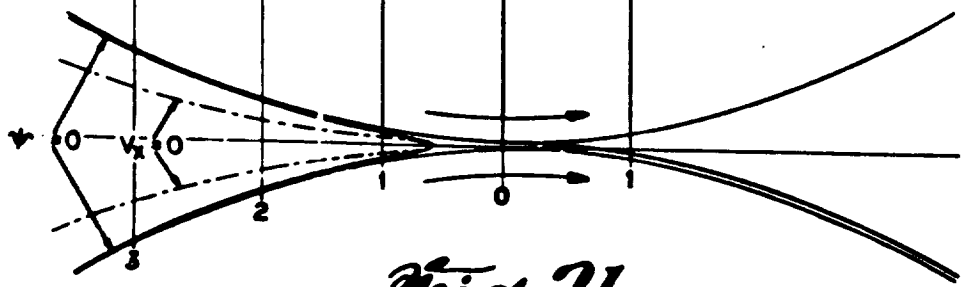

Fig. 2b

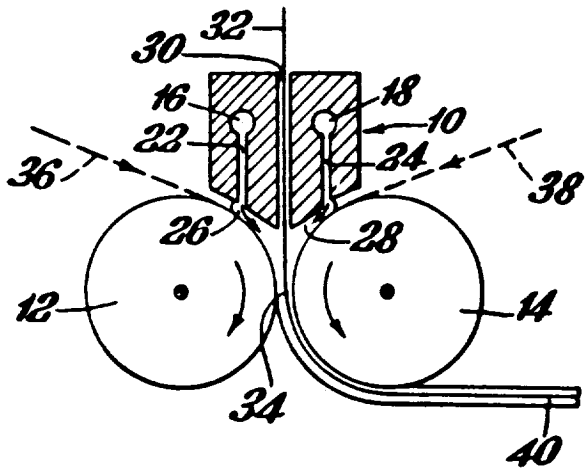

Fig. 3

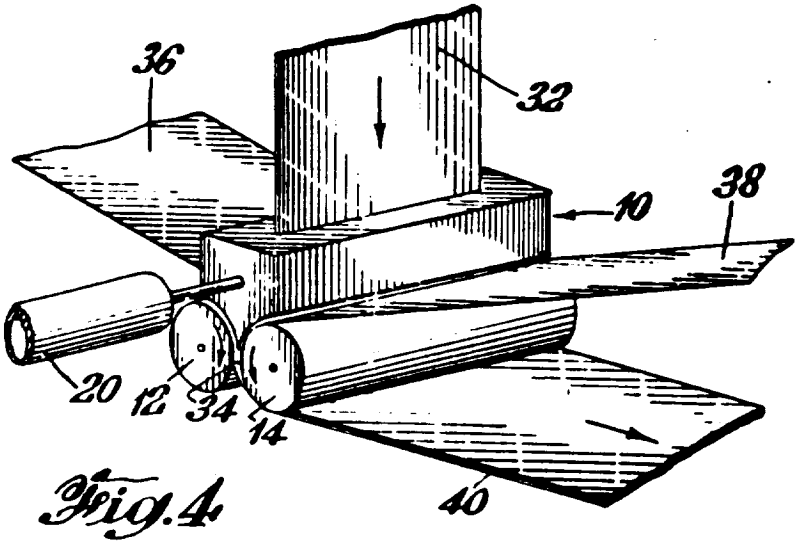

Fig. 4

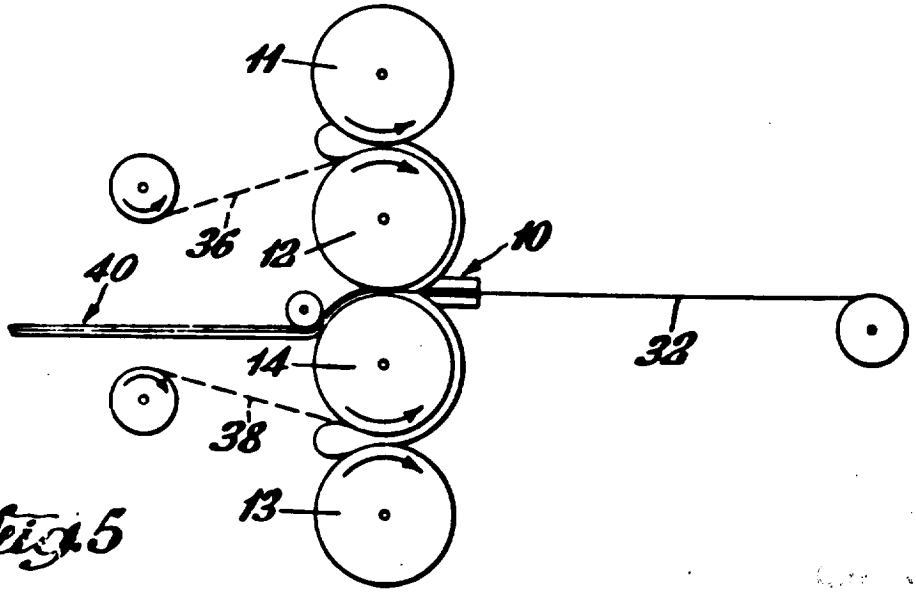

Fig. 5

improved flow and process control for making foam cored sheeting.

Embodiments of the invention are shown in FIGS. 3 through 7.

Referring specifically to the apparatus of FIGS. 3 and 4, an extruder die 10 is provided having a shape which will project into the bank of material which would otherwise form between counter-rotating rolls 12 and 14 of a calender. The die 10 extends across substantially the full width of the calender and has internal manifold passages 16 and 18 which receive molten, polymeric material from extruder 20 and feed it through die passages 22 and 24 to the passages 26 and 28 formed between opposite sides of die 10 and calender rolls 12 and 14.

Die 10 is also provided with a substantially axial passage 30 which permits the feeding of laminating sheet 32 directly to the nip 34 of the calender, between the two outer streams of molten, flowable polymeric material entering the nip through passages 26 and 28.

Additional webs or sheets of material 36 and 38 may optionally be fed, if desired, to the outer surfaces of rolls 12 and 14 to provide an outer surface for the resulting laminate 40.

The central laminating sheet, streams of molten, flowable polymeric material, and optionally outer additional webs are all continuously fed to and combined by passage through the nip 34 of the calender to provide the resulting laminated polymeric material sheet 40.

It is, of course, to be understood that volumetric obstruction die 10 is maintained across the full width of and between calender rolls 12 and 14. It has been found that the most forward (downstream in the direction of material passage) projection of the obstruction should be positioned so as to at least penetrate the bank of material otherwise formed between the pair of calender rolls upstream of the nip by the selection of calendering conditions.

It has been found preferable that the most forward projection of the volumetric obstruction be positioned well within the space between the pair of calender rolls beyond the position of merely slight penetration of the bank of material being calendered. However, any positioning of the most forward projection of the volumetric obstruction (within such penetration of the bank) between the rolls will provide a significant reduction in back flow and consequently improved calendering results.

It is most preferred that calendering operations be performed with the obstruction maintained at a sufficiently close distance to the nip to substantially reduce the calender back flow and thus eliminate the natural bank rotation typical of conventional calendering banks. This has been found capable of accomplishment by substantially contouring and positioning the volumetric obstruction with the stagnation zone or area as defined in my copending application Ser. No. 839,292. However, as pointed out hereinabove, this contouring and positioning is by no means critical and the desired results are progressively accomplished as a more substantial portion of the back-flow zone becomes occupied by the volumetric obstruction.

As mentioned hereinabove, it is optionally within the purview of the present invention to introduce webs (same or different kinds) along the two roll surfaces, thus enabling the forming of complex composite laminates in a single roll pass. The webs applied along the roll surfaces may be selected for decorative purposes and in addition to the web materials already mentioned, decorative webs such as wood veneer, cork, embossed or engraved metal foil, burlap, printed or otherwise patterned paper, natural or synthetic fiber fabrics, etc. may be used as exterior surfacing for the final sheeting. Furthermore, the flowable plastic materials introduced through manifolds 16 and 18 may be supplied by individual extruders or other melt pumps and thus provide laminates with different plastic interlayers. Similarly, the laminating web 32 introduced through passage 30 may itself by a multilayer composite thus resulting in the formation of multilayer composite laminates 40.

Another embodiment of the invention, as shown in FIG. 5, permits the same result to be obtained solely by the use of a four roll calender. As there shown, a calender is provided having rolls 11, 12, 13 and 14. The streams of flowable plastic and laminating webs are fed to the calender, through die 10, as in the embodiment of FIGS. 3 and 4, whereas the optional additional outer webs 36 and 38 are fed in the manner shown to the banks of material between roll pairs 11–12 and 13–14. The laminated polymeric sheet 40 is produced in the nip between the 12–14 roll pairs, as in the case of the embodiment of FIGS. 3 and 4.

FIGS. 6 and 7 show an embodiment of the invention as employed for making foam core laminates.

As in the case of FIGS. 3 and 4, additional exterior laminating webs 36 and 38 may be introduced along the surfaces of rolls 12 and 14. Also, it is apparent that the embodiment of FIG. 5 can be changed to produce foam core 41 sheeting by providing an expandable plastic material instead of laminating web 32 through the passage in flow obstruction 10. In this variation it becomes possible to manufacture foam cored sheeting and laminates directly on a conventional calender.

The flow system of the present invention conveniently circumvents the air rejection phenomenon of a conventional calendering bank referred to earlier. The expandable material in the center stream is enclosed on all sides and under elevated pressure until it has traversed the roll nip. Even then, the sheet surface consists of non-expandable plastic material and the gas is thus effectively trapped enabling the most efficient utilization of chemical blowing agents or injected gases.

A type of laminate which is becoming increasingly important is continuous fiber pre-pregs (pre-impregnated filaments) made from high strength, high modulus filaments such as graphite, boron or glass. These pre-pregs are webs of very accurately aligned and spaced filaments which are supplied to a coating apparatus as a warp, i.e., without any transverse filaments (filling or woofing). The polymeric coating is usually an epoxy or polyimid pre-polymer which is B-staged or advanced subsequent to the impregnation step. The tapes are then used for building up composite structures for ultra high strength parts such as structural air and space craft members by aligning the fibers according to the direction of the applied stresses. After final lay-up, the composites are fused together and cured by autoclaving.

It is extremely important to avoid formation of air bubbles in these composites because they become voids in the final composite which cause serious reduction in the mechanical properties of the composite by acting as stress raisers. Thus, the embodiment of the

April 25, 1972 F. H. ANCKER 3,658,978
CALENDERING OF POLYMERIC MATERIALS
Filed July 7, 1969
4 Sheets-Sheet 2

FIG. 3.

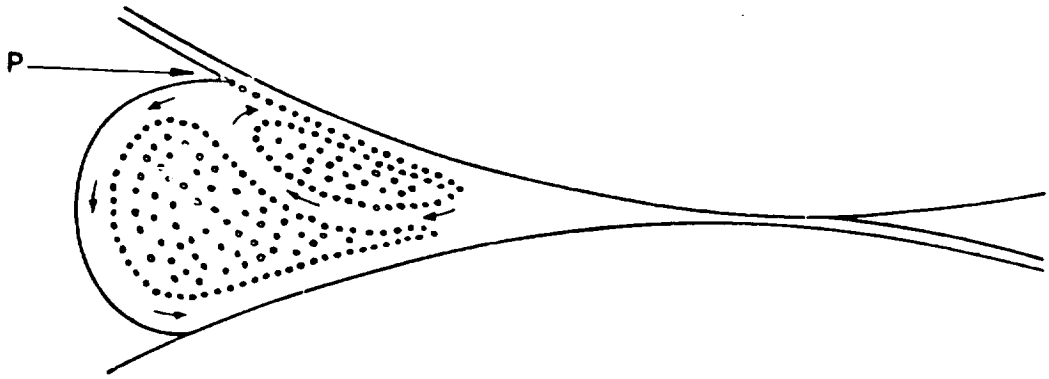

FIG. 4.

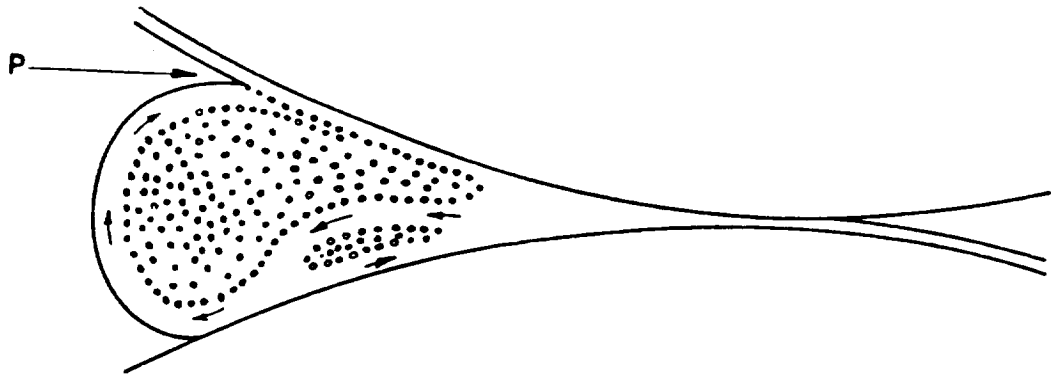

INVENTOR
FRED H. ANCKER
BY
ATTORNEY

April 25, 1972 F. H. ANCKER 3,658,978

CALENDERING OF POLYMERIC MATERIALS

Filed July 7, 1969

4 Sheets-Sheet 3

FIG. 5.

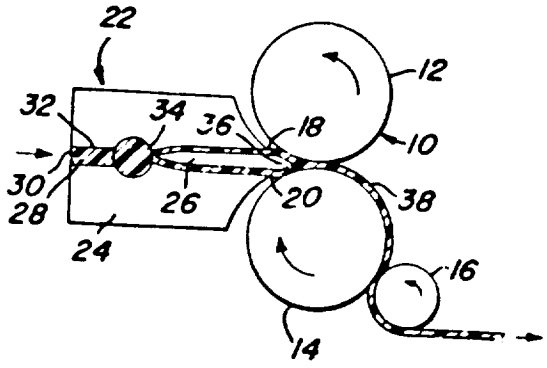

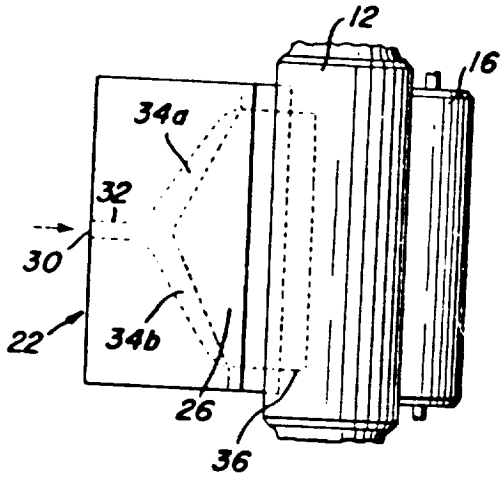

FIG. 6.

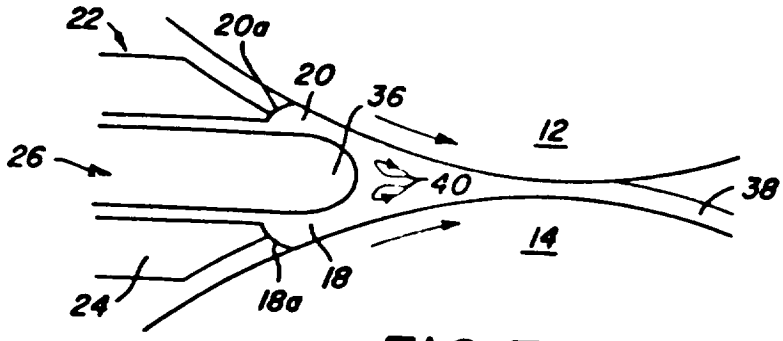

FIG. 7.

INVENTOR
FRED H. ANCKER
BY
ATTORNEY

tern of the actual calendering bank shown in FIGS. 3 and 4.

First, the maximum thickness limitation of about 25 mils for most calendered sheeting is due to the peculiar air entrapment and rejection behavior of a natural calendering bank. We have found that air bubbles almost invariably are introduced into the calendering bank where the hot sheet moves into the bank (points P on FIGS. 3 and 4), no matter in which direction the bank is rotating. If the bank surface is fluid and glossy, this tendency is generally less than when the bank surface is dry and matte, but some air is nearly always introduced. If the bank is cold and "folding," additional air is often introduced due to air cavities between the folds and due to formation of secondary vortices. Nevertheless, as long as the nip opening is small, the stagnation surface is very close to the roll surface, air becomes trapped within the stagnant flow zone and has no opportunity to pass thru the roll nip. Accordingly, it is often seen in calendering of thin films that the calendering bank is filled with air bubbles, yet the emerging film is completely free of air. However, as the nip opening is increased in order to produce thicker sheeting, this fortunate situation no longer exists. The stagnation surface will recede from the roll surfaces and the roll nip, the air bubbles introduced at point P now will be captured within the progressive or active flow zone and the emerging sheet will become porous and/or contain air streaks on the surface and be commercially useless.

Second, the problem of polymer decomposition encountered in attempting to calender thermally unstable, yet highly viscous, materials is also intimately connected with the natural flow pattern of a normal calendering bank. As the roll speeds increase, the residence time of molten polymer in the progressive zone of the bank decreases; however, the residence time of the polymer melt within the stagnant zone remains very great. Actually, because of the increase in viscous heat dissipation with increasing roll speed, the polymer within this zone may degrade severely before any visible degradation occurs in the emerging sheet. Thus, the stagnant flow zone with its associated extreme residence times is the major rate-limiting factor of the calendering process.

The third major problem of the conventional calendering process is the difficulty with which many polymer melts comply with the complicated film tracking and roll release required on a four-roll calender. The fact that three-roll passes are required to produce a calendered sheet of acceptable surface quality is, of course, the underlying reason for this limitation since tracking on a two-roll calender generally is quite simple. In studying the calender bank flow of many polymeric materials, it has been consistently surprising how seemingly minor flow disturbances on the inlet side of a roll nip often cause very objectionable surface defects in the sheet emerging from the roll nip. This phenomenon, which undoubtedly stems from the elasti. memory typical of high polymer melts, is believed to be responsible for the redundancy required in conventional calendering. In other words, the flow history, melt temperature, etc. within a calendering bank is not sufficiently uniform to obtain a high quality sheet unless the process is repeated at least once, usually twice or sometimes even three times over.

It is, accordingly, the prime object of the present invention to provide method and apparatus for the calendering of polymeric materials in which material thickness, degradation and surface defect limitations are greatly minimized or eliminated.

Other objects and advantages of the present invention will be apparent from the following description and appended claims.

In accordance with the present invention, method and apparatus are provided for the calendering of polymeric materials wherein said materials are fed thru the nip

opening of a pair of counter-rotating calender rolls while maintaining a volumetric obstruction across the width and between said pair of calender rolls, with the most downstream projection of said obstruction being positioned so as to at least penetrate the bank of material formed between the pair of calender rolls upstream of the nip by the selection of calendering conditions, and while concurrently feeding a stream of polymeric material to said nip opening on each side of said volumetric obstruction.

The present invention provides a simple and effective solution to the above-mentioned and other problems inherent in the calendering process. The solution to this problem is effected by removing a substantial part of the stagnant flow zone by placing within this region of flow a volumetric obstruction, while at the same time introducing the polymeric fluid in the form of separate streams conforming to the active or progressive flow zone, i.e., one stream on each side of the obstruction. The flow obstruction substantially reduces the natural back flow in the calendering bank and thus makes it possible to reduce or eliminate the usual bank rotation with its associated problems of air entrapment, thermal degradation, sensitivity to surface defects, etc. In fact, the present invention makes it possible to calender film and sheeting of excellent surface quality on a two-roll calender or mill by direct feeding from an extruder using a suitably designed die. Also, the invention makes it possible to calender much heavier gauge sheeting of a variety of polymers on conventional calenders or mills by the use of a suitably arranged obstruction.

The invention is more fully explained by reference to the apparatus embodiment shown in FIGS. 5 and 6. As there shown, calender **10** is provided comprising a pair of counter-rotating rolls **12** and **14** and stripper roll **16**. Calender **10** is directly fed two molten polymer streams **18** and **20** from extrusion die **22**, which comprises die housing **24** and flow divider **26**. A stream of molten polymeric material **28** is forced from conventional extruder means (not shown) and enters extrusion die **22** thru inlet means **30**. The polymeric material then passes thru passage **32** to internal die manifold **34**, having two manifold branches **34***a* and **34***b*.

Along the manifold edge, the molten polymeric material stream is separated into two streams by flow divider **26** which, in its most forward projection **36**, also serves as solid volumetric obstruction. Because the forward projection of the flow divider (volumetric obstruction) preferably occupies a substantial portion of the back-flow region (stagnant flow zone), smooth, gently curved bank surfaces **18***a* and **20***a* are formed between the die lips and the roll surfaces, as shown in FIG. 7 of the drawings.

It has been found that the forward projection of the flow divider (volumetric obstruction) does not have to conform closely to the particular stagnation surface resulting from a particular roll diameter and nip opening. Actually, it is preferable that the front end of the flow divider is considerably more blunt than the theoretical stagnation surface and that it stops somewhat short of the stagnation point. The reason for this is that the hydrostatic pressure in the roll nip is low in the outer region of the bank, whereas it increases steeply near the maximum pressure point (FIG. 1, $x=-x_e$). Consequently, if the front end of the flow divider (volumetric obsrtuction) protrudes only moderately into the bank, some misalignment of the die can be tolerated.

Furthermore, a blunt front end is more tolerant of operation with variable relative roll speeds which, as previously mentioned, changes the shape of the stagnation surface and thus the optimum position of the volumetric obstruction. On the other hand, if the front end of the flow divider is sharp and protrudes far into the roll nip, then the alignment of the die, i.e., volumetric obstruction, must be very accurate in order to avoid undesirable deflections and flow disturbances.

~~of temperature, pressure, viscosity etc~~ The basic assumptions made in development of the mathematical flow model are:

- The fiber bundle behaves as a nonlinear elastic porous media
- The aligned fiber bundle has transversely isotropic permeability
- The resin behaves as a Newtonian fluid during impregnation.

The viscous resin flow through a porous media can be described by Darcy's Law which states that the flow rate per unit area, q, is directly proportional to the pressure gradient as described by equation (1).

$$q = \frac{-S}{\mu}\frac{dp}{dx} \tag{1}$$

In this equation S is the permeability of the fiber bundle and μ is the Newtonian viscosity. The permeability, S, can be described by the Carman-Kozeny equation. For this case the equation shows the fiber volume fraction (V_f) dependence of the permeability.

$$S = \frac{r_f^2}{4k}\frac{\left(1-V_f\right)^3}{V_f^2} \tag{2}$$

Here r_f is the radius of the filament and k is the Kozeny Constant which describes the geometry of the porous media in the direction of flow. From this equation it can be seen that as the fiber volume in the impregnation zone increases the permeability, S, decreases. We have assumed that the fiber bundle acts as a non-linear elastic media, and as such, Vf is a function of the applied pressure (or stress on the fibers). The deformation behavior of the fiber bundle has been modelled by assuming that the fibers behave as bending beams between multiple contact points as shown in Figure 16. From this the following stiffness equation can be derived:

$$\sigma = \frac{3\pi E}{\beta^4}\frac{\left(\sqrt{\frac{V_f}{V_o}}-1\right)}{\left(\sqrt{\frac{V_a}{V_f}}-1\right)^4} = \Delta P \tag{3}$$

where:

ΔP = applied pressure
E = fiber bending stiffness
β = state of the bundle as described in Figure 16
V_o = initial fiber volume fraction
V_a = Maximum possible fiber volume fraction

Plotting the fiber volume as a function of the applied pressure as described by equation 3 we obtain the curve shown in Figure 17.

Substitution into Darcy's law (equation 1) to account for pressure gradients in the fiber bundle during impregnation and integrating to x = h allows us to determine the time required to impregnate the bundle:

$$t = \frac{\mu \left(1 - V_f\right) h_o^2}{2 \Delta p \, S_{zz}} \tag{4}$$

Note that the application of a large pressure gradient is not necessarily the way to speed impregnation since the applied pressure directly effects the permeability by increasing V_f. Applying the fiber deformation model to the permeability function results in a modified Carmen-Kozeny equation:

$$S_{zz} = \frac{r_f^2}{4 k_{zz}} \frac{\left(\sqrt{\frac{V_a'}{V_f}} - 1\right)^3}{\frac{V_a'}{V_f} + 1} \tag{5}$$

In equation (5) V_a' refers to the fiber volume fraction where the permeability of the bundle is effectively zero (i.e., the bundle is pressed closed). This is an important point because the fiber bundle is compressible therefore the permeability can go to zero before the volume fraction goes to 1. This point is not apparent in the unmodified Carmen-Kozeny equation (2).

Utilizing the rheology data presented in the previous section and substituting into equations 4 and 5, theoretical impregnation times can be calculated for the various conditions. Table 1 shows that impregnation times just over 1.5 min for LaRC TPI may be achievable. It is important to note that the times in Table 1 are only valid for the assumptions noted, and no account for the polymers shear stress relaxation has been made. It is also assumed that Beta=200 accurately describes the state of the bundle at the time of impregnation.

Holding all variables constant and changing only the viscosity of the resin, the time to impregnate would increase with increasing viscosity as shown in Figure 18. From this figure is appears that impregnation times less than 2 min are achievable with viscosities as high as 600 PaS.

Conclusions

The rheology and flow modeling results discussed above have numerous implications for thermoplastic melt impregnation of a towpreg. Importantly:

- Xydar LCP can be blended with LaRC-TPI to reduce the latter's shear viscosity by 80 percent; this reduction becomes larger at higher shear rates
- Based on processing and rheological studies with polypropylene, shear viscosities of 30 to 40 PaS (300 to 400 poise) or less are required for the polymer to penetrate the fiber bundle within 20 sec or less
- To reduce the LaRC-TPI shear viscosity to 40 PaS, at least 10 weight % Xydar LCP and 1000s^{-1} shear rates are needed
- LaRC-TPI and its blends with Xydar should be processed at high shear rates to reduce the residence time in the melt, thereby limiting the consequent increase in viscosity; melt temperatures of 350°C to 380°C should be used
- Shear stress relaxation times on the order of 1 sec at higher shear rates (greater than 10 s-1) limits the practicality of using high shear as the sole means of accomplishing high performance TP melt impregnation.

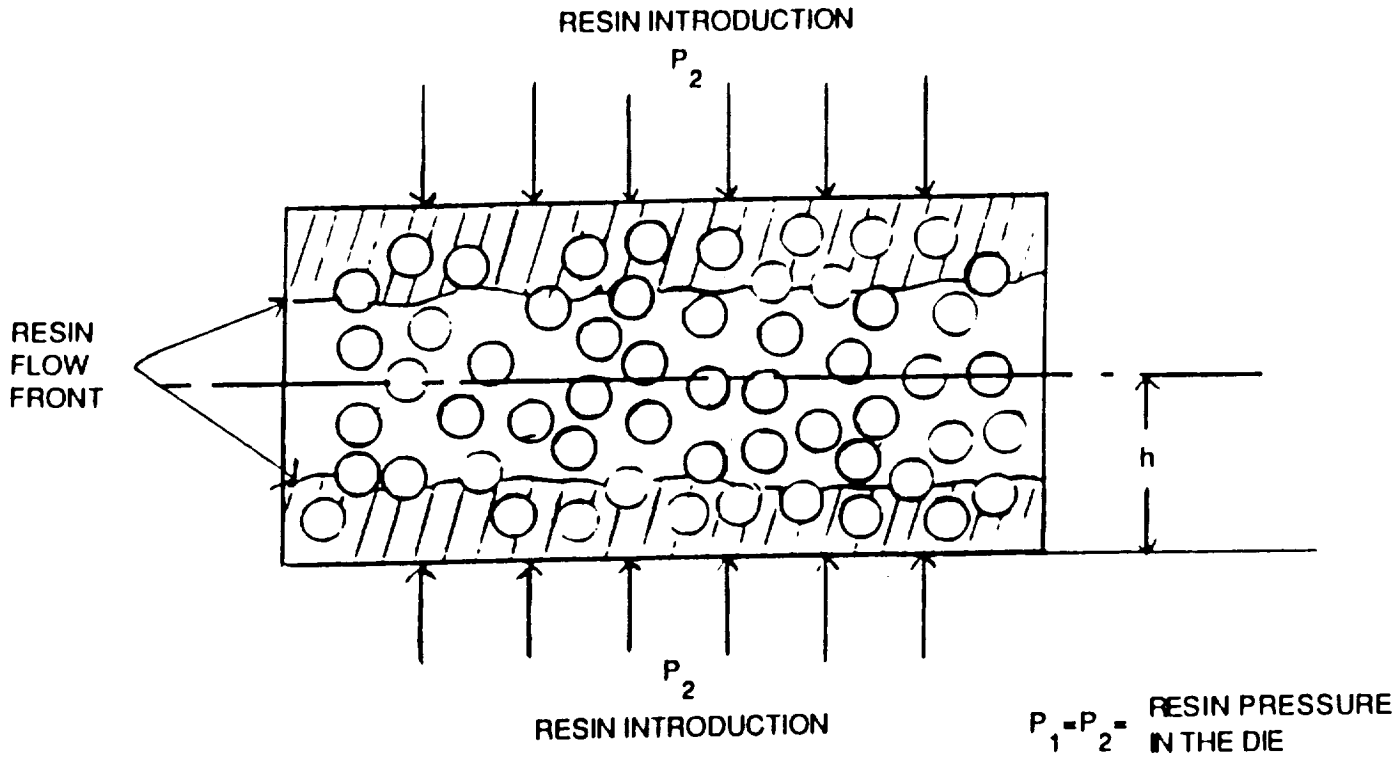

Figure 15. The Impregnation Model Adapted to the HSP Die

High Steam Prepregging

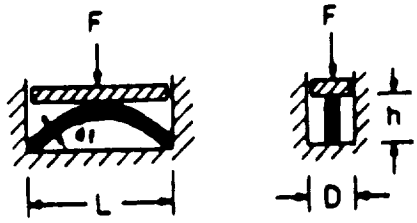

Geometry for a Unit Bending Cell Used to Derive the Stiffness of a Fiber Bundle. Note that the Parameter $\beta = \frac{L}{h-d_f}$.

Figure 16. Geometry for a Unit Bending Cell Used to Derive the Stiffness of a Fiber Bundle. Note that the Parameter $\beta = L/(h-d_f)$

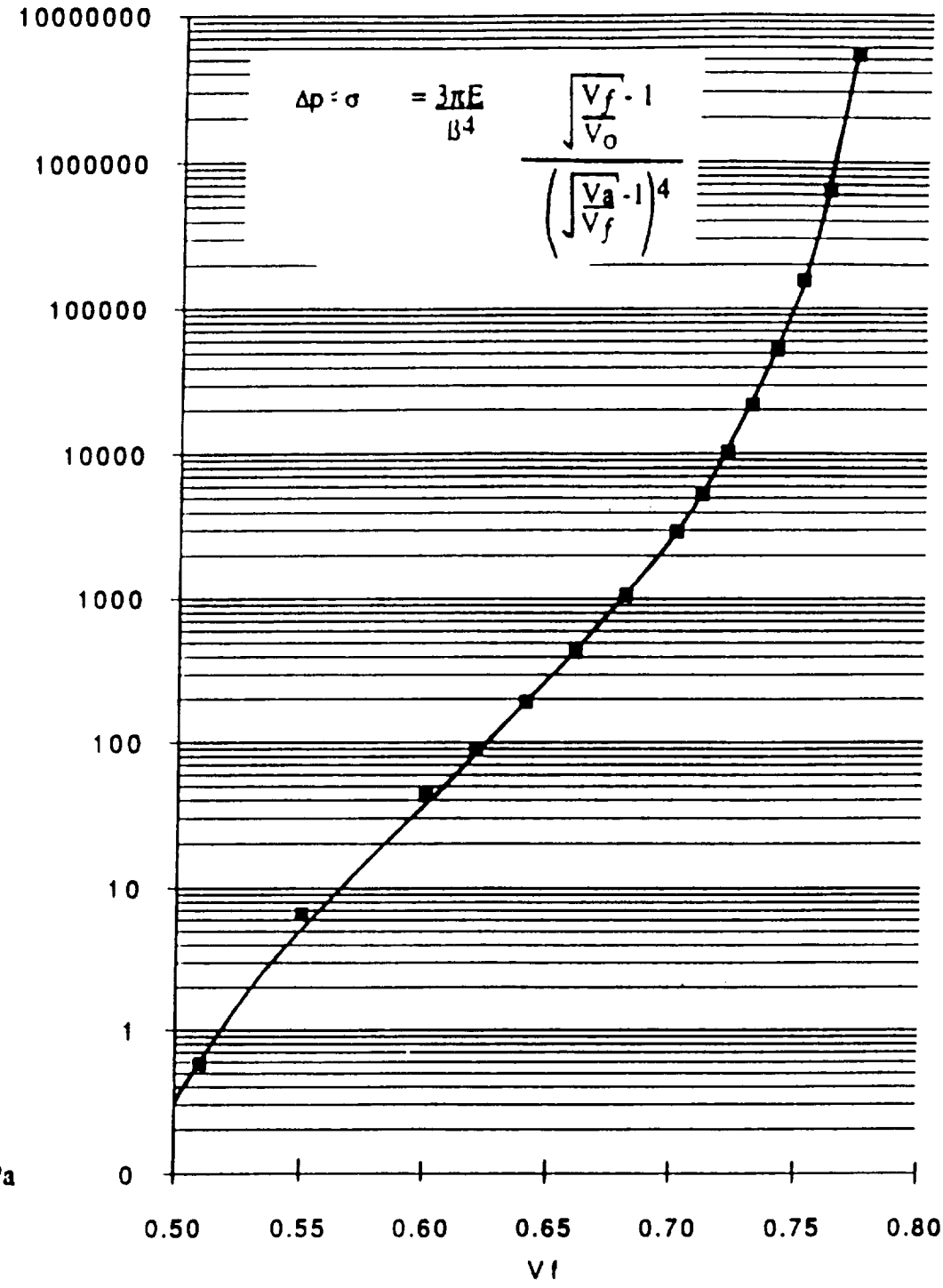

Note:

$E = 227(10^9)$ Pa

$V_a = 0.785$

$V_o = 0.5$

$\beta = 200 = \frac{L}{h - \delta_f}$

Figure 17. The Effect of Pressure on the Fiber Volume Fraction

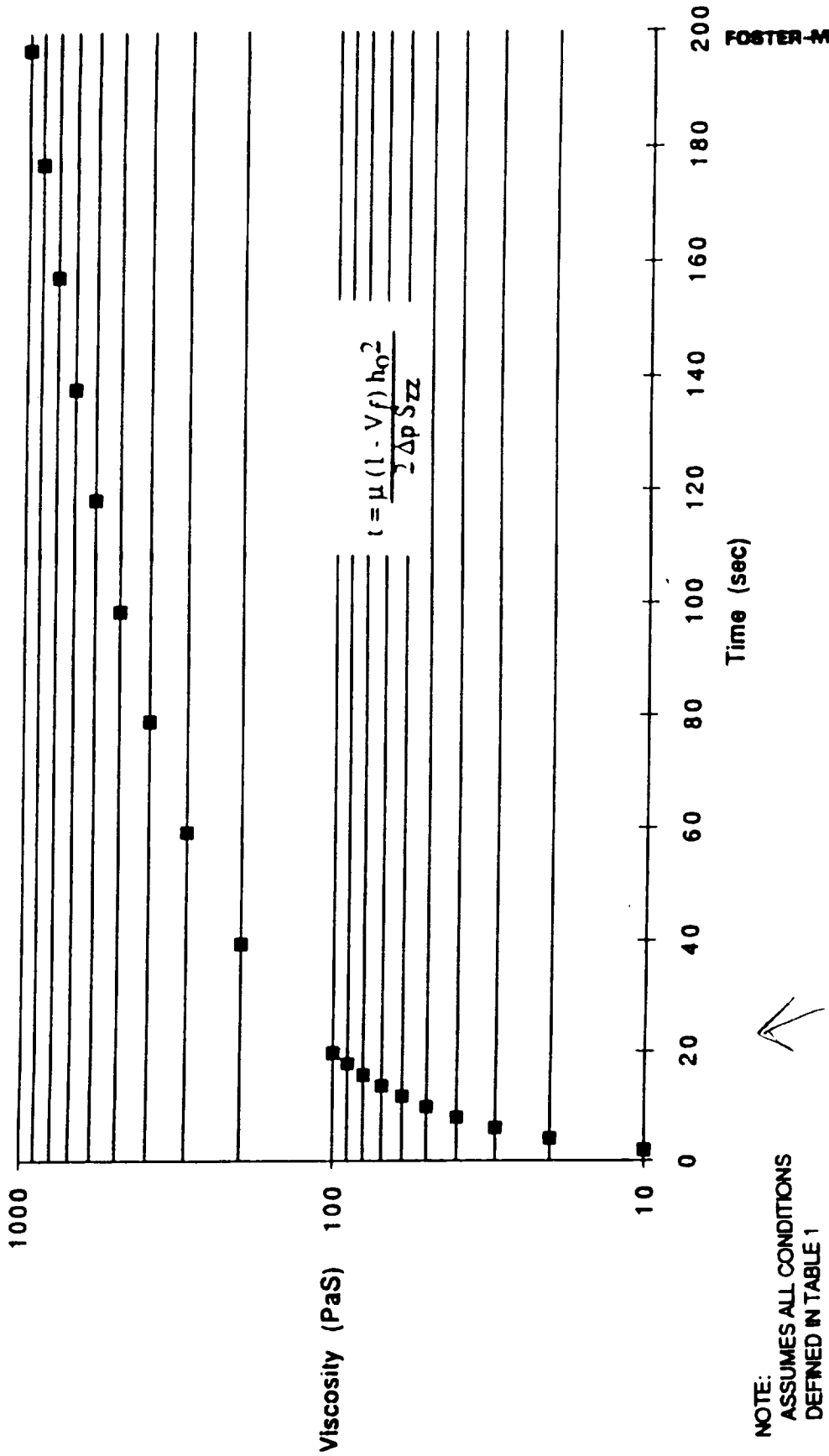

Figure 18. Increasing Viscosity Increases Time Required to Achieve Impregnation

...efore the viscosity of the molten PEEK 150P resin can be written as

$$\eta = 6.6 \times 10^{-9} \dot{\gamma}^{-0.0837} \exp\left(\frac{16260}{T}\right) \text{ Pa·s} \tag{21}$$

here $\dot{\gamma}$ is the shear rate in 1/sec and T is the absolute temperature. Figure 4 ows the comparison between the measured viscosity data and the viscosities lculated by Equation (21). For the impregnation process considered in this udy, the order of magnitude of the shear rate in the fiber bundle is about 10^{-1} = average resin velocity/fiber separation). The corresponding difference in vis-sity according to the power-law model from the Newtonian model is about)%, which shows that the non-Newtonian effect is important.

mpregnation Experiments

Experiments were performed to evaluate the validity of the model. In the ex-riments Toray T300 graphite fiber bundles were impregnated with PEEK 150P sin. Before the experiments the fiber bundles and PEEK 150P powder had been ied in a forced convection oven at 100°C for 30 minutes. Two fiber bundles ated in the above manner were placed in the cavity of a matched die mold. The old cavity was filled with PEEK 150P powder to make the fiber bundles sur-unded by the resin (Figure 5). Then the mold was placed in a hot press and ated to the test temperature without applying pressure. The mold was held at test temperature for approximately 10 minutes to reach the thermal equilib-im. Once the test temperature was reached, pressure was applied. After a pre-period of time the mold was removed from the hot press and cooled imme-ately to the room temperature. The specimen was removed from the mold, was t at right angle to the fibers, and the cross section of the impregnated fiber

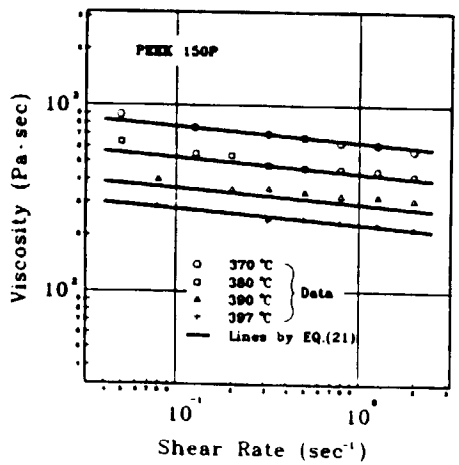

Figure 4. Comparison between measured and calculated viscosities.

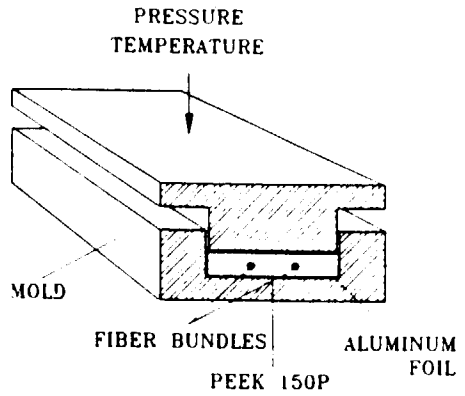

Figure 5. Schematic of the setup used in the impregnation experiments.

bundle was examined with an optical microscope. Typical micrographs thus obtained are shown in Figure 6. The number of impregnated fibers in a bundle was counted, and the degree of impregnation was estimated by the following expression

$$D_{imp} \equiv \frac{\text{Number of the Impregnated Fibers}}{\text{Total Number of the Fibers}} \tag{22}$$

This process was repeated for different durations of time (5, 10, 15, 20, 25, 30 minutes), different pressures (1, 2, 3, 4, 5, 6, 7, 8, 9, 10 atm), different temperatures (360, 365, 370, 375, 380, 385, 390, 395, 400°C), and different tow sizes (3, 6, 12 K). The data obtained are shown in Figures 7–10. The degree of impregnation was also calculated by the model [Equations (12)–(17) and Equations (19)–(20)] for the test conditions. The following values of the radius of the fiber bundle without applied pressure r_o and the fiber radius R were used [3]

$$r_o = 400 \ \mu\text{m for 6 K tow} \tag{23}$$

$$R = 3 \ \mu\text{m} \tag{24}$$

By fitting one data point (10 atm, 10 minutes, 370°C, 6 K tow) to Equation (17), the value of constant A in Equation (15) was obtained as

$$A = 6.91 \times 10^{-5} \text{ atm} \tag{25}$$

The comparison between the experimental data and the results of the calculations by the model are presented in Figures 7–10. Data obtained by Kim et al. [3] are also compared. As can be seen in the figures, good agreement was found between the model and the experimental data.

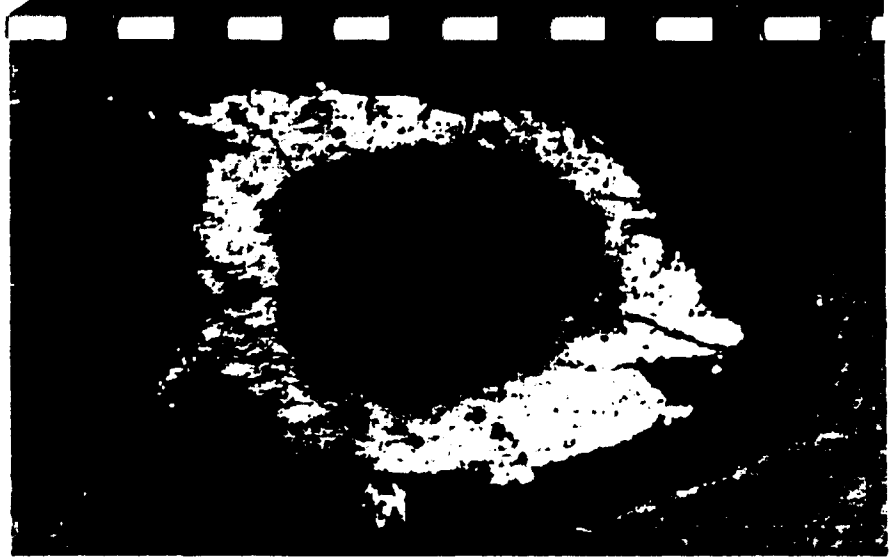

(a)

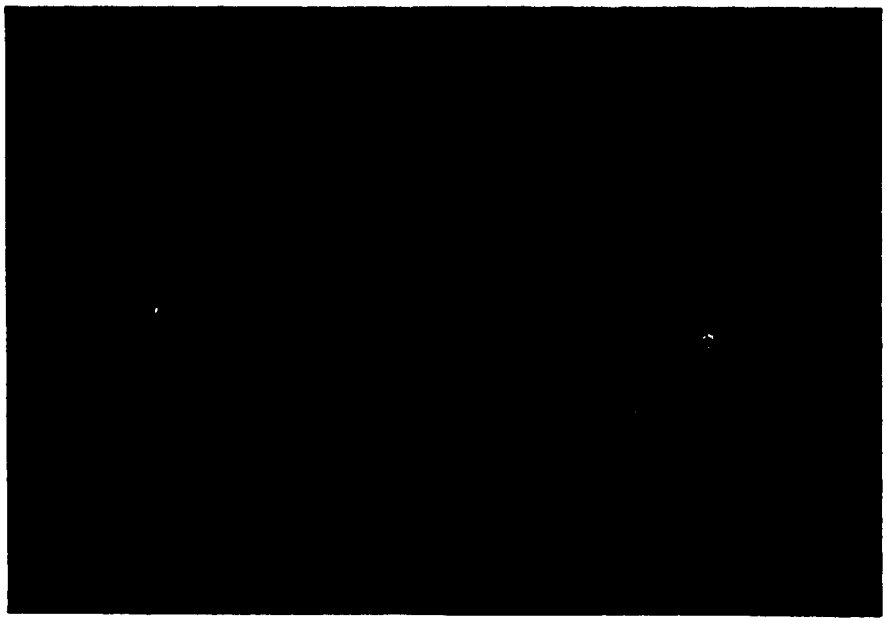

(b)

Figure 6. *Typical microphotographs of the cross sections of the impregnated fiber bundles: (a) P = 1 atm, T = 370°C, tow size = 6 K, t = 30 min (D_{mp} = 0.52); (b) P = 8 atm, T = 370°C, tow size = 6 K, t = 30 min (D_{mp} = 1.0); (c) P = 10 atm, T = 380°C, tow size = 6 K, t = 10 min (D_{mp} = 0.9); (d) P = 10 atm, T = 370°C, tow size = 12 K, t = 20 min (D_{mp} = 0.45).*

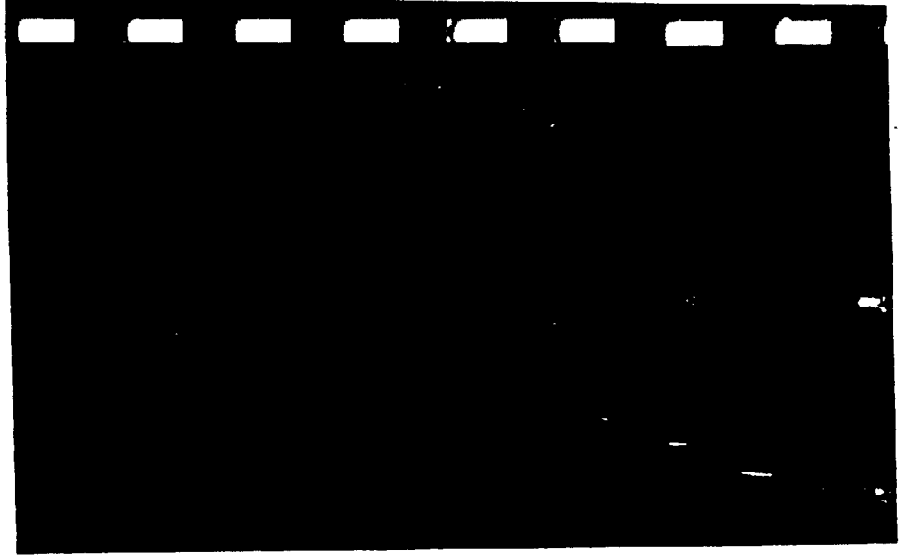

(c)

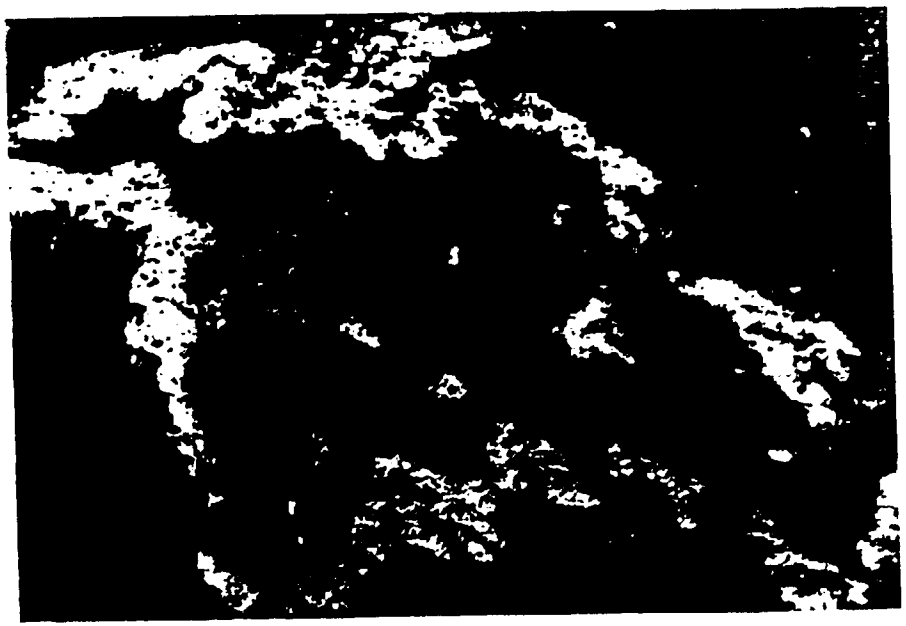

(d)

Figure 6 (continued). *Typical microphotographs of the cross sections of the impregnated fiber bundles: (a) P = 1 atm, T = 370°C, tow size = 6 K, t = 30 min (D_{mp} = 0.52); (b) P = 8 atm, T = 370°C, tow size = 6 K, t = 30 min (D_{mp} = 1.0); (c) P = 10 atm, T = 380°C, tow size = 6 K, t = 10 min (D_{mp} = 0.9); (d) P = 10 atm, T = 370°C, tow size = 12 K, t = 20 min (D_{mp} = 0.45).*

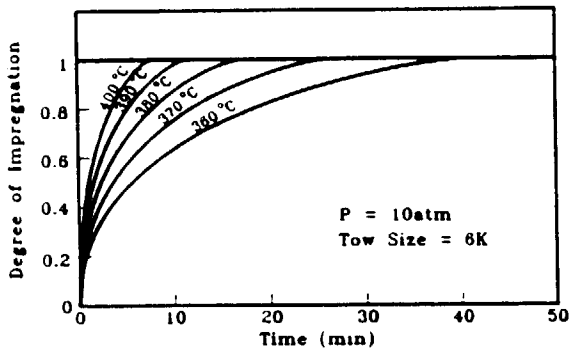

Figure 12. *Degree of impregnation as a function of time for different temperatures. Results calculated by model. P = 10 atm, tow size = 6 K.*

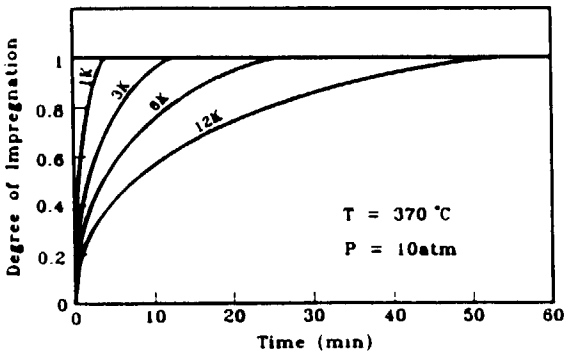

Figure 13. *Degree of impregnation as a function of time for different tow sizes. Results calculated by the model. P = 10 atm, T = 370°C.*

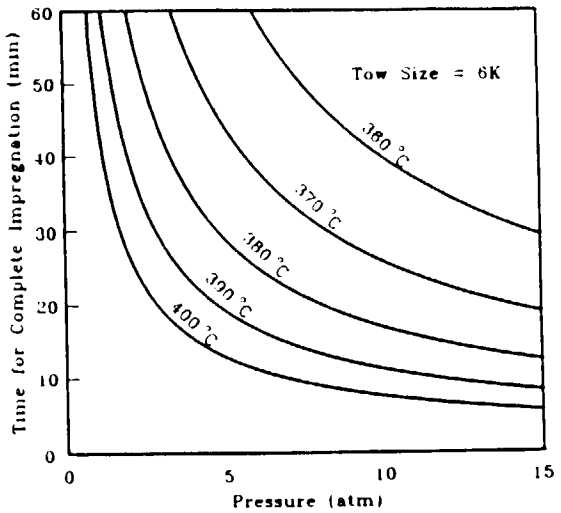

Figure 14. *Time for complete impregnation as a function of pressure for different temperatures. Results calculated by the model. Tow size = 6 K.*

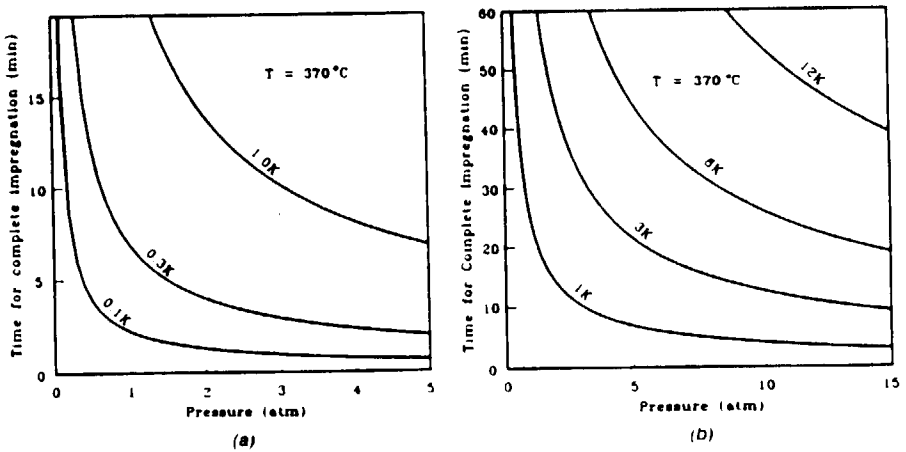

Figure 15. *Time for complete impregnation as a function of pressure for different tow sizes. Results calculated by the model. T = 370°C. (a) small tow sizes; (b) large tow sizes.*

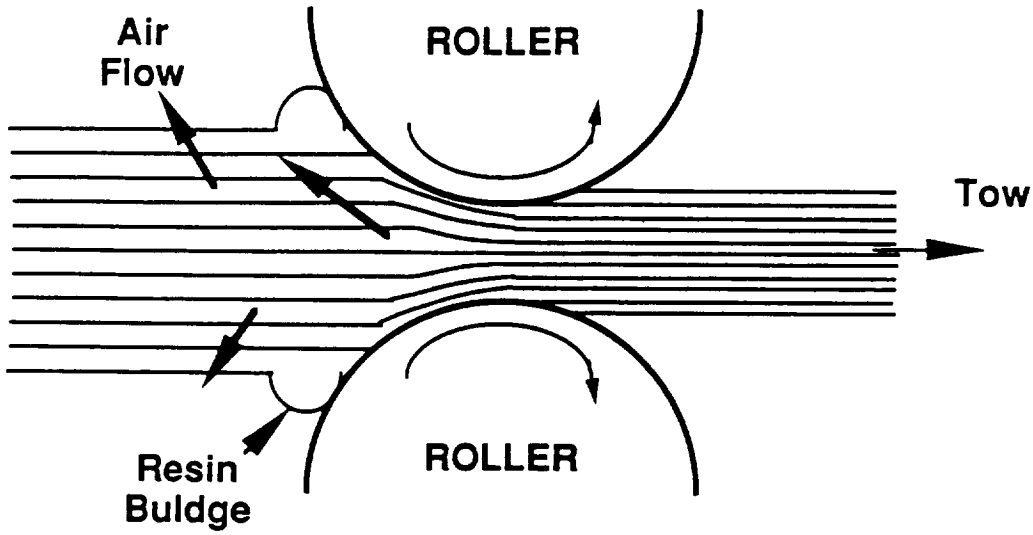

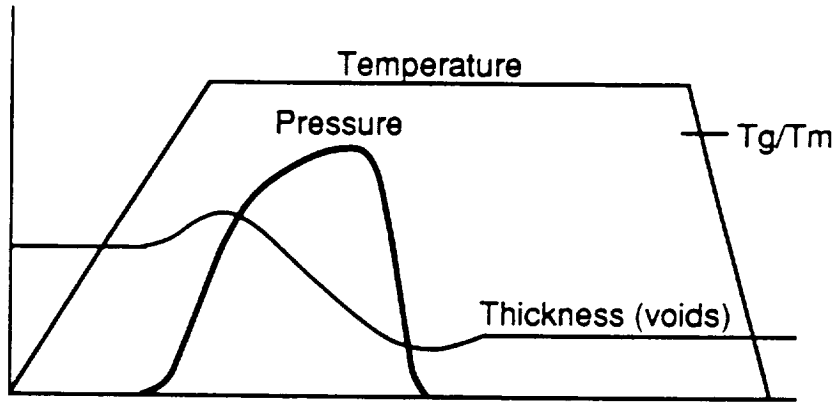

Preheated Tape and Hot Rollers

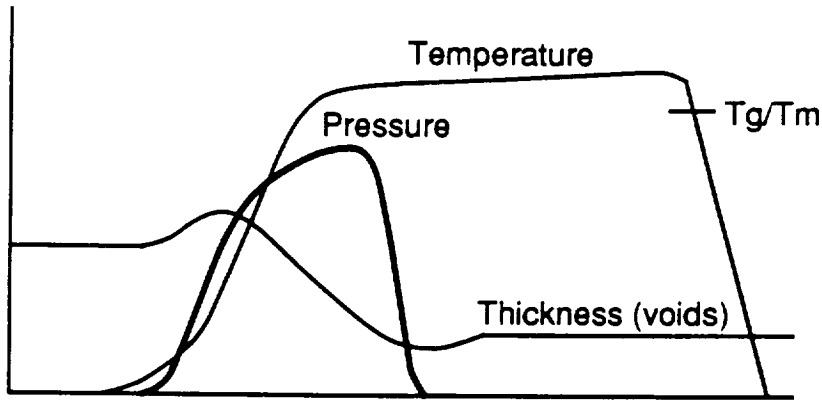

Cold Tape and Hot Rollers

NIP ROLLER CONSOLIDATION CYCLE

III. PULTRUSION

The computer model of pultrusion recently developed by Lee and Springer (7) describes the processing of thermoplastic matrix composites, and computes: the temperature, crystallinity, pressure, and consolidation inside the composite along the axis of the die; and, the required pulling force, see following pages. For APC-2 (carbon fibers melt impregnated with PEEK) prepreg tows, pulling forces range from 2,000 to 4,000 pounds at speeds of 2 to 5 inches per second.

In an experimental study of pultrusion, Astrom, Larson and Pipes (8) used APC-2 to determine the effect of pulling speed on the mechanical properties (compressive, flexural, and apparent interlaminar shear strength) of composites produced with a rectangular cross-section of 3.2 x 6.4 mm, see following pages. The ribbon was preheated and pulling rate ranged from 1 to 4 mm.sec. Mechanical properties were independent of pulling rate in that speed range.

Taylor and Thomas (9) studied the use of ultrasonics to aid pultrusion of thermoplastics. They made ribbon from a number of materials including BASF powdered towpreg of E75 carbon fiber with PEEK. The ribbon was 0.89 x 0.05 cm, for which they used six of the 12k PEEK powdered tows. At pulling rates of 1 to 2 m/sec the pultrusion ribbon contained less than 1 percent voids. Information about the die is not given, but if it were 0.5 m long, the pultrusion consolidation times were between 0.25 and 0.5 seconds.

In their discussion, Taylor and Thomas observe that "while ultrasonic activation of pultrusion dies has been shown to reduce die friction for thermoset pultrusion, the goal of the present work was to develop alternative methods to enhance consolidation rather than simply reduce friction ... since ultrasonic flow promotion is directly related to the power input to a power level determined by the specific resin, the ultrasonic power is generally not varied but maintained above the threshold for flow promotion and below the level leading to polymer degradation",see following pages.

Batch (10) analyzed temperature, cure, pressure, and pulling force for pultrusion in his PhD disseration. He developed mathematical models for (1) resin backflow, (2) thermal expansion, shrinkage, and compression of resin, and (3) the compaction of fibers. The pressure and

pulling force model was used to study the taper geometry at the die entrance. In his resin backflow model, Batch accounts for the difference between axial flow through rovings and through individual tows. The thermal analysis allows for thermoset polymerization and shrinkage with separation from the die wall in the release zone, see figure 10.12 in the following pages. His pulling force model includes bulk compaction traction, viscous traction, and frictional (fiber-wall) traction.

In his model of fiber deformation forces in composite processing, Batch draws on the work of Gutowski and of Gauvin and Chiboni to develop a "fiber contact" approach. Examination of experimental pulling force data indicate that viscous drag alone does not account for the measured forces. Friction between the moving fibers and the stationary die are the dominate component of the pulling force. Batch's model suggests that the greatest frictional resistance occurs after the resin gels (thermoset) at the wall and before it shrinks and separates from the die.

As part of their work on injection-pultrusion Kincaid, McCarthy and Fanucci (11) obtained pressure versus fiber volume in the absence of resin for several fiber orientations. The behavior of dry material is somewhat different from that of prepreg, see following pages. Stress relaxation times are about 10,000 seconds for random mat and 0/90 cloth and they are about 100,000 seconds for unidirectional straight rovings.

Fanucci, et. al. (12) developed a thin, disposable pressure sensor to monitor through the thickness consolidation forces during composite processing. Their data support Batch's predictions for thermosets, see fig 9 of the following pages, and indicates the importance of temperature in reducing consolidation pressure for thermoplastics, see fig 11 of the following pages.

provides the temperature, crystallinity and bonding inside the composite, and the required pulling force during pultrusion of fiber reinforced thermoplastic matrix composites.

2. PROBLEM STATEMENT

We consider the pultrusion process of thermoplastic matrix composites reinforced by unidirectional fibers (Figure 1). The composite (in the form of "prepreg" tows) is introduced into the die through a preheat oven. This oven is sufficiently long so that at its exit (and at the entrance of the die) the composite is at a uniform temperature T_o.

The die is a long, thin channel with a cross section symmetric with respect to the die's centerline. The die height H may vary with distance along the axis (i.e., along x) but is constant along the width. The die height is small compared to the width W and length L of the die ($H/L \ll 1$ and $H/W \ll 1$).

The specified die surface (wall) temperature T_w may vary along the die length but at each axial position is constant along the width. This, together with the geometric condition of $H/W \ll 1$, implies that variations in the properties need only be considered parallel and perpendicular to the die axis (x and z directions).

The composite is pulled through the die by a puller at a constant speed V. Between the exit of the die and the puller the composite is exposed to the ambient (which is at a temperature of T_a) and is cooled either by natural or by forced convection. The objective is to determine the following parameters as functions of position and time inside the

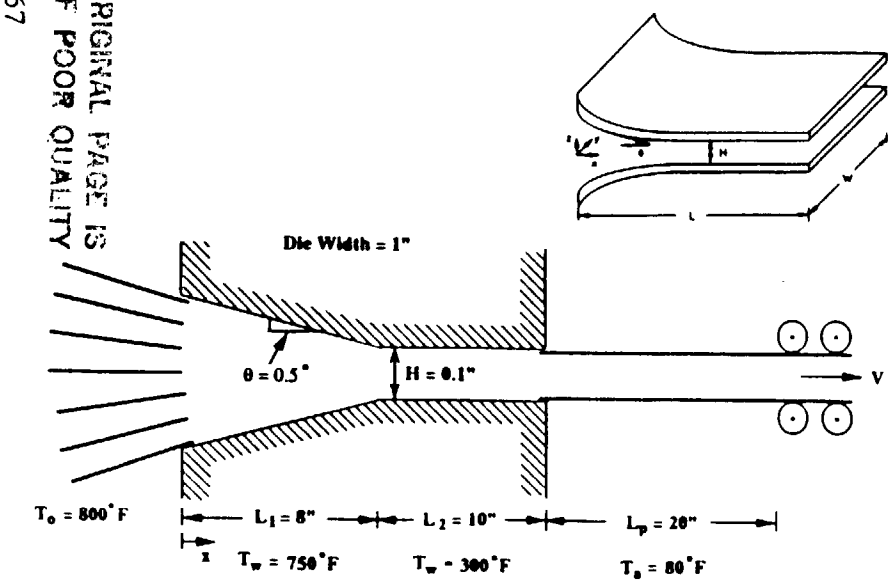

Figure 1. Description of the problem.

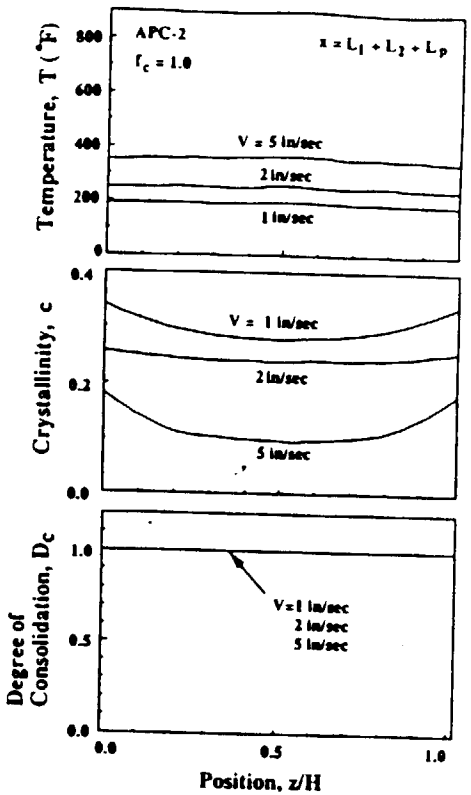

Figure 6. The temperature, the crystallinity and the degree of consolidation at the end of the puller. ($x = L_1 + L_2 + L_p$, Figure 1).

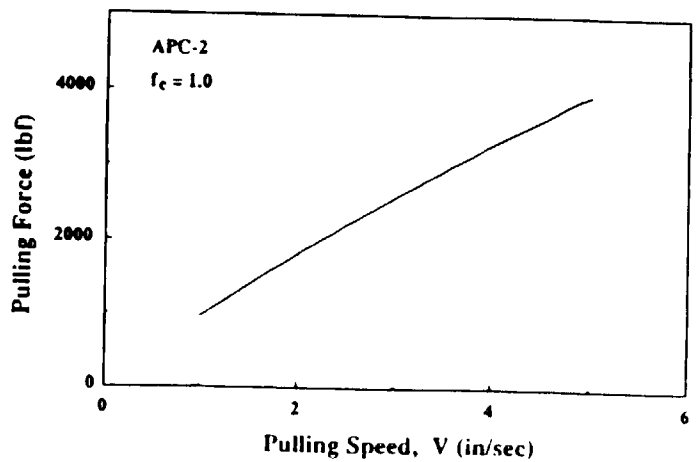

Figure 7. Pulling force versus pulling speed (see Figure 1).

3.4 Method of Solution Solutions to the submodels described above must be obtained by numerical means. A user-friendly computer code (designated as PULTR-PL) was written which can be used to perform the calculations. The type of information provided by this code is illustrated by the sample problem given in the next section.

4. SAMPLE PROBLEM

In this sample problem we consider the pultrusion of APC-2 prepreg tows. The material properties used in the calculations are summarized in Tables 1 and 2.

The temperature of the tows entering the die is 800°F. The die is made of two sections, a tapered section (exit height 0.1 inches for 20 consolidated plies of APC-2 prepreg) with a constant taper of $\theta = 0.5°$, and a 10 inch long straight section of height 0.1 inches (Figure 1). The width of the die is constant and is 10 inches. The die wall temperature is kept constant at each section. Along the tapered section the wall temperature is 750°F, and along the straight section the die wall temperature is 300°F. The ambient temperature outside of the die is $T_a = 80$°F. The distance between the die and the puller is 20 inches. The heat transfer coefficient between the die and the puller is $h_a = 10$ Btu/hr·ft^2·°F. It is assumed that no resin layer is present between the die wall and the composite.

The results are presented in Figures 4–7. In Figures 4–6 the temperature, the crystallinity, and the degree of consolidation are plotted across the composite for different pulling velocities. Figure 4 shows these results at the end of the tapered section, Figure 5 at the die exit, and Figure 6 at the puller. In Figure 7 the pulling force is plotted as a function of pulling speed.

The foregoing results show that the computer code is a useful tool for simulating the pultrusion process of thermoplastic composites. Thus the code can be used in designing pultrusion equipment.

Lee and Springer

Table 1
PROPERTIES OF APC-2 USED IN THE SAMPLE PROBLEM

Fiber	
Density	$\rho_f = 111.7$ lbm/ft^3
Specific heat	$C_f = 0.17$ Btu/lbm/°F
Thermal conductivity	$K_f = 15.0$ Btu/ft/hr/°F
Resin	
Density	$\rho_r = 78.8$ lbm/ft^3
Specific heat	$C_r = 0.32$ Btu/lbm/°F
Thermal conductivity	$K_r = 0.144$ Btu/ft/hr/°F
Initial thickness of one play	$S_o = 0.005$ in
Matrix mass fraction	$m_m = 0.31$
Rectangular element (Layer surface geometry)	
Original height	$a_o = 0.0007$ in
Original width	$b_o = 0.0022$ in
Original spacing	$w_o = 0.0022$ in

Viscosity-temperature relationship of composite

$$\mu_{mf} = 1.14 \times 10^{-12} \exp\left[\frac{26300}{T(°\mathrm{K})}\right] \quad \text{Pa} \bullet \text{sec}$$

Table 2
EQUATIONS AND CONSTANTS FOR CRYSTALLINITY OF APC-2

The relative crystallinity can be expressed as

$$\frac{dc_r}{dt} = -(1 - c_r)\frac{d\phi/dT}{(dT/dt)^{n-1}}$$

where T is the absolute temperature in degree Kelvin, and

$$\phi = \exp[-0.037T + 11.3]$$
$$n = 0.8$$

The relative crystallinity is related to the absolute crystallinity as

$$c_r = \frac{H_U}{H_T}\, c$$
$$\frac{H_T}{H_U} = -0.03 \ln\left(\frac{dT}{dt}\right) + 0.42$$

where dT/dt is in °C/min and $H_U = 130$ J/g.

for PPS and PEEK. Figure 1 shows that at a selected temperature, ultrasonic activation leads to greater flow than the nonultrasonic control. The data presented therein have been corrected to account for heating due to absorption of the ultrasonic energy and conversion to heat. While this work was with batch-type compression molding samples, it was felt that continuous processing such as pultrusion would be improved if the same flow promotion effect could be obtained. This would lead to complete consolidation at high pulling rates. While ultrasonic activation of pultrusion dies has been shown to reduce die friction for thermoset pultrusion [13], the goal of the present work was to develop alternative methods to enhance consolidation rather than simply reduce friction. Additionally, the ultrasonic application differs from traditional ultrasonic plastics welding in two important areas. First, the process does not rely on absorption of the ultrasonic energy to melt the resin and, second, it is designed to work on composite materials containing high fiber contents. Traditional ultrasonic welding techniques do not work well with high fiber-content thermoplastics since the fibers are good transmitters of ultrasonic vibrations. Hence, most of the vibratory energy is either transmitted straight through the laminate into the supporting structure or is transmitted and attenuated throughout the entire laminate rather than focused at the bond interface. The present process overcomes these problems and this paper reports on our preliminary studies of this novel pultrusion process.

2.0 EXPERIMENTAL

2.1 Pultrusion Procedure The developmental pultrusion line consists of the following individual components: a creel rack for feeding raw prepreg tape to the pultruder, the heated die section, the consolidation die section and optional cooling die section, and finally, the puller. All pultrusion tests were conducted by pulling prepreg tape through the dies at selected rates with the desired temperatures in the die sections. Temperatures were controlled with proportional controllers to ±10°F and consolidation die pressure was maintained by a pneumatic cylinder to ±5 psi.

2.2 Materials and Sample Analysis Raw materials for the pultrusion process are prepreg tapes. The following materials have been used in this work:

Taylor and Thomas

TABLE I

Raw Material Forms and Suppliers

Material	Supplier Mat'l ID	Form
AS4 carbon fiber/PEEK	ICI - APC-2	12" UD tape
AS4 carbon fiber/PPS	Phillips - AC40-60	8" UD tape
E-glass fiber/PPS	Phillips - AG40-70	8" UD tape
E-glass fiber/Nylon 12	BayComp - ATGA-300-052-65	1.16" UD tape
Carbon fiber/Nylon 12	BayComp - BTCA-127-030-45	0.50" UD tape
E75 carbon fiber/PEEK	BASF - Powder preform	6" UD fabric

from BASF

Pultruded samples were analyzed for fiber volume fraction and void content by ASTM 3171.

3.0 RESULTS AND DISCUSSION

This new pultrusion process is conducted very similar to other thermoplastic pultrusion in that the material is heated to a selected temperature, fed through an optional preforming die which starts to direct the fibers into the desired cross section shape without achieving significant consolidation, into the consolidation die which provides sufficient pressure to consolidate the material and finally through an optional cooling die. The primary difference in the new process is that ultrasonic energy is introduced into the material to induce resin flow. Then the resin temperature is generally at or just below the melting point as the material enters the consolidation die.

Hence, control of the process is derived from control of the heating die temperature and the pull rate which then controls the residence time in the heated zone. Since ultrasonic flow promotion is directly related to the power input up to a power level determined by the specific resin, the ultrasonic power is generally not varied but maintained above the threshold for flow promotion and below the level leading to polymer degradation.

An example of the effect of these variables on final pultruded product quality is shown by the data in Table II. Rods (0.635 cm dia.) were pultruded at constant ultrasonic power input but with varying heated die and consolidation die temperatures and pultrusion speed. Product quality, measured by void content, increases as residence time is increased by pulling at slower speed. Visually, the product also improves in appearance going from a milky, non-melted appearance to a glassy tan appearance

4) Pressures obtained in pultrusion by thermal expansion are usually enough to suppress void growth.

Finally, it will be assumed that the resin in the taper does not heat appreciably, and heat transfer can be neglected. The taper is usually less than an inch in length, so the taper residence time is less than 5 seconds for line speeds greater than 12 inches per minute. Moreover, heating in the taper is minimal because the front section of the die is often cooled to prevent heating the resin bath by resin backflow. This assumption decouples the heat transfer model of Chapter 8 from the flow model derived below. Also, the backflow model will use a constant resin viscosity. Beyond the taper, the effects of temperature on thermal expansion, shrinkage with cure, and viscosity will not be neglected.

Hence, the assumptions used in the flow model are:

1) Only aligned fiber rovings are present, and transverse flow is neglected. This reduces the flow problem to one dimension.

2) Flow occurs only in the taper section. After the taper, pressure changes with thermal expansion and shrinkage, but flow will be neglected.

3) Pressure from resin volatility will be neglected.

4) Heat transfer in the taper section is negligible, but will be considered after the taper section.

Two pressure models will be derived below: a backflow model which predicts pressure increase in the taper section only, and an expansion/shrinkage model which predicts pressure further inside the die in the absence of flow. These two modeling regimes are illustrated in Figure 10.3.

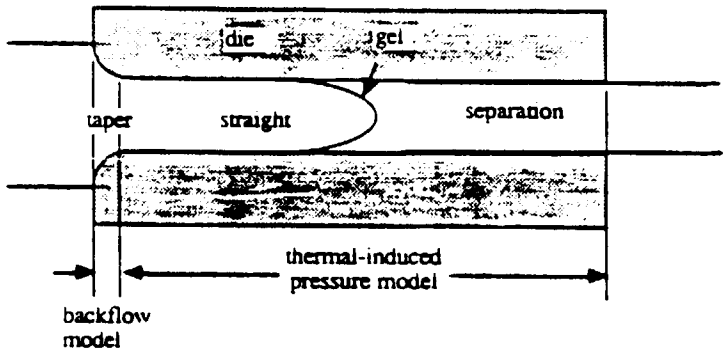

Figure 10.3. Illustration of typical die geometry, showing regions where the backflow pressure model and the thermally-induced pressure model apply.

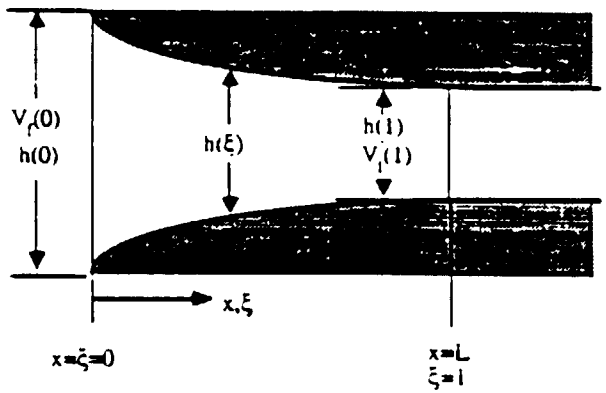

Figure 10.4. Geometry for backflow pressure model in the taper section of a die.

hence the former is considered negligible. The resistance from the die F_{tot} can be calculated from the surface traction S_s at distance x through the die.

$$F_{tot} = \int_0^{L_{die}} S_s(x)\, Z(x)\, dx \qquad (10.30)$$

where Z is the die perimeter, and total die length is L_{die}. Surface traction has three contributions: viscous drag before gel, bulk compressive forces at the die entrance, and friction.

$$S_s = S_{bulk} + S_{drag} + S_{fric} \qquad (10.31)$$

These tractions are shown schematically in Figure 10.12.

10.8.1. Bulk Compaction Traction

The bulk entrance force acts only at the die entrance and depends on resin pressure (calculated from the backflow model) and fiber elastic forces. Resin pressure P is isotropic and acts normal to the die surface. Fiber compaction force N is studied in the next chapter. For now, we will assume that N increases linearly with fiber volume fraction as fibers are squeezed into the die. N acts only perpendicular to the fibers, however, and the component of N normal to the die is N cos φ, where φ is the angle between the die surface tangent and the centerline ($\phi \geq 0$). The total traction at from bulk compaction is hence

$$S_{bulk}(x) = (P(x) + N(x) \cos \phi(x)) \sin \phi(x) \qquad (10.32)$$

where the factor sin φ accounts for the angle between the die surface and the direction of pull. Once beyond the die taper, the die walls are parallel ($\phi=0$), and Equation 10.32 predicts that bulk compaction forces are zero, as expected. For dies with round taper sections, such as the one in Sumerak's work, sin φ and cos φ are determined for $x<R_{taper}$ by trigonometry

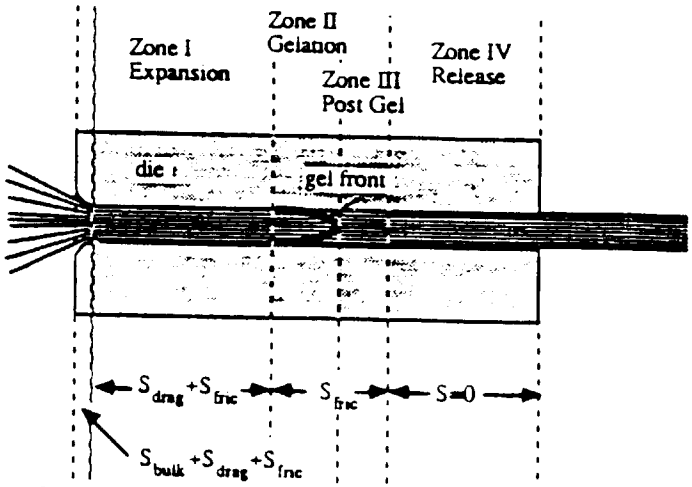

Figure 10.12. Zones in a pultrusion die (see Figure 10.1) and their corresponding surface tractions S in the pulling force analysis.

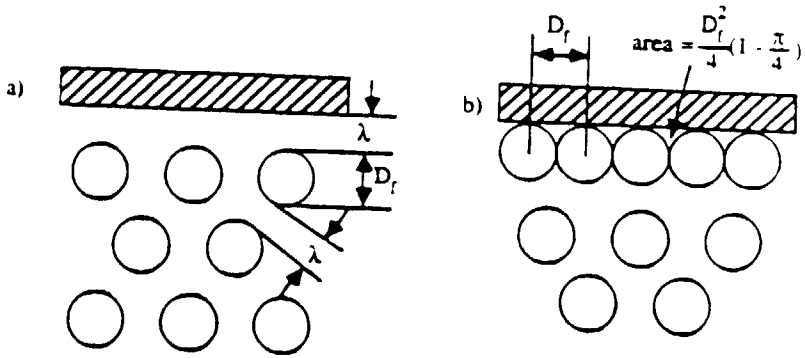

Figure 10.13. Two methods of determining the thickness of the resin layer between the moving fibers and stationary die wall: a) mean fiber spacing, b) direct fiber contact.

orce increases more rapidly, however, as fibers are compressed to higher volume actions. Ultimately, the fiber volume fraction will reach a limiting value V_{f_m} in which rther compaction is not possible without compressing the fibers themselves. This ter effect does not occur at pressures used for the processing of composites.

1.3.1. Assumptions

The model derived below will attempt to explain some of the fundamental fferences in the compression of random fiber mats and aligned fiber rovings. The sumptions of the model are as follows:

1) Stiffness of the fiber bed is assumed to increase proportionality to the concentration of fiber-fiber contacts. Fiber mats and rovings contain very many filaments of diameter 10-20μm. Unless these filaments are carefully aligned, voids will form where they cross. These voids give the fiber reinforcements their elasticity, and compression will close these voids by bending fibers around each other. As the fibers bend, they will contact each other at new locations. Hence further bending is more difficult because the applied pressure is distributed over an increasing number of contact points.

2) A single fiber interaction is assumed to represent of all fiber interactions during compression. Many fiber interactions occur in a fiber reinforcement (van Wyk (1946) calculated 10^7 fiber-to-fiber contacts per gram of wool); too many to be modeled separately. As shown in the schematic in Figure 11.4, fibers can have two-way interactions, three-way interaction, cross at a variety of angles, and can be both normal and parallel to the mold surface. Such a complex network is difficult to model. The simplified model using a single fiber is intended not to represent the shape of actual fibers in the fiber bed, but it is designed to contain the essential

physics of fiber-fiber interaction.

3) Friction between fibers are assumed negligible. The model derived below assumes that fibers are in equilibrium with surrounding fibers, hence sliding friction between fibers are neglected. Friction is responsible for the "memory" of fiber beds to retain deformed shapes. Friction would, for example, cause a fiber bed not to return to its original height after removing a load. Friction also would cause fiber deformation force to depend on the rate of deformation. A study of friction on fiber deformation is beyond the scope of this work.

Using these assumptions, the model for fiber deformation forces is derived below.

11.3.2. Fiber Deformation Cell

Initially, crossed fibers are shown in Figure 11.5, where the transverse distance between fibers is "c" and the distance between fiber contacts is L. The fiber is confined to the cell of length L and height c+d+e, where "d" is the fiber diameter, and "e" is an impenetrable portion during compression (not shown in Figure 11.5). The changes of fiber shape during deformation is shown in Figure 11.6. Initially, the fiber cell is shown in Figure 11.6a. As compression begins (Figure 11.6b), the fiber bends under the normal force N, decreasing the height of the cell by distance δ. In this mode of deformation, δ is proportional to N. Fiber motion along its axis will be neglected. When the deformation causes the fiber to touch the bottom of the cell (Figure 11.6c), force is now distributed to three points of contact. Further deformation now becomes more difficult as the fiber spreads a distance m along the symmetry line (Figure 11.6d). The ultimate compression at $V_f=V_{f_m}$ occurs when the ultimate contact length m_m is reached (Figure 11.6e).

As apparent from this simple illustration, fiber compaction has two regimes.

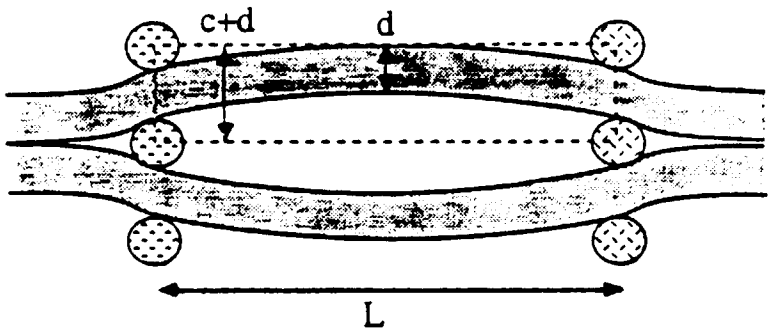

Figure 11.5. Schematic of fiber deformation cell used in the compaction model.

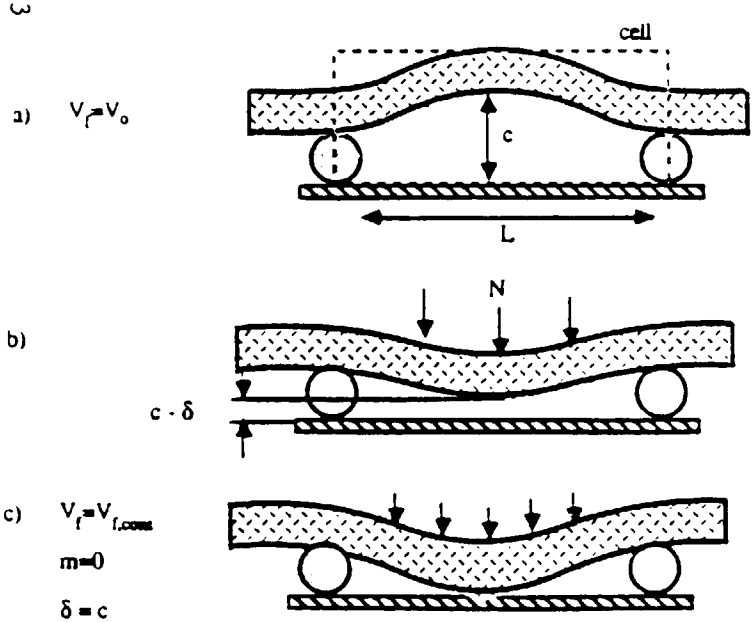

Figure 11.6. Steps in fiber deformation model. a-c: Hookean regime, d-e: nonHookean regime.

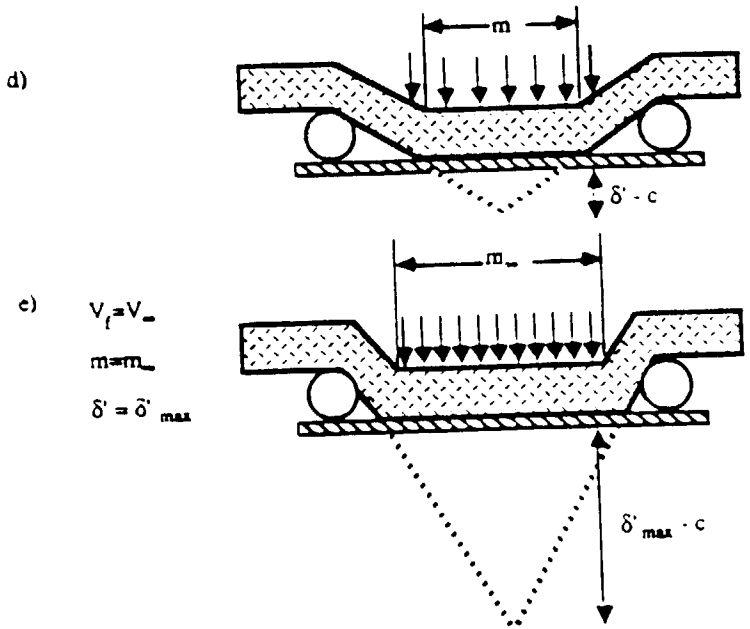

Figure 11.6. d-e: nonHookean regime (continued).

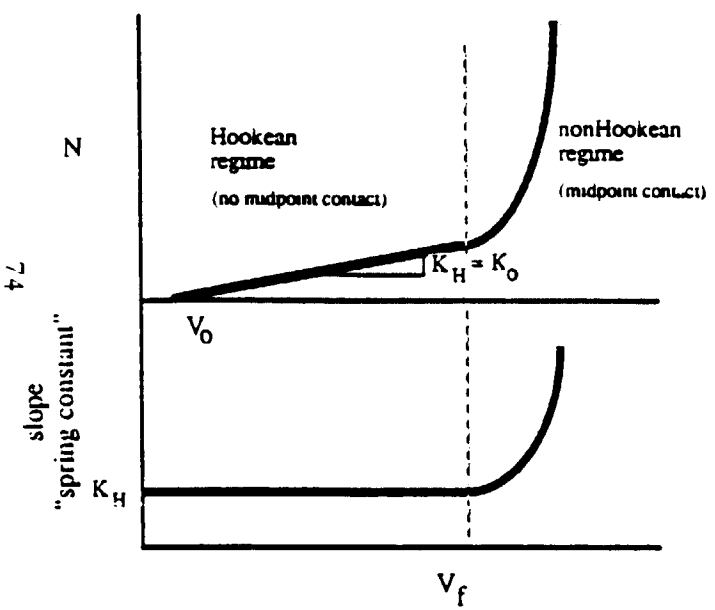

Figure 11.7. Illustration of two fiber contact regimes in model.

Hookean and nonHookean (Figure 11.7), the difference between them being the amount of fiber-to-fiber contact. The Hookean regime occurs at low volume fractions, where compression obeys Hooke's law.

$$N = K_H(V_f - V_o) \tag{11.6}$$

At higher volume fractions, the fiber spring "constant" K_{NH} increases due to increased fiber-to-fiber contact.

$$N = K_{NH}(V_f)\ (V_f - V_o) \tag{11.7}$$

Equations for the Hookean and nonHookean regimes are derived separately below.

11.3.3. Hookean Regime

The deformation model uses the strength of materials solution (Gutowski, 1985) for deformation of a beam supported a distance L apart

$$F = N A = \frac{E I}{\alpha L^3}\delta \tag{11.8}$$

where E is Young's modulus, I is the fiber cross section moment of inertia ($= \pi d^4/64$), and α is 1/192 when the ends are free to move only longitudinally. The area A normal to the compaction force is proportional to the fiber cross sectional area, d L,

$$A = d L / A_f \tag{11.9}$$

where the area fraction of fibers, A_f, is assumed to be equal to V_f. Substituting Equation 11.9 and the definitions of α and I into Equation 11.8, we find that compaction pressure is proportional to the reduced fiber deformation, δ/d.

$$N = \frac{3\pi d^4 E V_f}{L^4}\frac{\delta}{d} \tag{11.10}$$

Approximating V_f, V_o, and V_{max} from the height of the cells in Figures 11.6b, 6a, and 6c, respectively,

$$V_o = \frac{d}{c+d+e} \tag{11.11}$$

$$V_f = \frac{d}{c+d+e-\delta} \tag{11.12}$$

$$V_\infty = \frac{d}{d+e} \tag{11.13}$$

we can find the reduced fiber deformation, δ/d,

$$\frac{\delta}{d} = \frac{1}{V_o} - \frac{1}{V_f} \tag{11.14}$$

and the initial transverse fiber distance c,

$$\frac{c}{d} = \frac{1}{V_o} - \frac{1}{V_\infty} \tag{11.15}$$

Note from Equations 11.14 and 11.15 that δ approaches c as V_f approaches V_∞. Substitution of Equation 11.14 into Equation 11.10 gives the Hookean model for fiber deformation.

$$N = K_o (V_f - V_o) \tag{11.16}$$

where

$$K_o = \frac{3\pi E}{(L/d)^4 V_o} \tag{11.17}$$

A comparison of Equations 11.16 and 6 shows that K_H and K_o are equivalent, and a plot of compaction pressure N versus fiber volume fraction in the Hookean regime (i.e. Figure 11.7) will have slope K_o and x-intercept V_o. The definition of K_o in Equation 11.17 is the same as the definition of A_G in Equation 11.3 by Gutowski. The functional dependence on V_f for the two models, however, is different.

Equation 11.16 is valid if the nonHookean regime is not reached during compression. It is not accurate, however, for compression up to high fiber volume

fractions. The derivation below is for the nonHookean regime of compaction.

11.3.4. NonHookean Regime

Once fibers bend to touch each other at the midpoint (as in Figure 11.6c), the resistance to deformation increases. The spring constant K_{NH} diverges to infinity as the contact length m approaches m_∞. One simple expression to describe this dependence is

$$K_{NH} = \frac{K_H}{1 - m/m_\infty} \tag{11.18}$$

where K_{NH} approaches infinity as m approaches m_∞. Substitution of Equation 11.18 into Equation 11.7 will give the compaction pressure in the nonHookean regime, but first we need to find how m/m_∞ depends on V_f.

Assuming that the fibers deform linearly (Figure 11.6d), extrapolation of the two linear portions defines a new deformation, δ', which changes with m. By triangular similarity in Figure 11.6d, we can find m and m_∞ from δ' and δ'_{max}, respectively.

$$\frac{m}{L} = \frac{\delta' - c}{\delta'} = 1 - \frac{c}{\delta'} \tag{11.19}$$

$$\frac{m_\infty}{L} = 1 - \frac{c}{\delta'_{max}} \tag{11.20}$$

Dividing Equation 11.19 by Equation 11.20, we have

$$\frac{m}{m_\infty} = \frac{1 - c/\delta'}{1 - c/\delta'_{max}} \tag{11.21}$$

where c/δ'_{max} is a constant ($0 \le c/\delta'_{max} \le 1$). To find c/δ', we transform the deformation fraction δ/c from the Hookean model ($0 < \delta/c < 1$) into the deformation fraction δ'/δ'_{max}

in the nonHookean model ($0<\delta'/\delta'_{max}<1$).

$$\frac{\delta}{c} = \frac{\delta'}{\delta'_{max}} \tag{11.22}$$

Substituting δ of Equation 11.22 into Equation 11.14 and dividing by Equation 11.15 gives δ'/c.

$$\frac{\delta'}{c} = \frac{\frac{1}{V_o} - \frac{1}{V_f}}{\frac{1}{V_o} - \frac{1}{V_\infty}} \left[\frac{\delta'_{max}}{c} \right] \tag{11.23}$$

Note in Equation 11.23 that δ' approaches δ'_{max} as V_f approaches V_∞. Insertion of Equation 11.23 into Equation 11.21 gives the needed expression for m/m_∞ with three parameters: V_o, V_∞ and η ($\equiv c/\delta'_{max}$).

$$\frac{m}{m_\infty} = \frac{1 - \left[\frac{1/V_o - 1/V_\infty}{1/V_o - 1/V_f} \right] \eta}{1 - \eta} \tag{11.24}$$

where $0 < \eta < 1$.

Substitution of Equation 11.18 into Equation 11.7 and recalling that K_H and K_o are equivalent will complete the model for compaction.

$$N = \frac{K_o}{(1 - m/m_\infty)} (V_f - V_o) \tag{11.25}$$

where m/m_∞ is given in Equation 11.24. When $1/V_o - 1/V_f$ is small, Equation 11.24 gives $m/m_\infty<0$, which indicates that the midpoint fiber contact has not yet been attained, and thus deformation is in the Hookean regime. The new "fiber contact" deformation model is summarized by the expression

$$N = K(V_f)(V_f - V_o) \tag{11.26}$$

where

$$K = K_o \text{ for } V_f < V_{f,cont} \text{ (Hookean regime)} \tag{11.27}$$

$$K = K_o \frac{1-\eta}{\eta} \frac{1/V_o - 1/V_f}{1/V_f - 1/V_\infty} \text{ for } V_f \geq V_{f,cont} \text{ (nonHookean regime)} \tag{11.28}$$

and the transition from Hookean to nonHookean regimes occurs at volume fraction $V_{f,cont}$, determined by Equation 11.24 when $m/m_\infty=0$.

$$V_{f,cont} = \left[1/V_o - \eta (1/V_o - 1/V_\infty) \right]^{-1} \tag{11.29}$$

In summary, a "fiber contact" model has now been derived for the compression of fibers in both Hookean and nonHookean regimes. Since the model is mechanistic, the resulting parameters have physical meaning, and significance of these parameters will be discussed below. Finally, the model will be compared to experimental data for random fiber mats and aligned fiber prepreg to examine the effect of fiber form on compaction forces.

11.4. Interpretation of Model Parameters

The parameters η, K_o, V_o, and V_∞ are all related to the fiber structure and properties. Several of these parameters, in fact, are related to each other. The purpose of this section is to examine the physical interpretation of these parameters and their relation to each other.

An important parameter in the model is η, the fiber packing inefficiency, which measures the unattainable volume fraction during compaction. Unattainable volume is always present because fibers cannot exactly conform around each other. Some volume is "lost" whenever fibers cross. Thus, aligned fibers with fewer fiber crossings should have smaller η than random fiber mats.

The inefficiency η is important because it is inversely related to both V_o and

. Once these parameters can be expressed as a general function of η, they will no ger be independent and the compression model will have only two parameters, η . K_o. First, the packing inefficiency can be assumed to be proportional to the ıttainable volume fraction e/d. From Equation 11.13, η is inversely proportional to

$$\eta = \chi_1 \frac{c}{d} = \chi_1 \left[\frac{1}{V_\infty} - 1 \right] \tag{11.30}$$

ere χ_1 is a constant of order unity. Equation 11.30 is inverted to find V_∞ in terms of

$$V_\infty = \frac{1}{\eta/\chi_1 + 1} \tag{11.31}$$

e mitial void volume in the fibers c/d is related to the amount of kink in the fibers, ıich is also assumed proportional to η. Using Equation 11.11 and 11.30, we have

$$\eta = \chi_o \frac{c}{d} = \chi_o \left[\frac{1}{V_o} - \frac{1}{V_\infty} \right] \tag{11.32}$$

ıere χ_o is of order 10. Substituting Equation 11.31 into Equation 11.32 and solving r V_o, we have an expression for V_o in terms of η.

$$V_o = \frac{1}{\eta \left[\frac{1}{\chi_o} + \frac{1}{\chi_1} \right] + 1} \tag{11.33}$$

Once the constants χ_o and χ_1 are known, Equations 11.29, 11.31, and 11.33 n be used to generalize compaction behavior for a variety of fiber orientations. Using , of 10 and χ_1 of unity, the values of V_o, $V_{f,cont}$, and V_∞ are plotted as a function of in Figure 11.8. For aligned fibers, V_o and V_∞ are large, and deformation is also most entirely in the nonHookean regime since $V_{f,cont}$ is close to V_o. Hence, the ookean model would be of little use for rovings or aligned prepreg fibers, where η is ose to zero. For random fibers, V_o and V_∞ are smaller because more of more voids :tween the fibers and inefficient packing. The deformation is almost entirely in the

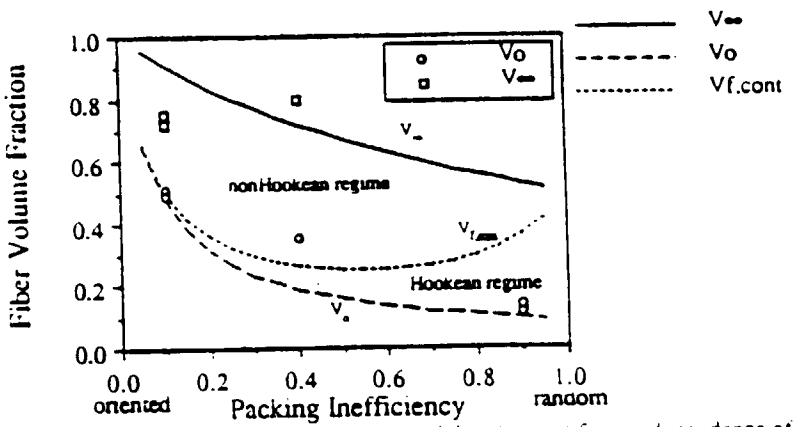

Figure 11.8. Model predictions (lines) and data (points) for the dependence of V_∞, V_o, and $V_{f,cont}$ on packing inefficiency of fiber reinforcements.

Hookean regime, except at high volume fractions when V_∞ is approached.

Figure 11.9 compares the compaction force of random and aligned fiber reinforcements. The compaction behavior of aligned fibers is nonlinear with higher initial and ultimate volume fractions than the more random type of fibers. As fiber randomness increases, the predictions become more linear in volume fraction until V_∞ is approached, then pressure increases rapidly. The transition between Hookean and nonHookean regimes sharpens as η increases.

In addition to affecting the shape of the compaction behavior, the packing inefficiency also affects the magnitude of pressure rise. As shown in Figure 11.9, N generally is greater for random fibers than aligned fibers at the same fiber volume fraction. Qualitative differences in parameters for random and aligned fibers are also shown in Figure 11.9.

The Hookean spring constant K_o is related to the mean dimensionless distance between fiber crossings, L/d, using Equation 11.17. As fibers become more randomly oriented (η increases), L/d is expected to decrease, K_o increases, and the fibers become harder to compact. L/d is difficult to measure, however, but it can be inferred from K_o if the Young's modulus of the fibers and initial volume fraction are known.

$$\frac{L}{d} = \left[\frac{3\pi E}{K_o V_o}\right]^{1/4} \qquad (11.34)$$

This expression will be used below to determine an effective L/d from experimental values of K_o.

In summary, the deformation of mats is expected from the model to be different than that of rovings in two regards: the slope (spring constant) of the Hookean regime is larger for mats because the fiber contact distance L is smaller, and 2) random mats have are more Hookean than for aligned fibers. These results agree qualitatively with

parameter	random fibers	aligned fibers
η - packing inefficiency	large	small
V_∞ - ultimate fiber volume fraction	small	large
K_o - Hookean spring constant	large	small
V_o - initial volume fracuon, N=0	small	large

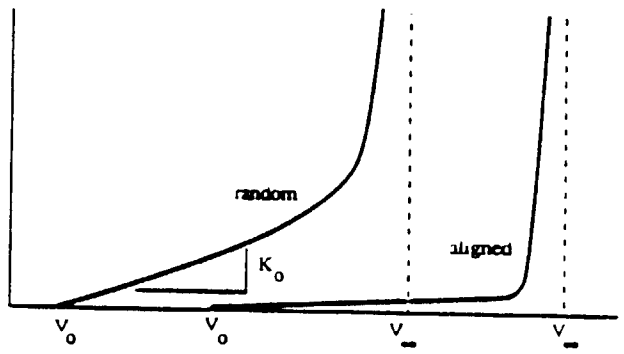

Figure 11.9. Compaction behavior for random fiber mats and aligned fiber rovings, highlighting fundamental differences between model parameters.

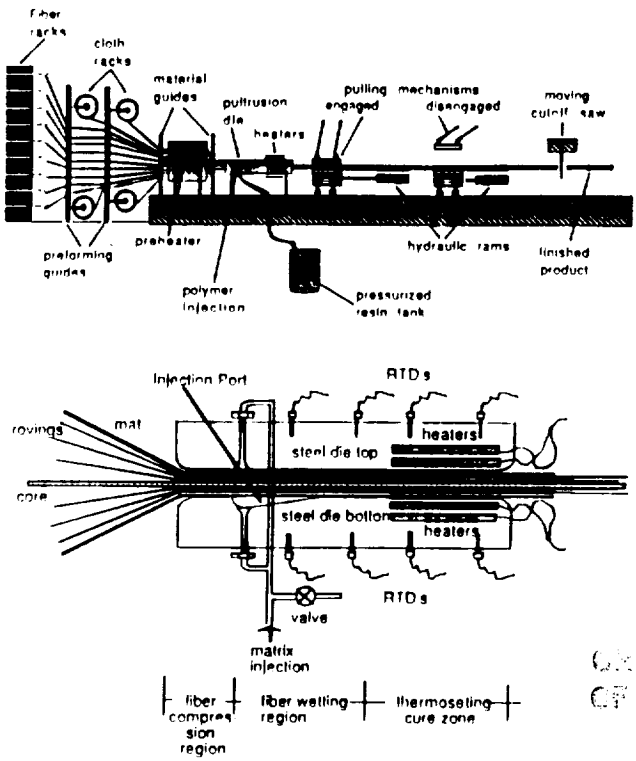

Fig. 1. Typical injection-pultrusion system and die.

surfaces are generated both by compaction of the reinforcing fibers and pressurization of the matrix materials. Both effects act to increase the total pulling force required to move the product through the die (2). In the injection-pultrusion process the reinforcing fibers are dry as they enter the die. Therefore, only fiber compaction contributes to the pulling force that arises in the compression region of the die. The ability to predict the pulling load associated with the compaction of arbitrary combinations of reinforcing materials is essential for proper design of injection-pultrusion tooling, machine size selection, and product design.

The main purpose of this study is the generation of a data base of compressibility information for a variety of fiber reinforcements of interest to pultruders. This information will be used in the development of an analytical model of the injection-pultrusion process. This paper will present results of an experimental and analytical investigation of the response of various dry reinforcing materials subjected to compressive forces applied normal to their principle plane. Stress versus fiber volume data generated during tests of both individual materials and various combinations of reinforcement will be illustrated. Discussion regarding compressibility and relaxation behavior of fiber reinforcements will be presented.

THEORY OF COMPRESSION

The consolidation of composites has been studied by a number of investigators. Among them, Gutowski (3–7) has published extensively on the subject. His research has suggested that the fiber network can be modelled as having the following characteristics. At or below a certain initial fiber volume fraction, V_0, the fibers carry no load. As fiber volume fraction, V_f, is increased, the network can carry a rapidly increasing load. Eventually, the fiber volume fraction of the network approaches a theoretical maximum based on close packed geometry, and can not increase without an enormous increase in load. In this region, V_f approaches a maximum available fiber volume fraction, V_m. When the fiber network is perfectly aligned, V_m is almost always between the limits for a square array, $V_m = 0.785$, and a hexagonal array, $V_m = 0.907$. Gutowski developed a mathematical expression for the transverse stiffness of a bundle of confined, approximately aligned fibers by assuming that the fiber will be slightly arched so that the applied load comes to rest on the beam section between multiple contact points, and not on the end points. The stress taken by the fiber network in bending is then

$$\sigma = A_s \frac{\sqrt{\frac{V_f}{V_0}} - 1}{\left(\sqrt{\frac{V_m}{V_f}} - 1\right)^4} \tag{1}$$

where A_s is a constant dependent on the geometry and properties of the fiber network within the ply. *Equation 1* assumes some transverse fiber rearrangement during compression. He expressed that

$$A_s = 3\pi \frac{E}{\beta^4} \tag{2}$$

where E is the bending stiffness of the fiber, and β is the typical span length/height ratio for the fiber beam network. A computer program was used to find the three variables (A_s, V_m and V_0) that produced the best fit to the data.

Another approach to modeling the compression behavior of fibers was taken from the field of soil mechanics (8, 9). This theory assumed that the voids were completely filled with water, that both the water and the solid constituents were perfectly incompressible, that Darcy's law was strictly valid, and that the coefficient of permeability, k, was a constant. Taylor (9) used a model of a spring immersed in a water cylinder. A frictionless and tightly fitting piston was placed in the cylinder and loaded with weight. The piston was provided with a stopcock, which was assumed to be closed so that no water could escape. When the stopcock was opened, the water flowed out due to the pressure with which it was subjected. In the first instant, the pressure conditions were unchanged. As the water escaped, the piston moved lower and lower, compressing the spring. The spring, consequently, carried more weight, until finally it carried all the weight. The length of time required for the spring to support all the weight depended on the rapidity with which the water escaped, that is, on the size of the stopcock opening. If the spring were more compressible, more water would have to escape in order to produce a

given change in consolidation. Consequently, a longer time would elapse. In the mechanical analogy, the spring represented the compressible fiber reinforcements and the water in the cylinder represented the resin in the void space of fiber network. An empirical relationship between fiber volume fraction and effective stress was expressed as follows:

$$V_f = V_1 + C_c \log_{10}(\sigma/\sigma_1) \quad (3)$$

where σ_1 was usually taken as unity (1 psi or 1 kg per sq·cm), and C_c was called the compression index or expansion index. V_1 was the fiber volume fraction when the effective stress, σ, was unity.

THEORY OF RELAXATION

The phenomena of relaxation of fiber reinforcements during compression can be explained by the Maxwell-Wiechert viscoelastic model (10), which consists of an arbitrary number of Maxwell elements connected in parallel as shown in *Fig. 2*. In each element, the modulus, E, characterizes the response of the spring while the viscosity of the liquid in the dashpot, η, defines the viscous behavior. From here, relaxation time, $\tau_z (= \eta_z/E_z)$, is determined. During compression each fiber is stressed. If we assume that all fibers act independently, we can describe the total stress as the summation of the stresses of the individual elements.

In a stress relaxation experiment, one compresses the sample instantaneously to some strain, ϵ_0, and studies the stress, $\sigma(t)$, necessary to maintain the constant strain. The instantaneous strain will be realized only in the spring element. The dashpot will gradually relax so that the stress decreases as a function of time. In this model the spring represents the compressible fiber reinforcements with a spring constant related to the elastic properties of the fiber and the material geometry. The dashpot represents the structural rearrangement of fiber and/or breakage of fiber during compression. From this model we can describe

$$\frac{\sigma(t)}{\sigma_i} = \frac{\sigma(0)_1}{\sigma_i} e^{-t/\tau_1} + \frac{\sigma(0)_2}{\sigma_i} e^{-t/\tau_2} + \frac{\sigma(0)_3}{\sigma_i} e^{-t/\tau_3} + \ldots \frac{\sigma(0)_n}{\sigma_i} e^{-t/\tau_n} = \sum_{z=1}^{n} \frac{\sigma(0)_z}{\sigma_i} e^{-t/\tau_z} \quad (4)$$

where $\sigma(0)_n$ is the stress on the nth element at time equals zero, and σ_i is initial stress applied on the sample. Thus, the total stress relaxation is the summation of the responses of the individual elements.

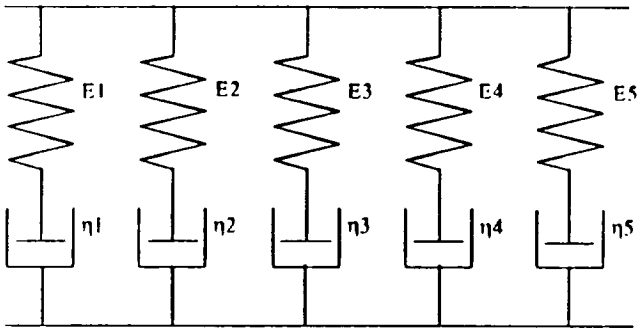

Fig. 2. Maxwell-Wiechert model for relaxation.

EXPERIMENTAL PROCEDURE

Compression Test

Materials used in this study are shown in *Table 1*. Cloth and mat samples were cut to 15.24 cm × 15.24 cm. For unidirectional samples, roving was wound onto a thin 15.24 cm wide steel plate, taking care to keep each new winding parallel to its adjacent winding. The edge was then cut to allow the sample to be laid flat. Samples were weighed and then put into a 15.3 cm × 15.3 cm bottom test fixture. Normal compression force was applied to the samples using a 15.24 cm × 15.24 cm upper test fixture installed in 250,000 N Instron testing machine. In general, 20 to 40 layers of material were used for each test sample. Compression force versus sample thickness was measured. Sample thickness was recorded on a strip chart using a magnification factor of 100. From that data, the stress versus fiber volume fraction was determined. Fiber volume fraction was calculated from the known sample thickness and the weight and density of the fibers being compressed. Fiber densities of 2.62 g/cm^3 for E-glass and 1.79 g/cm^3 for graphite were used (11). Fiber samples were compressed at a cross-head speed of 2 mm/min.

Table 1. Fiber Information for the Compression Test.

Materials	Orientation	Type	Manufacturer
Straight roving	Unidirection	1062	PPG
Fluffy roving	Unidirection	N/A	Scandinavian Glass Fiber in Sweden
Spun roving	Unidirection	G135 Type A	Owens Corning
0/90 plain weave cloth	Bidirection	Style 3	Bean Glass Fiber Inc.
	Bidirection	HWR-240	PPG
Random mat	Quasi-isotropic	ABM	Bean Glass Fiber Inc.
Combination mat	Combination[a]	WOVMAT Type 1524	Bean Glass Fiber Inc.
Graphite roving	Unidirection	IM7	Hercules

a: Combination of unidirectional and 0/90 cloth.

Relaxation test

An initial stress, σ_i, was applied to the samples at a speed of 2 mm/min, and then the machine was stopped. Stress was measured as function of time while sample thickness was held constant. From that data, the ratio of (current stress/initial stress) versus time was determined. Effects of initial stress and fiber orientation on stress relaxation were studied.

RESULTS AND DISCUSSION

Compression study

Figure 3 shows the effect of cross-head speed on compressibility. From this figure it is seen that as cross-head speed decreased, the curve moved slightly to the right. Slow speed appeared to allow more time for fiber rearrangement and relaxation to occur, and thus required less load to compress. *Figure 4* shows the result of repeating compression on the same sample. Tests made using two different material types showed that the first run required much more stress to produce a certain fiber volume fraction, particularly in the low stress range (<4 MPa). These results demonstrate non-equilibrium effects related to fiber movement in the mold. If the compression force is applied very slowly, the curve for the first compression cycle will shift close to the second cycle curve. Note that repeated compression on the same sample continues to shift the curve to the right gradually. This differs from Gutowski's results (6) which showed that, while the second compression test on the same sample shifted the curve to the right, the third and subsequent compression tests did not cause any further significant shift. This difference might be due to the use of dry samples for the current experiment, while Gutowski used prepreg specimens. Use of dry fibers may have resulted in increased fiber misalignment and/or fiber breakage because friction between fiber to fiber contact points would be higher. Dry materials were used for this experiment because they better represent the behavior of materials used in the injection-pultrusion process.

Figure 5 shows the effect of lubrication on compressibility. A mold release agent was applied to a sample. During this test, the lubricated sample showed less initial thickness than the dry sample even before compression. From the figure, it is clear that the lubricated sample was easier to compress. From this experiment we can conclude that lubricating the material eased fiber rearrangement at low stress levels, and at high stress levels reduced fiber breakage.

Figure 6 shows the effect of fiber orientation on compressibility. These results indicate that compressibility is strongly dependent on the fiber orientation. For the case of straight roving, at least, compressibility seems to be less dependent on fiber material stiffness, as demonstrated by the similarity of the curves for straight glass and graphite.

Figure 7 shows the effect of combining two different fiber orientations on the compressibility of the

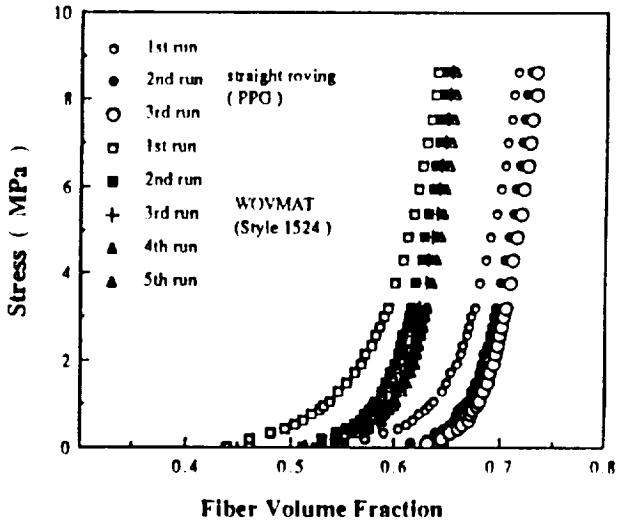

Fig. 4. Effect of repeated compression on same sample.

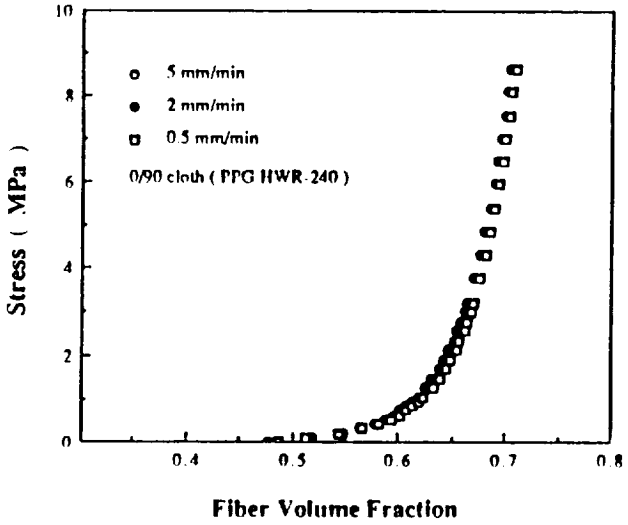

Fig. 3. Effect of cross-head speed on compressibility.

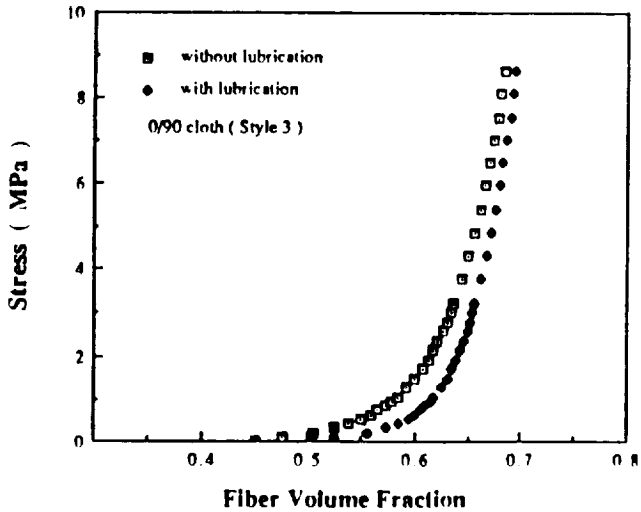

Fig. 5. Lubrication effect on compressibility.

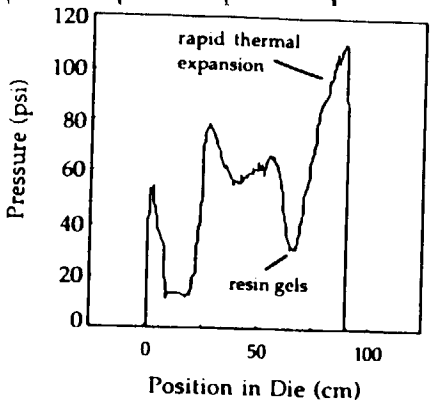

Figure 8. Glass/phenolic resin.

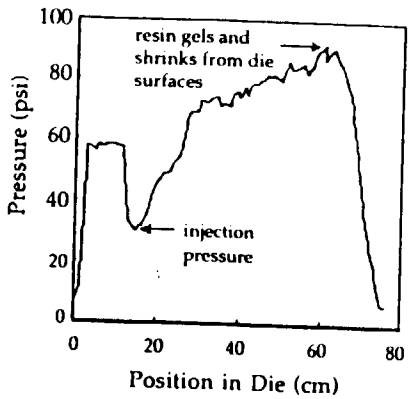

Figure 9. Glass/polyester resin

Figure 9 illustrates the pressure profile of a polyester resin, the mainstay of the pultrusion business. The data were generated using the same die as the previous two examples. Thermal expansion of the fiber/matrix system results in peak pressurization at the point of gelation, a very desirable behavior. Little or no shrinkage of the resin occurs before the gel. High pressurization at gel maximizes consolidation and surface quality. Shrinkage of the resin during the gel stage releases the part from the die and pressure goes to nearly zero. The die length is 100 centimeters and the pressure drops quickly at about 70 cm. The dry fiber compression at the die inlet and the 30 psi injection pressure in the wet-out section of the die can be clearly seen in the data.

One of the classic failure modes of the pultrusion process is a die jam. Die jams occur when resin builds up on the surface of the die, causing a local reduction in the cross sectional area at that point. This in turn leads to increased pulling forces as the same amount of fiber is forced through the smaller section. The tendency is for the residue thickness to gradually increase until either the pultrusion machine lacks the capacity to apply the force necessary to pull the part through the die, or the pulling load exceeds the strength of the laminate and the product breaks. Figures 10a, 10b and 10c show three pressure profile snapshots of various stages of resin build up during a development run of a fiberglass/epoxy part made with 43.5% fiber volume and pulled at a speed of 30 cm/min. Figure 10a shows an apparently normal process in operation, with a slight increase in pressure observable approximately 60 cm into the die. Figure 10b illustrates the data from a sensor passed through the die a few minutes later. A marked increase in pressure is now apparent at the 60 cm position, indicating that resin build up is occurring. Figure 10c shows data from a sensor run made a few minutes prior to a jam which exceeded the machine's pulling capacity. Pressure at the 60 cm position exceeded 550 psi.

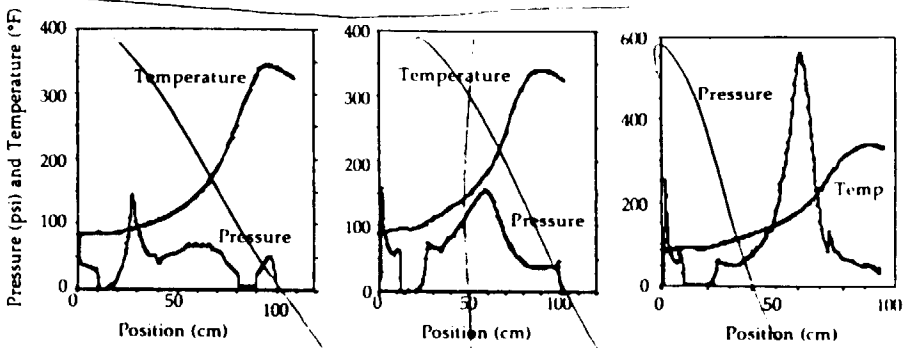

Figure 10a. Time 1. Initial indications of resin build-up at 60 cm.

Figure 10b. Time 2. More obvious build-up at 60 cm.

Figure 10c. Time 3. Resin build-up prior to process failure.

Figure 10. Fiberglass/epoxy bar pulled at 30 cm/min, V_f = 43.5%

5. PROCESS MONITORING IN THERMOPLASTIC PULTRUSION

Careful tailoring of the distribution of compression forces applied to the thermoplastic composite as it is pultruded is required in order to optimize part quality and production rates. Prior to the development of the disposable pressure sensor discussed in this paper, there was no technique for directly measuring the pressure history of the laminate as it passed through the multiple stages of the pultrusion tooling. Setting the die gaps that control pressure distribution relied primarily on trial and error. The low profile of the new sensor makes it possible to pass the gage through the series of dies along with the structural materials by simply laying the sensor between layers of prepreg as it enters the die.

The following plots illustrate typical pressure and temperature data measured by passing sensors through an eight die set during the pultrusion of graphite/ULTEM thermoplastic. Final thickness of the pultruded part is 3.17 mm (0.125 inch). Figure 11a shows data from a run made early in the test program. Even with a relatively low fiber loading with 16 plies of prepreg, pressures measured in the first few die stages are relatively high because the matrix has not yet reached the melting point. In the fourth die the material finally melts, making it more easy to compact. The pressure therefore drops significantly. Pressure again rises in the final cooling stage as the material solidifies. The large pressure spike measured in the first few die stages is undesirable. Applying high compaction loads to the unmelted thermoplastic contributes little to the final consolidation of the part, but greatly increases pulling load. A more optimized process should have a more constant pressure distribution from stage to stage.

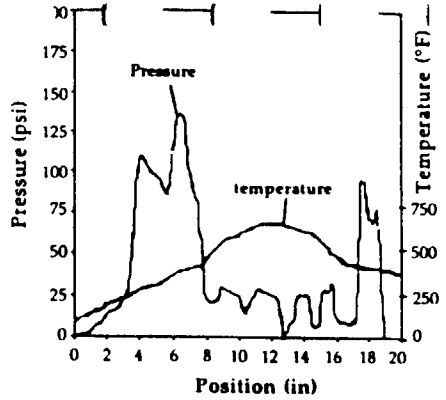

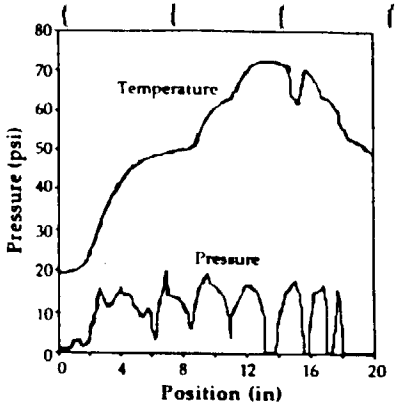

Figure 11. Pressure profiles from thermoplastic process development runs.

Figure 11a. Uneven pressure distribution causes poor consolidation.

Figure 11b. Even pressure distribution results in good quality part.

Figure 11b illustrates a temperature and pressure run made after adjusting processing conditions to attempt to more evenly distribute the application of pressure to the laminate. The pressure in die stages 2 through 8 is reasonably constant, except for the drops that occur in the small gaps between stages. This pressure trace suggests that a set of more optimized processing parameters has been established, and illustrates the usefulness of the disposable pressure sensor in quantitatively converging on the optimum process.

6. CONCLUSIONS

This paper has described the characteristics and application of a new type of pressure sensing device designed specifically for measurement of locally applied pressures in composite material processes. Until this device was developed, no cost-effective method for making many of the processing pressure measurements described in the preceding sections existed. The sensor's small size and thickness permit it to be placed directly at points where pressure information is desired, rather than following the previously conventional method of inferring pressures from far field measurements. Its low cost, similar to that of a thermocouple, allows it be a disposable item to be scrapped along with other materials such as bleeder and peel ply layers used in autoclave processing to support laminate curing. The versatility of the device allows it to be used as a simple vacuum bag leak detector, to locate bridging in complicated bagging situations, to measure compaction forces during winding of thick composite shells, to monitor loads in compression molding, to be used as a tool for press alignment and in a wide variety of other processing situations. As illustrated in this paper, it is also capable of generating processing data for pultrusion, one of the most difficult composite manufacturing techniques to observe directly

IV. ADVANCED TOW PLACEMENT

In March 1991, Norm Johnston and I visited MacAir, Hercules and Cincinnati Milcron. The purpose of our trip was to learn about automatic tow placement and the tow properties that are required for it. The key feature of the advanced tow placement equipment under development is the automated robot head, which lays adjacent tow ribbons on the part surface while applying heat and pressure to adhere them. The process is similar to its forerunner the automated prepereg tape laying operation, the difference being that of laying an array of tow ribbons rather than a tape.

Advanced tow placement utilizes robotic technology to apply as many as 32 adjacent impregnated tows simultaneously on complex part surfaces. The ability to lay a number of adjacent narrow (1/8 to 1/4 inch wide) tows has two advantages over wider tape laying operations. First, wrinkle free turns, with radii as small as 5 inches, are possible by laying the outer tapes faster than the inner ones as the turn is made. Second, the number of adjacent tows being laid may be increased or decreased to accomodate changes in part geometry. That is, the ribbon of tows may be narrowed or widened by dropping or adding tows as the head moves over the surface. The robotic heads designed to achieve these two functions utilized towpreg in the form of a fairly stiff ribbon of uniform width.

Another objective of advanced tow placement research is "on the fly consolidation". The goal of these efforts is to eliminate the need for autoclave consolidation once the tow has been laid. To achieve this end, laser, infrared, or gas heaters are used to deliver thermal energy to the tows at the point where they are laid on the part surface. This hot zone of freshly laid tows is immediately subjected to high pressure by the roller, which extends from the robot head to the surface, see subsequent section.

The goal of the Hercules/NASA ACT program (13) is to demonstrate the low cost potential of the automated fiber placement process. As shown in the following pages, a 32-tow head is used. Tow-tow gaps are kept within 0.75 mm (0.031 in) and scrap rates as low as 5 % have been achieved.

Automated fiber placement studies by Cincinnati Milacron and Thiokol (14,15) cover the performance of 24-

tow machines involving in-process compaction, individual tow cut/start capabilities, resin tack control, differential tow payout, and low fiber tensioning. The fiber placement process is usually run at 454 g (1 lb) of constant tension for each individual tow. The system is capable of tensions up to 6.8 kg (15 lb) per tow. The tack control system decreases or increases the "B" stage prepreg tow material tack at critical points along the cut/clamp/ restart operation in the robot head. Compaction uses a pneumatically controlled flexible elastometric roller that can conform to a convex or concave 15.2 cm (6 inch) cross band radius and apply even pressure across the width of the roller. Machine capabilites are described in the following pages, note the 5 inch turning radius in fig 5 and in table 3 the range of towpreg bandwidths.

Ghasemi-Nejhad, et. al. (16) conducted an analytical and numerical thermal analysis for the melting and consolidation taking place during thermoplastic tape laying. The objective was to identify the processing window for thermoplastic tape laying. APC-2 was taken as the composite material. The window requires that the interface temperature exceed the melt temperature and at the outer surface, where the heat is applied, the temperature should be below the degradation level. This provides the temperature difference across the tow for heat conduction through it.

The authors (16) conclude that, " to maximize velocity (output), one should use a heater width (length in the laydown direction) of at least 0.02 m. This 0.02 m heater width would allow for speeds above 0.1 m/sec; however, in this range the processing window is very small. Clearly, well focused <u>lasers are not at all suitable</u> for the example developed herein. Unless a very high degree of process control is employed, one would be wise to operate below the maximum allowable velocity in order to 'widen' the processing window, which allows for some variation in the absorded heat intensity without adversely affecting part quality. Finally, regardless of the heater width and speeds used, heating devices which provide absorbed intensity less than $0.25 \times 10^6 W/m^2$ and greater than $1.4 \times 10^6 W/m^2$ are of little or no value". The estimated maximum flux appears to be based on staying below the degradation temperature, while the minimum seems flux seems to be based on a lowest flux that will achieve adhesion at the interface.

Anderson and Grant

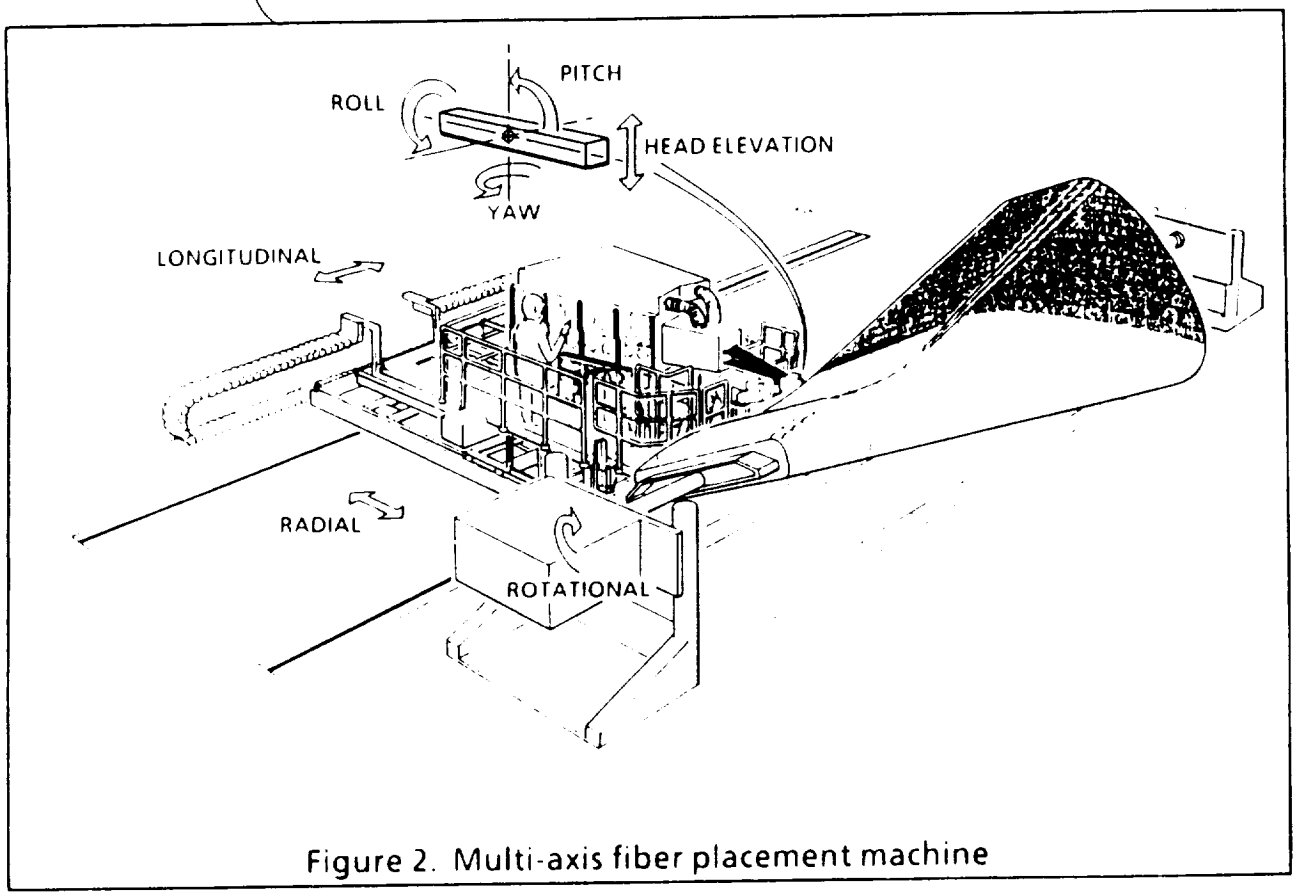

Figure 2. Multi-axis fiber placement machine

We currently have two delivery head designs that are operational on our fiber placement machines. The tow cut and add head allows for individual tow cutting and adding for ply tailoring on complex, nongeodesic structures. The band cut and add head is used for all structural shapes that do not require individual tow cut and add capabilities. Both of these delivery heads are designed for 12 tows. We also have a tow cut and add head that is designed for 32 tows. The 32-tow head was used on the MANTECH V-22 Aft Fuselage shown in Figure 1.

Fiber tow placement offers many improvements over hand lay up that contribute directly or indirectly to cost savings. Tow width control allows for non-standard ply thicknesses which optimize part design while maintaining constant band width. Gaps and overlaps are kept within a tolerance of 0.75 mm (0.030 in.). Constant ply thickness can be maintained by adding or dropping tows as the part changes cross section (Figure 4). Tow and band cut/add features reduce material scrap to as low as 5% by placing the material only where required. Fiber placement also uses prepreg tow that is projected to be the lowest cost material form available. The tow-placed product is also comparable in performance to hand lay up prepreg tape parts (Figure 5).

During the fiber tow placement process, a conformable roller rides directly on the part or tool, providing in-process compaction while delivering the tow material. This minimizes the need for intermediate compaction steps. The placement head flexibility allows fiber placement on convex and concave surfaces. The delivery head delivers individual tows as a flexible band to minimize material distortion. This flexibility provides fiber angle control that allows for fiber placement of non-geodesic shapes which cannot be fabricated with filament winding (Figure 6).

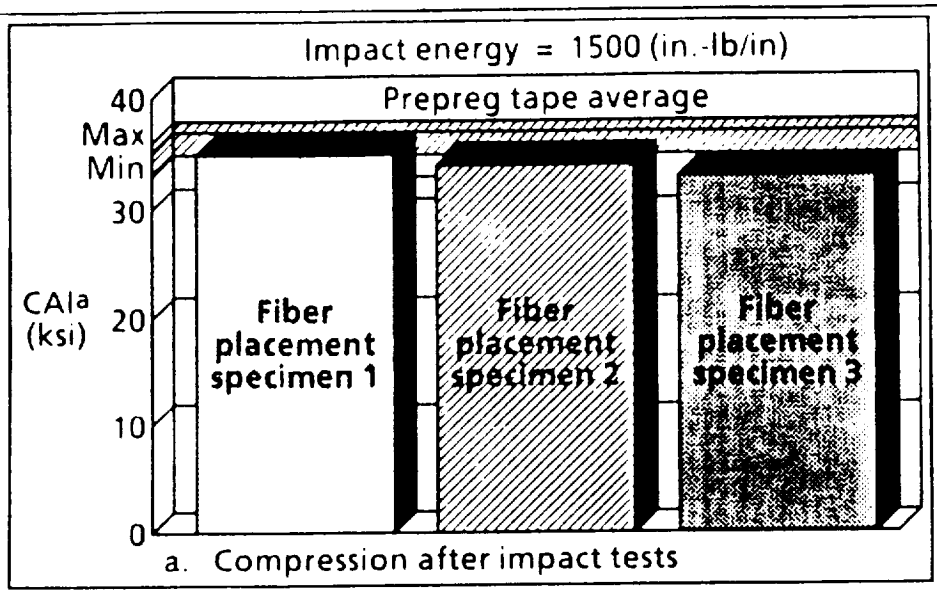

a. Compression after impact tests

- Damage tolerant IM7/8551-7A towpreg demonstrated
- Fiber placement process CAI results demonstrate equal quality to prepreg layup process
- Concave surface, variable skin thickness, tapered cross section and thin ply laminates now possible with automated process

Figure 5. Compression after impact test data

Item	Filament Winding (Wet)	Fiber Placement (Prepreg Tow)
Void content	4-8%	<1%
Thickness	• 0.010-0.025 in/ply • Not constant for tapered parts	• 0.005 - 0.015 in/ply • Constant for tapered parts
Tow cut and add	No	Yes
Winding angle	>15° 15 - 90°	No limit 0 - 90°
Laps and gaps	0.125 in.	0.030 in.
Geometry	Best for bodies of revolution	• Complex • Concave
Scrap rate	20 - 40%	5 - 20%

Figure 6. Filament winding/fiber placement comparison

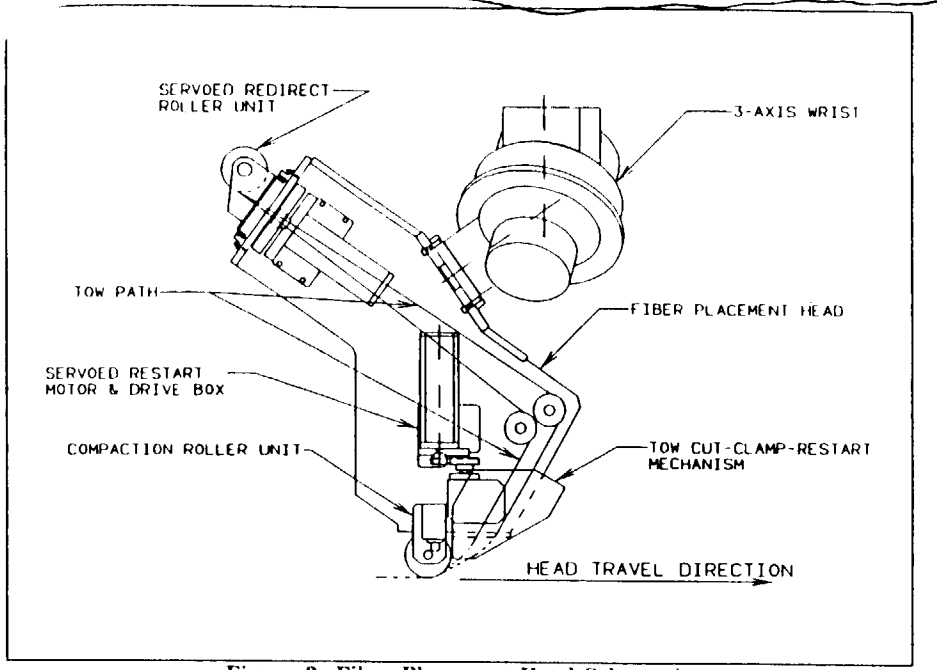

Figure 2 Fiber Placement Head Schematic

configuration simplifies the tow tensioner requirements and the creel design.

Experts from Morton Thiokol's Strategic Operations were consulted on the fiber band collimation technique that is used on the creel. Morton Thiokol has a strong interest in the fiber placement process for fabrication of both rocket motor casings and aerospace structural parts. Complex geometries, localized reinforcements, load bearing joints, and thick wall sections all require additional processing beyond filament winding. Currently this processing is labor intensive, making it expensive and time consuming. Preliminary studies of past and current production parts indicate significant cost savings are possible with the fiber placement process.

Cincinnati Milacron is actively engaged in a project to validate the fiber placement process using a T3-886 gantry robot to manipulate a prototype fiber placement head. See Figure (3). This work began in October of 1986. At this time a fully automatic head that is capable of laminating up to eight tows over complex lay-up molds or rotary mandrels is operational. The advantages of Fiber Placement are being demonstrated with this system.

2.0 FIBER PLACEMENT

Figure (2) shows a schematic of the fiber placement head and the necessary process functions. The key process features of fiber placement that were developed at Cincinnati Milacron are:

1. Delivery of the fiber band past three axis wrist
2. Differential tow payout
3. Cut-clamp and restarting of the tows
4. Compaction

2.1 Fiber Delivery

It is necessary in fiber placement to be able to deliver the fiber band, which is collimated at the creel, past the three axis wrist to the fiber placement head. The fiber band must be delivered in such a way that it does not greatly restrict the operating zone of the head. Head manipulation is necessary for maintaining the head centerline coincident with the mandrel or mold surface normal at any given point along the fiber path. The action of the head moving relative to the creel defines an ever changing vector for the fiber delivery path. The best way to deliver a collimated band of tows through this vector is to pull the band through redirect roller sets located at the creel and head. These redirect roller sets must be mounted in a pivotable base that automatically positions proportional to head motion.

2.2 Differential Tow Payout

The second key feature of fiber placement is the individual tow payout speeds made possible by the independent delivery guide system for each tow. Each tow must have its own set of delivery guide rollers from the spool to the compaction line. This feature is required to allow each fiber within the band width to subtend a unique line length as the laminating action of the head pulls the fibers off the spools and presses them on the part surface. When the head is required to laminate a curved path, the outer tows of the band will pull more length than the inner tows. Similarly, as the head laminates over a contour, some tows must dispense more length than others. With fiber placement a small relative difference in fiber payout speed is necessary and must be permitted.

2.3 Cut Clamp and Restarting of the Tows

The third feature of fiber placement, and probably the most challenging, is automatic cutting and restarting of the tows. It is necessary to individually cut-clamp and restart the tows without stopping the laminating motion of the head. As part of the off line software, commands which signal cut-clamp and restart sequences must be programmed based upon the requirements of the lay-up geometry. This feature allows all or any combination of tows to be removed or added to the band width in increments equal to one tow width. With this capability, it is possible to decrease the band width to prevent excessive material build-up. Also cutting the entire set of fibers at the part edge will save the material that would otherwise be wasted in a turn around area.

2.4 Compaction

A final feature of the process is the use of a mechanical compaction device to laminate the prepreg tow onto the mold or part surface. Compaction is the action of mechanically pressing the tows onto the part or mold surface so entrapped air and inner band gaps are removed from the band width. The compaction device used during initial head development was a soft, 7.6 cm (3.0 in) diameter roller. In most situations it is necessary to introduce heat into the compactor nip area to decrease the resin viscosity of the tows. This part of the process is referred to as tack enhancement. Heat promotes resin flow thus enabling the compactor to remove gaps between adjacent tows easier. Increased tack also enables the incoming fibers to adhere more quickly and remain in place on the mold or previously laid courses.

to calculate a lamina which will satisfy the customer requirements and be processible. Once the simulator indicates that the lamina is feasible, the lamina is down loaded into the 975F controller.

Finally, the lamina is dry run on the mandrel to ensure that tow cut/clamp and restarts mechanisms are working correctly. Machine paths are verified for collision detection and the part is ready for fabrication.

2.5 Machine Capabilities The FPX machine has seven primary axes of machine motions. These include the typical three axes of movement found on a basic filament winder, two linear axis (carriage and cross slide), and a spin table axis. In addition, there is a robotic wrist on the end of the arm which provides three axes of machine motion and a tilt axis on the machine which tilts the entire creel and delivery head assembly. In summary, the primary axes are:

Primary Axes of Motion

Carriage axis:	Moving carriage and assembly for longitudinal movement
Cross slide axis:	Moving the cross slide for cross movement
Mandrel axis:	Rotating the workpiece parallel to the carriage axis
Tilt axis:	Moving the tilt saddle for vertical (tool point) movement

Robotic Wrist Axes of Motion

Roll 1 axis:	Rotating the entire wrist and head about the cross slide axis
Bend axis:	Rotating the head perpendicular to the Roll 1 axis rotation
Roll 2 axis:	Rotating the head about an axis perpendicular to the head mounting plate

Figure 1 shows the world coordinate or programmed axes of motion which do not directly correspond to the machine axes. Movement in the world coordiante frame is dynamically transformed into machine axis motion. Also there are three additional secondary machine axes of motion on the machine. A servo-driven redirect roller is used in the fiber delivery system to provide a constant alignment of the tows to the delivery head as the machine moves about in three-dimensional space. An additional servo-motor (restart axis) is used to advance the tows when additional tows are required in a layup. Additionally, a fiber axis for the fiber's linear motion is monitored by the tension controller device. The fiber axis is somewhat of a redundance of the restart axis. A summary of the secondary axes controlled by the Acramatic 975F controller:

Secondary Axes

Redirect roller axis:	Angular position of the servo-driven redirect roller unit
Restart axis:	Linear position of the tows between the restart rollers
Fiber axis:	Linear position of the tows at the tool center point

The mandrel capacity of the machine is as follows:

Diameter	2.134 m (84 in.) swing
Length	8.687 m (342 in.) maximum
Weight	9,091 kg (20,000 lb)
Inertia	32,000 in.-lb/sec**2

that uses thermoset prepreg tows. The design of the fiber delivery path is such that differential tow payout is possible. Differential tow payout is the ability to have individual tows within a band of tows running at different speeds. This reduces the possibility of developing catenary in the delivered band, as found in the process of tape laying on rapidly changing contours. Differential tow payout allows the user to fabricate more complex shaped parts, and to add and drop tows within a ply.

Another feature that differential payout adds to the process is the ability to steer the band of tows on the mandrel. A steered band path will benefit both the designer, by reducing the number of discontinuous load paths, and the manufacturing engineer, by reducing the need for hand layups within the composite. A minimum radius of 12.7 cm (5 in.) has been demonstrated (Figure 5). The ability to steer the band allows for the benefits described in the following list:

- Constant fiber angles on changing geometry
- Continuous fibers around holes and ports
- The ability to place the fibers on critical load paths

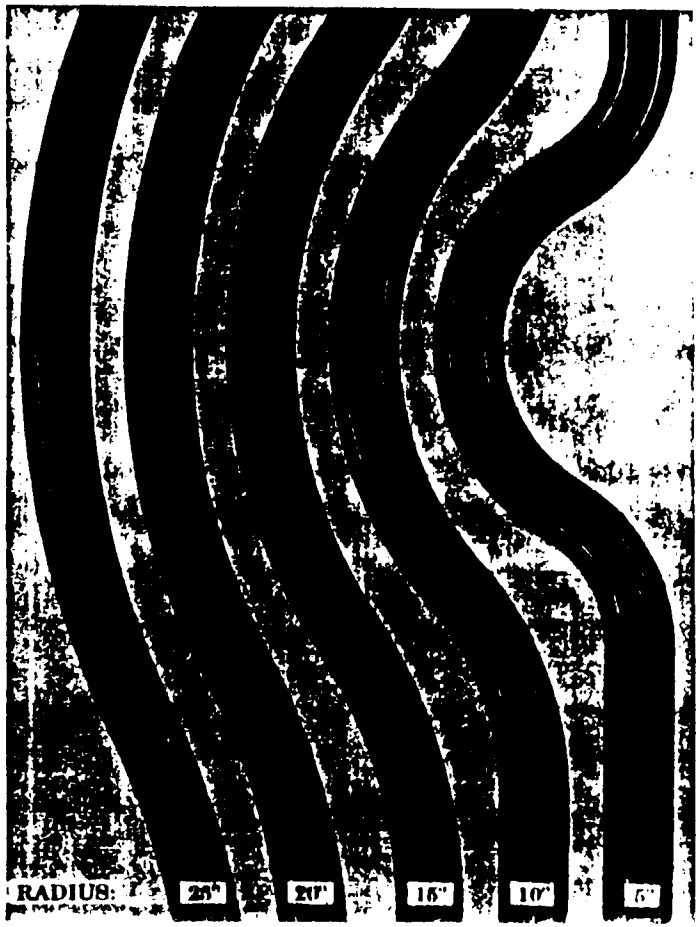

FIGURE 5 Fiber steering with differential tow payout

other processing attribute of the FPX machine is its ability to automate the fabrication of a hybrid composite lamina. Because tows can be individually added or dropped within the ply, the machine could be set up to operate two bands of dissimilar materials. The tows can be programmed to be added or dropped as desired by a customer to create a hybrid layup.

The fiber placement process can now create composite laminates which are designed as tape layups. With the previous filament winding processes this was not possible because off-axis plies had to be wound as layers of materials containing plus (+) and minus (-) fiber orientations. In addition, these off-axis layers of fibers contain "crossovers" wherever the bands intersect as the winding pattern is created. These crossovers can contribute to a slight loss in composite strength due to fiber waviness [Ref. 3]. The FPX machine can fabricate entire areas of off-axis plies in either the plus or minus orientation without any crossovers. The ability to fabricate an entire ply of a singular fiber orientation can allow the designer the freedom to intersperse the composite lamina.

3. MATERIAL ISSUES

Integral to the success of any new manufacturing process is the quality of the material used. Industry acceptance of fiber placement will be influenced by its material requirements and availability. The material form required for fiber placement is towpreg, which is currently produced for the filament winding process. This product typically does not exhibit the lot-to-lot consistency of tapes and broadgoods prepreg products. In particular, tow bandwidth and tack are critical to process performance. Unfortunately, present control of these parameters is only marginally acceptable for fiber placement. Incorporation by the material vendors of various in-line control mechanisms and real-time feedback will raise product consistency for both fiber placement and filament winding.

Critical parameters, such as bandwidth, influence the rate performance of the machine and the end product lap/gap tolerances. Intarband gaps are a direct result of input material bandwidth: each 0.025 mm (0.001 in.) less than nominal width results in a maximum 0.076 mm (0.002 in.) gap. Interband laps are fixed by machine limits at a maximum of 0.635 mm (0.025 in.). Machine programming can control intraband gaps/laps per part requirements. Therefore, towpreg quality is critical to full development and performance of the fiber placement technology.

Recognizing the importance of materials relative to process performance the Thiokol/Milacron team has worked closely with towpreg material suppliers. Table 3 lists the targeted property parameters desired.

4. PART DEMONSTRATION

A number of composite parts have been successfully fabricated using fiber placement technology through the Milacron prototype gantry system [1] and with other similar systems [4]. The FPX machine at the time of this writing has had limited use to date because of its newness; however, a few basic evaluation parts have been fabricated on the machine. The evaluation

TABLE 3 THERMOSET TOWPREG PHYSICAL PROPERTIES REQUIREMENTS

Bandwidth, Individual Spool	• 3.2 ±0.4 mm; target ±0.13 mm (0.125 ±0.015 in.; target ±0.005 in.)
Tow Cross Section	• Rectangular cross sectional geometry
Tack Level	• Medium to low
Drape	• Drapeable on mandrel at 32°C (90°F)
Spool Package	• Minimal de-spooling force (less than 2.2 kg (1 lb)) • No fuzz or foreign material • No tow band twist • Full impregnation of tow (no dry spots or dry tow interior allowed)
Strand Flexibility	• No cracks when 1 ft of tow is bent 180 deg around 5 cm (2 in.) dia roller
Volatile Content, Individual Spool	• Standard for product
Resin Content, Individual Spool	• % required to produce a 60% (±3%) fiber volume laminate assuming a net process
Out of Storage Life	• Target for 240 h at 24°C (75°F) maximum temperature

parts include a simple 45.7 cm (18 in.) diameter cylinder, a complex cone shape, and a 45.7 cm (18 in.) diameter bottle. All the evaluation parts used ICI Fiberite T300-12K/934 prepreg tow material.

The 45.7 cm (18 in.) diameter cylinder (Figure 6) was used as an article to test the basic functions of the FPX machine. The cylinder was a 16-ply layup consisting of interspersed 0, 90, and ±45 degree plies with a cylinder length of 61 cm (24 in.). Due to the development stage of the machine the overall processing speed was low, but an entire ply of 45 degree orientation was laid down in 13 min, demonstrating a through-put of 40 in./min.

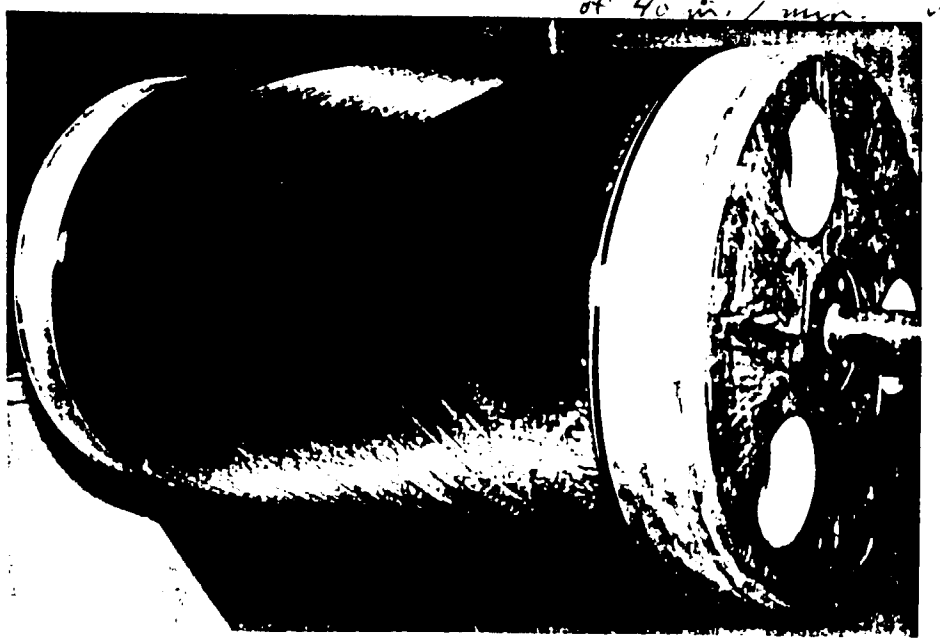

FIGURE 6 45.7 cm (18 in.) diameter fiber placed cylinder

Thermal Analysis of *in-situ* Thermoplastic Composite Tape Laying

M. N. GHASEMI NEJHAD, R. D. COPE AND S. I. GÜÇERI
Department of Mechanical Engineering
and Center for Composite Materials
University of Delaware
Newark, DE 19716, USA

(Received December 3, 1990)

ABSTRACT: This paper presents analytical and numerical thermal analysis for melting and consolidating impregnated composite tapes in the presence of a localized heat source. This analysis also leads to the prediction of the processing window for a given tape-laying configuration. Heat of melting/solidification is included in the form of a heat generation term. A separation of variables method is employed to solve the governing equations analytically. In the numerical analysis, the governing equations are discretized using a nonuniform mesh and are solved using a finite difference approach. The processing parameters, such as consolidation speed, heat intensity, heat source width, etc., as well as material properties are incorporated within the analysis. The results show large thermal gradients in the vicinity of the consolidation point. The error between the analytical solution and the numerical result is found to be 3% for the maximum temperature, and the maximum error for the temperature over the entire domain is observed to be 7%. The effects of processing speed, heat intensity, and the width of the local heat source are investigated, and the overall optimization of the process is discussed.

1. INTRODUCTION

RECENT DEVELOPMENTS IN high-temperature, advanced thermoplastic resins have opened new opportunities for their application in thermoplastic composites for producing high-performance parts. The advantages of thermoplastic composites over those based on thermoset resins are well known and include superior fracture toughness, infinite shelf life and easier processibility. An excellent review of the current status of thermoplastic composites is presented by Chang and Lees [1]. In thermoplastic-matrix composites, the research issues center on the development of new material systems and the development of processing techniques to produce parts in a cost-effective way. The processing of thermoplastic composites differs completely from that of thermoset composites in that it is based on the melting and solidification of the matrix which is based on the transport of energy, often in the form of heat [1–4].

The tape-laying process for thermoplastic composites is a manufacturing method that appears to be suitable for producing parts with large surfaces and mild curvatures, like those seen in aircraft wing skins. It offers the possibility of combining the laydown, melting and consolidation steps in a continuous process, thereby eliminating the curing steps that are necessary with thermosetting materials. Also, whereas producing thick cross-section parts is very difficult using thermoset resins because of their exothermic reaction and heat diffusion limitations, there is conceptually no limitation on the thickness of an *in-situ* consolidated thermoplastic part. This is due to localized melting and solidification during consolidation that prevents the build up of large residual stresses from the high temperature gradients in thermoset curing or the large volumetric changes in post consolidation of thick-section thermoplastic parts.

One of the major characteristics of composite materials is the strong coupling between their microstructure and processing history. In semicrystalline thermoplastics, this coupling occurs most significantly in the final crystallinity of the resin, which can range from low percentages in quenching-like processing conditions, to more than forty percent for processes in which the rate of heat transfer is very slow. General treatment of this subject is reported by Seferis [5], Velisaris and Seferis [6], and Blundell et al. [7]. Recent studies by Motz and Schultz [8,9] present an excellent analysis of crystal morphology and kinetics for Polyetheretherketone (PEEK).

In addition to crystallinity, the prediction of residual stresses during processing of thermoplastic composites also largely depends on the information about their thermal history. In an *in-situ* thermoplastic tape-laying process, a localized heat source generates a molten region around the laydown point. The prepreg tow is consolidated through a melting diffusion process under the pressure of a consolidation roller. The solidification of the material occurs as a result of heat removal as it consolidates and moves away from the laydown point. The temperature field is altered with the variation of the processing parameters, such as processing speed, heat input, size of the heater, thermal boundary conditions. A parametric study can be used to determine the processing window that indicates the bounds on the heat flux at any given manufacturing speed and configuration.

In the current study, analytical and numerical thermal analysis for melting and consolidation taking place during thermoplastic tape laying is presented. A continuous manufacturing process (*in-situ*) in the presence of a localized heat source is considered. The primary objective of this study is to identify the dominant processing parameters and observe their effects on the thermal history, as well as to determine the overall feasibility of *in-situ* thermoplastic tape laying. An analytical model and a numerical technique are presented that allow for the prediction of the temperature fields in the anisotropic composite. The results are assembled in a way to develop a processing window that can be applied to a wide range of material and processing configurations. The analytical solutions are compared with the results obtained using the numerical method to assess the accuracy in computations.

2. THERMAL ANALYSIS

A schematic description of a typical *in-situ* tape-laying process is depicted in

0892-7057/91/01 0020–26 $6.00/0

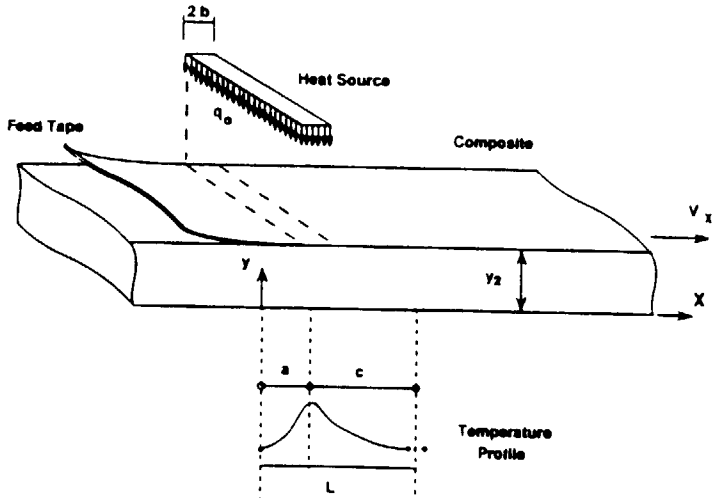

Figure 1. The geometry and Eulerian control volume (ECV) for a tape laying process.

igure 1. The localized heat source of finite width is applied at the consolidation oint, and the tape lay-up is achieved by moving either the heat source or the omposite substrate. A descriptive temperature distribution around the consoli- ation zone is also indicated in this figure. In a realistic tape-laying process, the uminate is relatively long with respect to the width of the local heat source, /hich has been a common assumption in some of the earlier studies by Beyeler 0], Beyeler and Güçeri [11], Beyeler et al. [3], and Grove [12,13]. Therefore, a wo-dimensional heat transfer analysis becomes necessary to accurately represent ie thermal diffusion and its effects on the material properties.

Figure 2 depicts the geometry considered in the present analysis and indicates ie various boundary conditions. The formulation of the governing equations is erformed by assuming a local heat source fixed with respect to inertial coor- inates x and y, and the process-relative velocity V_x is assigned to the laminate id the base plate as a whole. The length of the domain for the analysis is taken ; L, which is sufficiently greater (to validate the boundary conditions) than the idth of the heat source $2b$. The portions of the substrate upstream and down- ream from the consolidation point are indicated as a and c respectively.

The tape laying is a transient heat diffusion problem in a Lagrangian frame- ork, i.e., from a material point of view. On the other hand, in a steady opera- on of continuous process, an Eulerian Control Volume (ECV) enveloping the gion influenced by the local heat source can be identified, and a steady-state rmulation can be developed (Eulerian approach). This steady-state approach ecomes possible since at every instant, neglecting the edge effects, the tempera- re distribution would remain unchanged with respect to a fixed coordinate ame. However, the ECV must be chosen large enough to satisfy the boundary nditions at the upstream and downstream ends with respect to the heat source.

As shown in Figure 2, the temperature T_ε of the material entering the control volume at the left side of the ECV can be assumed to be the composite/base-plate temperature sufficiently far away from the local heat source. For the right side of ECV, a gradient type boundary condition becomes applicable, indicating that the primary heat transport is due to the motion of the substrate rather than thermal diffusion. Considering the relatively shallow zone experiencing temperature variations and the high speed (relative to diffusion speed) of motion at this intersection, this assumption can be easily justified [11,14]. Moreover, it is assumed that the thickness of the composite substrate at the instant when the analysis is performed is at least an order of magnitude greater than the thickness of the prepreg tow (approx. 0.125 mm) being consolidated. Therefore, the effect of the ply-drop is assumed to be negligible, leading to a rectangular domain for the analysis as shown in Figure 2. The accuracy of this assumption increases with increasing substrate thickness. It is also assumed that the prepreg feed-tape is at a uniform specified temperature.

A change of variable is introduced by defining an excess temperature as $T = T_{act} - T_\varepsilon$ where T_{act} and T_ε are the material and ambient temperatures, respectively. q_0 indicates the amount of heat supplied by the localized heat source and can be absorbed by the composite over the exposed area. It has a non-zero value only in the interval $a - b \le x \le a + b$. A factor of A_e/A is introduced to modify the q_0 term at $y = y_2$ boundary condition for the numerical analysis. This term accounts for the effective area, on the surface of the composite, which absorbs heat and can be found using a control volume approach. For example,

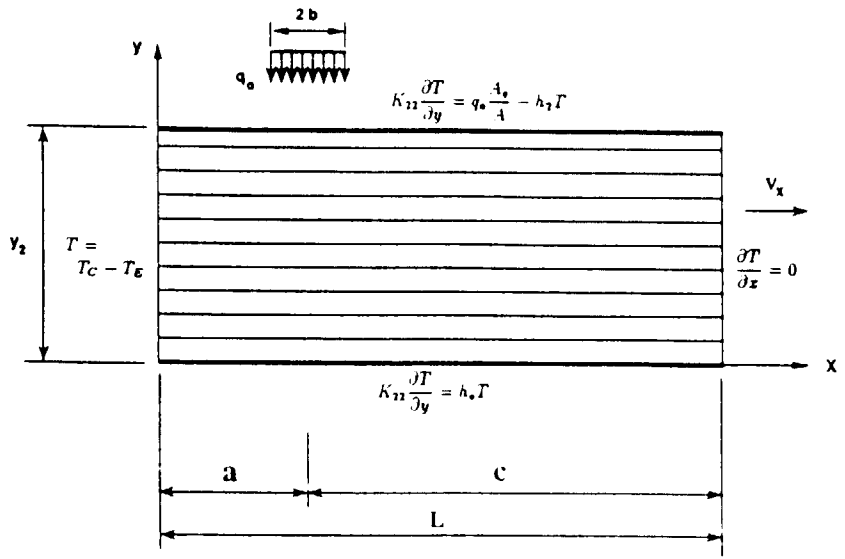

Figure 2. The anisotropic domain for the analysis and the boundary conditions used in generating the results.

istory of the upstream region (Gosman et al. [19], Anderson et al. [17], Güçeri [8]). The mesh parameters are modified using the Newton-Raphson method to nsure that mesh points lie on the boundary of the area exposed to the heat ource. Additional details of the numerical procedure can be found in the study f *in-situ* thermoplastic-matrix composite filament winding reported by Ghasemi lejhad et al. [14].

4. ACCURACY ASSESSMENT

For this study, APC-2 is taken as the composite material, and the average asso-iated properties used are those reported by Grove and Short [12], Cattenach and 'ogswell [20], and Blundell and Willmouth [21], with 60 percent fiber volume raction; i.e., T_f = 550°C, T_m = 340°C, T_g = 140°C, K_{11} = 6.0 W/m·°C, $_{22}$ = 0.72 W/m·°C, ϱ = 1.56 × 10^3 kg/m³, C_p = 1.425 × 10^3 J/kg·°C, and = 10^4 W/kg. U and C_p are taken as constants and obtained by averaging the alues from experimental data reported by Beyeler and Güçeri [11] and Ghasemi lejhad et al. [14]. The laminate is assumed to rest on a solid surface (base plate) esulting in a convection coefficient at the bottom surface of 10^3 W/m²·°C and ie top surface is exposed to air with a convection coefficient of 5 W/m²·°C Beyeler and Güçeri [11]).

Due to the presence of the exponential terms within the analytical solution with the material properties appearing in the power) difficulties are faced in ob-aining an analytical solution. However, to assess the accuracy of the numerical ode, the results obtained from the numerical method are compared with the ana-ytical solutions for smaller values of the material properties. To achieve this oal, all the material properties input into the problem were taken as those re-orted for APC-2 in the literature except the value of the heat capacity which was educed to 10 J/kg·°C. The value of the heat generation was also reduced to 10, ccordingly. The dimensions and processing parameters taken in this section are: = 0.005 m, c = 0.01 m, y_2 = 0.005 m, $2b$ = 0.002 m, T_c = 100°C, T_ε = 2°C, V_s = 0.05 m/sec, and q_0 = 4 × 10^5 W/m².

The temperature profile obtained analytically for the surface of the composite, /here the error is maximum, is given in Figure 3. The analytical results are ob-ained using the first 20 terms of the series. However, it should be mentioned that ie difference between the results obtained using 10 and 20 terms is insignificant, nd they remain practically unchanged beyond 20 terms.

The result obtained from the numerical method is also shown in Figure 3 for omparison with the analytical solution. A transformation on the x-axis (i.e., ' = $x - a$) is performed, in this figure, to clearly show the location of the heat ource at $x' = 0$. The relative error at the maximum temperature is 3%, and the iaximum relative error is 7%, which indicates excellent agreement between the nalytical solution and the numerical results.

5. PROCESSING WINDOW

In an effort to understand the effect of typical processing parameters on *in-situ* ape laying, a parametric study was conducted. Due to the limitations imposed by

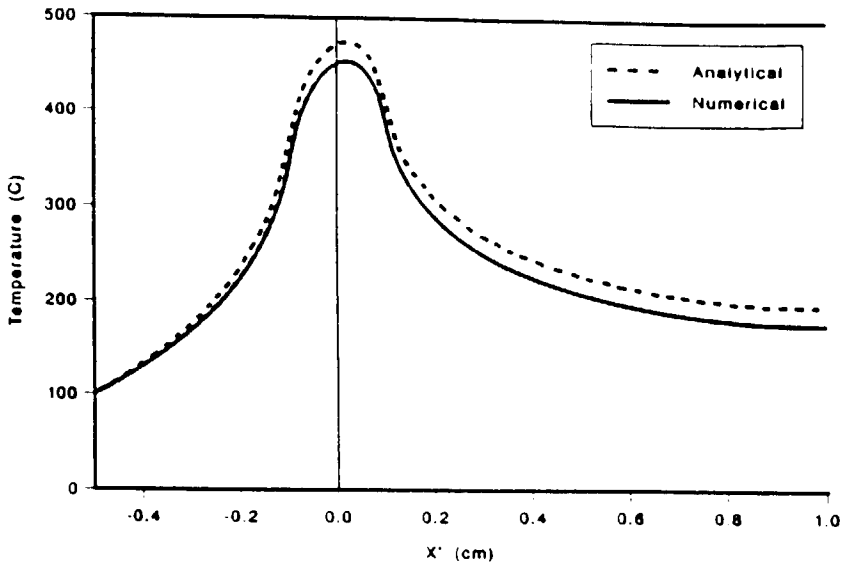

Figure 3. Comparison between the analytical and numerical results for the temperature profile at the top surface of composite (where the maximum error occurs).

the analytical solution concerning the material properties and realizing the close agreement between the analytical and numerical approaches, the numerical approach was used exclusively in the following analysis. APC-2 was taken as the composite material, and the associated properties are provided in the beginning of Section 4. U and C_p are taken as functions of temperature employing the experimental data reported by Beyeler and Güçeri [11] and Ghasemi Nejhad et al. [14]. For the process of *in-situ* tape laying, typical processing parameters were identified to be the heat intensity, q_0, the speed, V_s, and the width of the heater, $2b$ (see Figure 2). These parameters must be adjusted so as to prevent the degradation of the outermost surface while still assuring melt at the first ply interface. For the modelled process, T_c and T_ε are assumed to be 40°C and 22°C, respectively. A typical mesh concentration in the vicinity of the local heat source used in this study is shown in Figure 4. Figure 5 shows typical temperature contours within the laminate during the process.

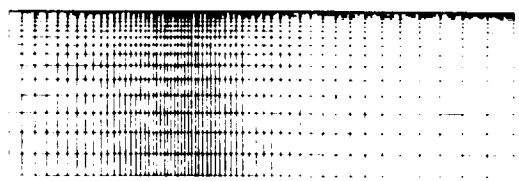

Figure 4. The non-uniform mesh used in the numerical analysis.

elated to heater width raised to some power less than one. In an attempt to tch the above noted trends, a variety of equation forms were fitted to the nurical data. For each equation form attempted, an iterative scheme using a Tayseries expansion of the particular equation was used to determine the "best," l least squares sense, values of all unknown coefficients. Surface and interface ximum temperatures were examined separately, although a common form was d for both. Equations with up to 10 unknown coefficients were investigated, h a total of 27 numerical trials used as the basis to determine the coefficient ues. Ultimately, the form that was found to provide the best fit of the numerical ximum temperature data was:

$$T_{max} = A + B(cq_0^{0.3} + Dq_0^{0.6} + q_0^{0.9})(EW^{0.3} + FW^{0.6} + W^{0.9}) \times \left[G\left(\frac{W'}{V}\right)^{0.3} + H\left(\frac{W'}{V}\right)^{0.6} + \left(\frac{W'}{V}\right)^{0.9}\right] \quad (43)$$

ere W is the full heater width or $W = 2b$. By the nature of its determination, uation (43) is valid only over the interpolated region of the input data (see Figs 11 and 12). This corresponds to $150°C \leq T_{max} \leq 1000°C$ in Equation 3). For the 27 temperature distributions determined using the numerical heat nsfer analysis, Equation (43) was able to fit all of the maximum interface and rface temperature values within 3%. The optimum values of the coefficients are pplied in Table 1. These values are based on a tape thickness of 0.005 inches. ice the "best fit" coefficients were determined, Equation (43) was then used to ovide those values of heat intensity, heater width and speed which produced the sired maximum temperatures at the interface and at the surface. Once again, the interface the minimum condition is $T_{interface}$ equal to T_m, while at the surce the maximum condition is $T_{surface}$ equal to T_d. Replacing T_{max} in the interface

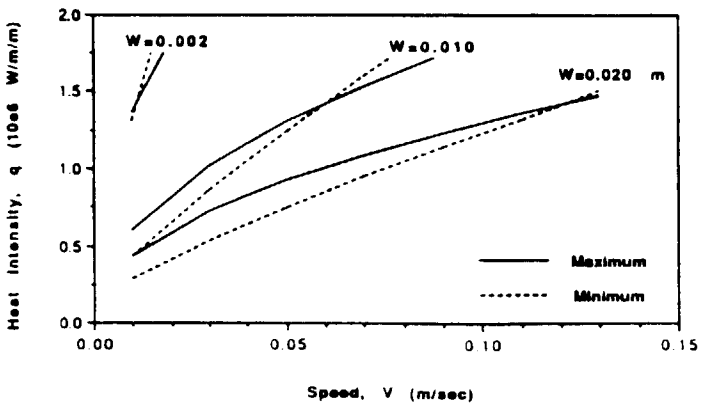

gure 11. Processing windows for various heater widths W = 0.002 m, 0.010 m, and 020 m. Note that the processing window is bound by polymer degradation (upper limits) id insufficient melting (lower limits).

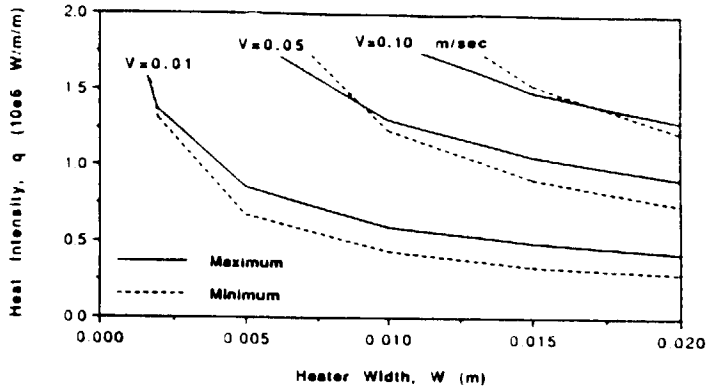

***Figure 12.** Processing windows for various processing speeds V = 0.01 m/sec, 0.05 m/sec, and 0.10 m/sec. The processing windows are bound by the polymer degradation (upper limits) and insufficient melting (lower limits).*

and surface forms of Equation (43) with T_m and T_d, respectively, provides the lower and upper bounds of the processing window. This approach resulted in the typical plots shown in Figures 11 and 12 where the dashed line indicates the minimum process conditions and the solid line represents the maximum conditions. The processing window is the zone above the dashed line and below the solid one. It should be realized that Figures 11 and 12 are two views of the process surfaces.

As can be seen in Figure 11, for a heater width of 0.002 m (i.e., $b = 0.001$ m), no viable process conditions exist for speeds greater than 0.01 m/sec. If the curves are extrapolated, a narrow processing window does exist for speeds below 0.01 m/sec. At the other extreme, for a heater width of 0.02 m (i.e., $b = 0.01$ m) viable processing conditions can be found for speeds up to approximately 0.12 m/sec, with heat intensities ranging up to approximately 1.4×10^6 W/m^2.

Figure 7 shows that the temperature decreases with increasing processing

Table 1. Coefficients for Equation (43).

	Interface T_{max}	Surface T_{max}
A	52.745	53.613
B	-4.125×10^{-3}	1.955×10^{-6}
C	-724.55	187.110
D	18.550	-13.881
E	0.556	-0.101
F	-0.996	-1.450
G	1.452	-11.318
H	-5.255	-13.536
I	0.727	0.0

eed for a given heat intensity and heater width; however, to achieve sufficient elting the heat intensity should increase. It is found that the temperature gradit through the thickness increases with increasing processing speed and heat inisity. Therefore, the height of the processing window decreases with increasing ocessing speed for a given heat source width. Also, Figure 11 shows that for a ven heat intensity, an increase in the heat source width not only increases the ea of the processing window but also increases the processing speed which, in rn, increases the production rate. Of some interest is the fact that for the heater idths shown, no viable process conditions exist for heat intensities in excess of iout 1.4×10^6 W/m², and the maximum viable heat intensity drops only ightly with increasing width.

Examining Figure 12, the dependence on heater width becomes evident. For eeds in excess of 0.1 m/sec, the interpolated results show limited process conditons. However, at speeds of 0.01 and 0.05 m/sec a range of conditions is possible. f interest is the anticipated inverse relationship between heater width and heat tensity. From a process development viewpoint, there is a diminishing value in ing progressively wider heat zones. Except for the leftmost edge of the processg window, the process appears to be relatively insensitive to changes in heater idth, but allows only small variations in heat intensity.

From a practical viewpoint, Figures 11 and 12 are the key to the development f a viable process. Although the data presented here was interpolated only from ie initial numerical analysis results, it appears that to maximize output, i.e., to iaximize velocity, one should use a heater width of at least 0.02 m. This 0.02 m eater width would allow for speeds above 0.1 m/sec; however, in this range the rocessing window is very small. Clearly, well-focused lasers are not at all uitable for the example developed herein. Unless a very high degree of process ontrol is employed, one would be wise to operate below the maximum allowable elocity in order to "widen" the processing window, which allows for some variaon in the absorbed heat intensity without adversely affecting part quality. Fially, regardless of the heater width and speeds used, heating devices which proide absorbed intensity less than 0.25×10^6 W/m² and greater than 1.4×10^6 W/m² are of little to no value.

The effect of the consolidation roller at the top surface of the composite was aken into account by modifying the top surface boundary condition. This effect vas found to be insignificant due to the fact that the contact area is extremely mall compared with the total top surface.

The number of nodes taken in the analysis is 61×21 in the x and y directions, espectively. Doubling the number of the nodes had an insignificant effect on the esults obtained. Since the computational model relied on experimental measurenents of thermal properties which do not have similar accuracies, the results vere considered to be satisfactory. The Gauss-Seidel iteration method is emloyed in the numerical analysis. The convergence tolerance (i.e., the relative error between the consecutive values of the iterations) was taken as 10^{-4}. Successive over/under relaxation did not enhance the convergence in this study. Additional information on the numerical study will be reported in [22].

The above example was developed to demonstrate the usefulness of the numerical technique in developing and analyzing a given fabrication process. All parameters are easily adjusted to suit any alternate process. Typical run times for a single case require 1 to 5 minutes of cpu time on a VAX 11/780. Unusual geometries and drastic temperature variations may require considerably more time.

6. CONCLUSIONS

Analytical and numerical thermal analysis for *in-situ* thermoplastic tape laying using a local heat source are presented. The results show large temperature gradients in the vicinity of the local heat source. The accuracy of the numerical method is assessed by comparing its results with those obtained from the analytical analysis. Very good agreement exists between the two methods. Using the more general numerical technique, the influence of the processing speed, heat flux and heater width on the nature of the overall heat transfer is demonstrated. A methodology is presented to characterize all viable processing conditions based on a finite set of numerical results of the general problem. The processing window is shown to vanish as heater width decreases, speed increases or heat intensity increases. Indeed, bounds on all three conditions are indicated.

The availability of such an analysis is expected to provide the basis for future studies on heating/cooling rates, microstructure, and state of residual stresses. It also forms a bridge linking processing, microstructure, and material performance, which are strongly coupled in the case of composite materials.

NOMENCLATURE

A_q/A	nodal area fraction for the surface exposed to the heat source
a	upstream distance from the heat source, m
b	half-width of the heat source, m
c	downstream distance from the heat source, m
C	heat capacity, J/kg·°C
D	a constant in the analytical solution
G	a constant in the analytical solution
h_0, h_1	convection coefficients, W/m²·°C
h	maximum length in numerical transformations
K_{11}	conductivity in x-direction, W/m·°C
K_{22}	conductivity in y-direction, W/m·°C
q_0	absorbed heat supplied by the heat source, W/m²
T	temperature, °C
U	heat generation, W/kg
V_x, V	processing speed, m/sec
W	width of the local heat source, m
x, y	Cartesian coordinates, m
x'	x-axis shifted to the location of the heat source, m
$\bar{x}, \bar{y}$	transformed Cartesian coordinates, m
$\bar{x}_r$	$\bar{x}$ at the right-hand side boundary, m
$\bar{y}_t$	$\bar{y}$ at the top-surface boundary, m
$\bar{x}_{bm}, \bar{x}_{bp}$	$\bar{x}$ at the left and right edges of the local heat source, m

V. ON THE FLY CONSOLIDATION

A. Introduction

Consolidation during automated tow placement, a.k.a. "on the fly" or "in-situ", requires that void elimination and resin adhesion be accomplished in the short periods of heating and pressure rolling that follow towpreg placement by the robot head. For thermosets it also includes the resin curing process, and for semi-crystalline resins some degree of crystallization.

As mentioned in the previous section, research on "on the fly consolidation" is being conducted at Hercules, Boeing, MacAir, and by Cincinnati Milacron with Thiokol. During their visit last September to ICI, Paul Hergenrother and Maylene Hugh learned about ICI's research. See following pages, especially the towpreg development summary and areas for future research. Note, for example, the tow laying speeds are 1.5 inches per second, which with a compliant roller correspond to pressure intervals of about one second.

During a trip to Boeing last September, Paul Hergenrother, Ruth Pater and I toured the B-2 wing fabrication facility and discussed fabrication concerns Boeing has with composite parts they currently make for commerical aircraft. We also were appraised of their plans for composites in the 777 aircraft. Automated six inch tape laying is used for the B-2 wing. Hand layup is needed in difficult areas. After layup the wing is placed in a 90 foot long, 27 foot diameter, autoclave for curing, with subsquent C-scanning in an equally large test facility. Tape gaps are about 1/8 inches for the automated laying process.

An important ATP discussion topic during our meeting was the difficulty with layup on concave surfaces where tack causes problems. It was agreed that"tack on demand" could solve this problem. That is, a tackless towpreg, or tape, could more easily be placed on the concave surface and simultaneously tacked to it, avoiding the current air pocket problems when laying tacky tape on concave surfaces.

Prior to discussing aspects of rapid consolidation, heat transfer, and voids, a brief review of some of the physical factors involved seems worthwhile. Features of the robot head were outlined in the previous section on ATP. Once the towpreg band, of up to 32 tows, is laid on the surface, it is heated over a length ranging from a

Key Equipment

from Visit by Paul & Mayfield Sept 1991

- **Automated Dynamics Corporation**
  Processing Head Technology
  - Hot Gas Heat Source
  - Pressure Applied Through Compaction Roller Assembly
  - Computer Controlled, Electro-Mechanical System

- **ICI Fiber Placement Platforms:**

  Research Cell
  - 4-Axes Winder
  - 1/4" Tow / Tape
  - Part Sizes Approaching 24" Diameter and 20" Length

  En-Tec
  - 6-Axes Winder
  - 1/4", 1" and 3" Tow / Tape
  - Part Sizes Approaching 52" Diameter and 120" Length

.4lb/hr - .9lb/hr. w/ 1/4" tape.

97 C-2

ICI COMPOSITE STRUCTURES

In-Situ Consolidation Process Optimization
Design of Experiments – Fractional Factorial
APC2/AS4 – Initial Results

Rate (ips)	Temperature (°F)	Compaction (lbs.)	Flow (scfh)	ILSS (ksi)
1.5	1550	56	110	9.30
1.5	1550	9	90	8.99
1.5	1350	56	90	8.10
1.5	1350	9	110	6.86
0.5	1550	56	90	13.60
0.5	1550	9	110	11.90
0.5	1350	56	110	11.30
0.5	1350	9	90	9.57

DESIGN OF EXPERIMENTS PRELIMINARY CONCLUSIONS AND RECOMMENDATIONS FOR FUTURE WORK

- Initial results indicate that autoclave consolidated properties achievable with in-situ consolidation
- Feed rate is most significant process parameter given current equipment
- Minimize process dependence on feed rate by:
  - Improving material quality
  - Increasing compaction load capability
  - Increasing time under pressure (eg, compliant compaction roller)

Tow Development Task

1st Level Testing (Screening)

NOL Tubes (5.75" ID x 0.125" thick x 3" long, all hoop orientation)

1. Density/Resin Content/V_f, V_V
2. Photomicrograph/Image Analysis
3. DSC/GPC (Depending on polymer selected)
4. C-Scan (pulse echo)
5. Short Beam Shear (ASTM D2344)
6. Split-D Tension (ASTM 2290)

2nd Level Testing (Performance Assessment)

Flat Panels

1. Density/Resin Content/V_f, V_V
2. Photomicrograph/Image Analysis
3. C-Scan (thru-transmission, pulse echo)
4. Filled-Hole Tension per BSS 7320
5. Open-Hole Compression per BSS 7260
6. DCB (6ic) per BSS 7273

Tow Development Task

1st Level Testing (Screening)

NOL Tubes (5.75" ID x 0.125" thick x 3" long, all hoop orientation)

1. Density/Resin Content/V_f, V_v
2. Photomicrograph/Image Analysis
3. DSC/GPC (Depending on polymer selected)
4. C-Scan (pulse echo)
5. Short Beam Shear (ASTM D2344)
6. Split-D Tension (ASTM 2290)

2nd Level Testing (Performance Assessment)

Flat Panels

1. Density/Resin Content/V_f, V_v
2. Photomicrograph/Image Analysis
3. C-Scan (thru-transmission, pulse echo)
4. Filled-Hole Tension per BSS 7320
5. Open-Hole Compression per BSS 7260
6. DCB (6ic) per BSS 7273

Areas for Future Research

- Thermoplastic Tow Development
  - Tailor to In-Situ Processing Requirements
- Complaint Roller Development
  - Increase Throughput and Improve Processing of Complex Contoured Parts
- Tooling Concept Development
  - Cost Effective Tooling Concepts for In-Situ Processing of Large Complex Curvature Skins
- Low Cost Feedstock for Stamping Process
  - Alternative to Preconsolidated Sheet

few inches to about one foot and then pressure rolled.

The roller footprint depends upon the roller diameter and the initial and final thickness of the compressed towpreg. Ardichivili (17) and Gaskell (1) developed equations for the length ,L, of the roller footprint from the point of initial contact to the nip. The sketch below illustrates the situation.

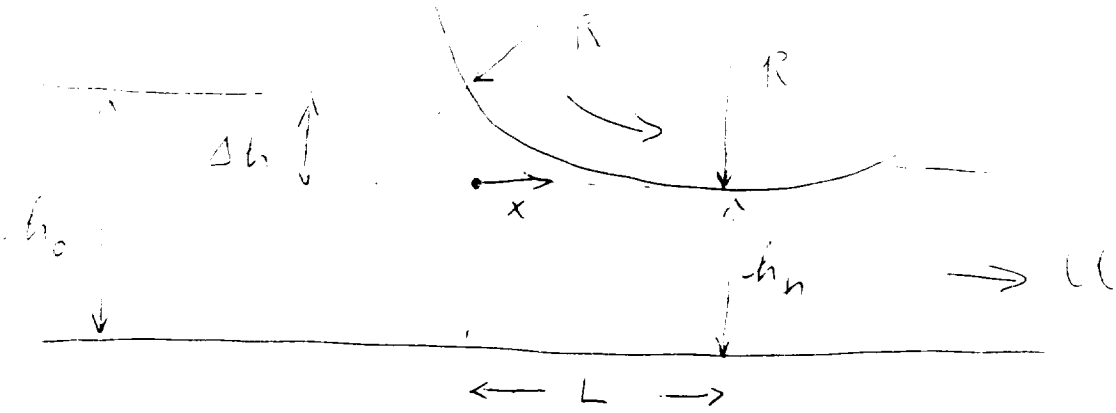

As indicated in the figure: h_o is the thickness at the initial point of contact, h_n is the nip thickness, R the roller radius, and U the linear speed. For the right triangle with sides R and L and hypotenuse approximated by R + Δh,

$$(R + \Delta h)^2 = R^2 + l^2$$

assuming that $(\Delta h)^2 << 2(\Delta h)R$ and L^2

$$L = [(h_o - h_n)2R]^{1/2}$$

or

$$h_o = h_n + L^2/2R$$

Using this relationship they further assumed that along the footprint length L, the variation in h was approximated by the relation

$$h = h_n + (L - x)^2/2R$$

This expression for thickness as a function of distance was used in through-the-thickness resin flow models to calculate the pressure profile as the material passes through the nip region. Ardichvili (17) obtained:

$$P = 4\mu UR(h - h_n)/gh^2$$

This equation adequately predicts the peak pressure for both Newtonian and non-Newtonian fluids, but does not fit the profile for non-Newtonian flow. Gaskell (1) extended the analysis to non-Newtonian flow pressure profiles,

obtaining a fairly complex equation that gives good agreement with experimental data.

This equation for the pressure required during through the thickness resin flow can be used to illustrate a significant difference between calendering and on-the-fly consolidation.

For a high flow resin having a viscosity of 10 poise, at a roller speed of 0.01 m/sec, with a roller diameter of 0.3 m, an initial tow thickness of 0.00020 m and a nip space of 0.00015 m, substituting gives L = 0.0055 m and P = 133 atm. For a roller width that accommodates 32 tows each 1/8 inches wide (0.0022 m) and assuming the roller footprint is 2L = 0.011 m, to deliver 133 atm of pressure the weight applied to the roller mount must be 12,700 kg (28,000 pounds).

It is unlikely that most tooling could be designed to accommodate such heavy weight. Thus, through-the-thickness resin flow, as is used in calendering between two rollers, is ruled out for on the fly consolidation. Prepregged tows need to be used so that roller pressure over the tool surface serves only to force rein and fibers into towpreg gaps and to ensure adhesion at the laydown surface.

Other dimensional aspects of concern are the range in towpreg widths and resulting tow gaps. The data reported by Enders and Hopkins (15) for 1/8 inch (3.0 mm) wide towpreg, having rectangular cross section, showed width variations of as much as 0.4 mm. The laid down tow gaps average about 0.20 mm. Hercules (13) reports laid down tow gaps of 0.75 mm with 1/4 inch towpreg tape.

Finally consideration must be directed toward what might be considered commercial ATP speeds. A 12 k AS-4 towpreg (35 wt% resin) weighs 1.3 g/m. For 32 towpregs, the weight per meter of length would be 43 g/m. A tape laying rate of 1 m/sec corresponds to 42 g/sec or 333 pounds per hour, which may be an acceptable commercial rate. As will be discussed in a later section, a speed of 1 m/sec is within the ATP heat transfer process window. It may not be within the pressure process window.

Compliant roller footprint lengths are about 1 cm, so that roller compression time would be 0.01 seconds at a speed of 1 m/sec. Ultrasonic pultrusion of powder coated tow has been achieved in times of about 0.25 seconds, which suggests that consolidation at 1 m/sec may not be possible. For a compression time of 0.25 seconds, the laydown rate would be 4 cm/sec or 13.3 pounds per hour. Using two rollers in sequence might double the rate. Other methods of achieving high rate may be

possible through optimization of towpreg architecture.

B. Consolidation

The August 27 memorandum reviewed consolidation processes and highlighted those aspects that are important for the use of textile and robotic technology in part fabrication. It began with a discussion of material preparation, or pre-consolidation, and the differences between hot melt, solution, commingled, and powder coated prepregs. This was followed by a discussion of fiber wetting, bulk (initial) consolidation, resin flow, polymer interface adhesion, and relaxation of network elastic stresses, all of which occur more or less in sequence during the consolidation process.

Attention in this section is directed toward the rate at which the various phases of consolidation take place. Because they have already been polymerized, thermoplastics can be processed faster than thermosets. In addition, heat transfer is simpler because thermoplastics need only to be heated, whereas thermosets must be heated and then cooled to remove the polymerization heat of reaction, see previous section on pultrusion.

For ATP the towpreg must be produced as a stiff ribbon with less than one percent voids, see subsequent discussion of voids. For weaving, to retain flexibility, the powder coated tow receives only enough heat to adhere particles to the fibers. During the brief heating period, thermoplastics retain much of their particle shape, while high flow thermosets flow over the fibers forming a sheath or film coating.

The theory for the wetting of fibers by polymers follows the work of Brochard (18),who studied the spreading of liquid drops on thin cylinders. Surface tension and long range van der Waals forces govern the spreading process and the coating sheath formation, see following pages. The capillary penetration of polymer melt into a slit was investigated by Van Oene, et. al. (19). Examination of the role of surface tension and wetting angle indicates that for a polymer having a viscosity of 1,000 poise the wetting times are of the order of 5 seconds, see following pages.

Bulk consolidation, resulting in intimate contact at the polymer-polymer interface at numerous sites, requires network deformation and polymer flow. The rate of compaction depends upon the equipment used. For a roller compaction will occur in fractions of a second, depending on rpm and radius. As pointed out in the introduction to this section, through the thickness resin

Spreading of liquid drops on thin cylinders: The "manchon/droplet" transition

F. Brochard
Laboratoire de Physique de la Matière Condensée, Collège de France, 11 Place Marcelin-Berthelot, 75231 Paris Cedex 05, France

(Received 29 May 1985; accepted 2 January 1986)

We discuss the spreading of liquids on thin cylinders (radius b), including the effects of long range attractive van der Waals (VW) forces. For volatile liquids, the vapor adsorbs on the cylinders; the thickness e of the film is given by a balance between the disjoining VW pressure and Laplace pressure ($e^3 = ba^2$, where a is a molecular size). For nonvolatile liquids, a liquid drop cannot spread out over the cylinder if the spreading coefficient S is smaller than a critical value S_c. For $S = S_c$, we find a first order transition between a droplet and a sheath structure ("manchon"). For $S > S_c$ the droplet spreads indefinitely. The thickness of the manchon is equal to the thickness reached by a drop spreading over a plane surface. We also calculate the liquid profile just below the threshold S_c. When $S \to S_c$, a precursor manchon appears at the two poles of the droplets.

I. INTRODUCTION

The wetting of fibers has many important industrial applications (dyeing, protection, and greasing of synthetic fibers in the textile industry, hair industry, etc.). However the spreading of a liquid on a thin cylinder is far less understood than the wetting on a plane surface.

1. *On a flat solid*: A nonvolatile liquid drop spreads *partially* until a finite contact angle θ_e is established, or *completely*, depending upon the "spreading coefficient" S,

$$S = \gamma_{SO} - \gamma_{SL} - \gamma, \tag{1}$$

where γ_{SO} and γ_{SL} are the interfacial energies between solid/air and solid/liquid and γ is the liquid/air interfacial tension.

$S < 0$ correspond to partial spreading. The liquid forms a spherical cap (if gravity is negligible: small droplet); the contact angle θ_e is given by $\cos\theta_e = (\gamma_{SO} - \gamma_{SL})/\gamma$.

$S > 0$ corresponds to total wetting and has been analyzed in detail by Joanny and de Gennes.[1] The drop spreads out over the surface to form a "pancake." Contrary to common belief the liquid does not always spread down to a monomolecular layer. The thickness $e(S)$ of the pancake is fixed by a competition between S and long range forces—essential for thin films—which tend to thicken the film. For pure VW forces the result is

$$e(S) = a\sqrt{\frac{3\gamma}{2S}}, \tag{2}$$

where a is a molecular size. In general, $\gamma/S \simeq 1$ and $e_{(S)} \simeq a$. But if S is small, $e(S)$ can be relatively large. With $\gamma/S \simeq 10^2$, $a \simeq 3$ Å, one expects $e(S) \simeq 30$ Å.

2. *On a thin cylinder (radius b)*: The situation is quite different. The threshold between wetting and nonwetting cannot be exactly at $S = 0$. To understand this, we discuss first two extreme limits: (a) $S = 0$ and (b) S positive and large.

(a) The case where $S = 0$ exactly has been discussed by Carroll.[2,3] Then a drop of large size, when put into contact with a long fiber, does not spread out. In a flat geometry, a film can build up because (for $S = 0$) the increase in liquid/air surface energy at the outer surface (γ) is balanced exactly by a gain in interfacial energy at the solid ($\gamma_{SO} - \gamma_{SL}$) surface. But, to cover a fiber, we need more area at the outer surface (radius $b + e$, where e is the film thickness) than at the inner surface (radius b).

In fact, the macroscopic equilibrium shape of a droplet for this special case $S = 0$ has been computed; it does not extend at infinity along the fiber. The shape is mostly spherical, with two small protruding regions (of nearly zero total curvature) in the direction of the fiber (Fig. 7).

(b) On the other hand, if S is large and positive, the liquid will clearly wet the fiber; the curvature of the fiber (which is very weak at the molecular level) cannot suppress the wetting.

Thus in between the two regimes (a) and (b) there must exist a critical value S_c for wetting. This paper analyzes the structure of S_c for the simple case of pure van der Waals fluids. Most of our attention will be focused on nonvolatile fluids, where the solid–gas interface is "dry." However, for reference, it will be useful to discuss also the case of strongly volatile fluids, where the vapor and the fiber are everywhere in equilibrium; in this case we always have a liquid film on the fiber, but the equilibrium thickness of this film will depend on the fiber radius.

In Sec. II we define the appropriate free-energy functionals (free energy for the dry case, where the number of liquid molecules is fixed, and grand chemical potential for the wet case). In Sec. III we derive the equilibrium film thickness $e(b)$ for the wet case. In Sec. IV we return to the dry case, and discuss in detail the wetting transition at $S = S_c$. Below S_c we have a droplet and a dry fiber. Above S_c we have a manchon (sheath) covering the fiber—possibly coexisting with a residual droplet. Section V is devoted to a numerical analysis of the shapes. The physical implications of the manchon structure are discussed in Sec. VI.

II. FREE ENERGY OF A LIQUID ON A CYLINDER

A. Long range forces

An essential observation, going back to Derjaguin,[4] is that thin liquid films are very sensitive to long range forces. This can be described in term of a long range energy P (per unit area of film) depending upon the thickness ζ of the film.

 0021-9606/86/084664-09$02.10

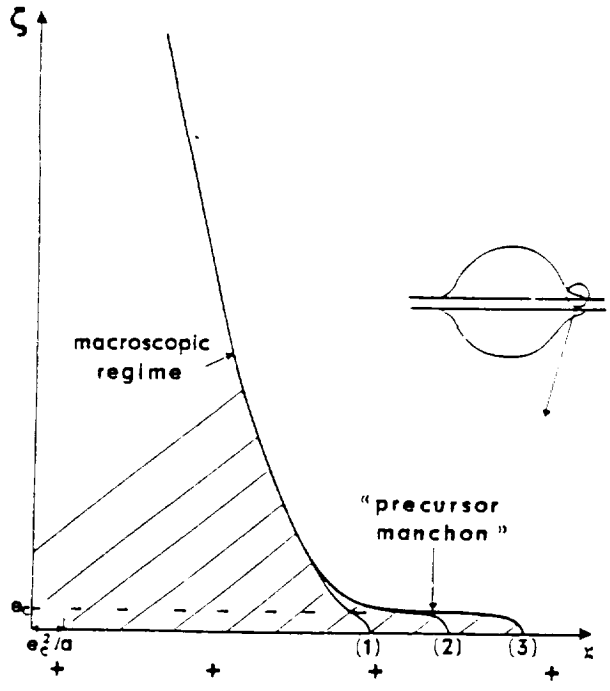

FIG. 7. Profile of a droplet on a cylinder for $S<S_c$. If $S \to S_c$, a precursor manchon appears on the two poles: (1) $(S-S_c/S_c)=\frac{1}{3}$; (2) $(S-S_c/S_c)=\frac{1}{3}\times10^{-3}$; (3) $(S-S_c/S_c)=\frac{1}{3}\times10^{-4}$, calculated numerically from Eq. (30) by Levinson.

$$\zeta_l/e_c = 1 - e_c/a\sqrt{\frac{2S}{3\gamma}}$$

in Eq. (34):

$$a\frac{x_l}{e_c^2} = \frac{1}{\sqrt{3}}\log 2\frac{(\sqrt{3}-1)}{(\sqrt{3}+1)} - \log\frac{e_c}{3a}\sqrt{\frac{2\Delta S}{3\gamma}}. \quad (43)$$

At $a=1$, $e_c=10$, $\Delta S/S_c=\frac{1}{3}\times10^{-4}$, then $x_l=310$ Å. The size α of the manchon diverges at S_c:

$$\alpha \sim \xi\left|\log\frac{(S-S_c)}{\gamma}\right|, \quad (44)$$

where $\xi=e_c^2/a$ is the scale length of variation of ζ near $\zeta=e_c$.

B. Droplets on a horizontal fiber

This case is more complex because p_0 has to be adjusted. We calculate now the shapes of the droplets, stable for $S<S_c^*$, and the profiles of the manchon, stable for $S>S_c^*$, near the contact line where S_c^* is given by Eq. (23).

1. $S<S_c^*$: Regime of droplets (Fig. 7)

For $S<S_c^*$, the liquid does not wet the fiber. *Macroscopically*[6]: one observes an "unduloidal" droplet. The shape, largely discussed in the literature,[26] is a sphere of radius R which matches the cylinder with a near zero surface curvature (Fig. 7). The internal pressure is $p_0=(2\gamma/R)$. The apparent contact angle is given by the Young equation if $S<0$ and is zero if $S>0$.

Microscopically: the profile at the top of the drop ($\zeta<b$) is given by

$$\tfrac{1}{2}\left(\frac{d\zeta}{dx}\right)^2 - \frac{\zeta}{b} - \frac{a^2}{2\zeta^2} + \frac{2\zeta}{R} = -\frac{S}{\gamma}. \quad (45)$$

The additional term $2\zeta/R$ is negligible compared to the term ζ/b and can be omitted. The previous discussion (vertical ascension in zero gravity) applies; when $S \to S_c^*$, a "precursor" manchon appears at both end of the droplet. It is shown in Fig. 7 for three values of $(S-S_c)$. At the critical value of S ($S=S_c^*$), the size of the manchon is from Eqs. (23) and (38),

$$\alpha = \xi\left|\log\frac{e_c}{R}\right| \quad (46)$$

with $e_c=100$ Å, $\xi\simeq1\,\mu$, and $\alpha\simeq$ several μm.

2. $S>S_c^*$ = manchons

For $S>S_c^*$, the droplets spread out on the fiber. The profile is deduced from Eq. (29) with p_0 given by Eq. (26). It leads to

$$\tfrac{1}{2}\dot{\zeta}^2 - \frac{a^2}{2\zeta^2} - \frac{a^2}{e^3}\zeta = -\frac{S}{\gamma}. \quad (47)$$

The profile starts with a sharp edge at $x=x_0$ [$\zeta\sim\sqrt{a(x-x_0)}$] and reaches the equilibrium thickness $e=\sqrt{(3\gamma)/(2S)}\,a$ in a distance e^2/a.

C. Remark: Cylinder of finite size

If $S>S_c^*$, the droplet spreads out over the cylinder. If the size L_F of the cylinder is smaller than the size L of the manchon, the drop cannot spread, as explained in Sec. IV D; we expect a drop and a film. The pressure inside the precursor film has to be zero. The film thickness is then equal to e_c whatever the value of S, provided that $S>S_c^*$. The profile is then given by Fig. 6(c) as for a vertical cylinder in contact with a reservoir when $S>S_c$ in the range $\zeta>b$.

VI. CONCLUSIONS

(1) A liquid droplet spreads over a thin cylinder only if the spreading coefficient S is larger than a threshold value S_c. Equivalently for a given pair solid + liquid characterized by (S,γ), a cylinder of radius b can be wet by the liquid if $b>b_c$,[7] $b_c=a(3\gamma/2S)^{3/2}$. When $\gamma/S\simeq1$, b_c is very small. But if $\gamma/S\simeq100$, $b_c\simeq1\,\mu$. One can currently produce ultra thin fibers of radius ranging from 100 to 1 μ. By monitoring the spreading of small droplets on fibers of different sizes, it will be possible to test our theoretical predictions for b_c. For $S>S_c$, a droplet flows out from both poles to form the stable manchon. A simple way to display the apparition of the manchon is to start with two small droplets: as the two manchons touch each other, the smaller droplet will flow into the larger droplet through the manchons. On the other hand, if $S<S_c$ the two droplets will be stable.

The manchon could be detected by various methods: (a) electrically using a conducting liquid and measuring the electrical resistance between two electrodes attached on the fiber; (b) for dielectric liquids on a metallic fiber, the thickness e could be derived from capacitive measurements; (c) optically: using the available optical fibers, and observing the changes in propagation features induced by the film.

The Rheology of Wetting By Polymer Melts

H. VAN OENE, Y. F. CHANG AND S. NEWMAN

Ford Motor Co., Scientific Research Staff
Dearborn, Michigan 48121

(Received November 20, 1968)

ABSTRACT

Theoretically, the rate of capillary penetration of a polymer melt into a slit, a model for a surface irregularity, has been shown to depend on $\gamma\cos\theta/\eta$ where γ refers to the surface tension of the liquid, η its viscosity and θ a time-dependent contact angle. Analytical expressions relating the depth of penetration with time have been experimentally verified by observations of the penetration of molten polyethylene and poly-(ethylene-vinyl acetate) into aluminum channels. Values of η, calculated from the observed data, agree closely with independent determinations of this material parameter. A theoretical treatment has also been developed which describes the velocity of spreading of a liquid drop over a flat surface. Flow equations for the flow of free films were adapted for this purpose. The spreading velocity is predicted to depend on the product of three factors (1) a scaling factor, $(\gamma/\eta R_o)$, where R_o is the initial radius of curvature; (2) $\cos\theta_e\ (1-\cos\theta/\cos\theta_e)$ where θ_e refers to the equilibrium value of θ, and (3) geometric terms. After demonstrating that a drop of molten polymer may be treated as a spherical cap, the predicted dependence of spreading rate on drop size, $\cos\theta_e$ (nature of the substrate) and the scaling factor was experimentally verified. Some discrepancies noted at long times and high temperatures are discussed.

INTRODUCTION

THE FORMATION of an adhesive bond between an adhesive, organic coating or polymer melt and a surface depends on the development of a maximum area of molecular contact and the displacement of air from surface irregularities. While much attention has been given to the thermodynamics of wetting and adhesive forces, little quantitative work has been carried out on the rate of approach to equilibrium conditions for viscous systems.

Accordingly, the flow of a polymer melt over a surface under the influence of surface tension forces has been studied by observing separately (a) the kinetics of spreading of a drop—to obtain information about the mechanism of surface transport, e.g., viscous flow or surface diffusion, and (b) the rate of penetration into a channel or slit—a system which is a model for a surface irregularity. The important factors controlling the rate of wetting were

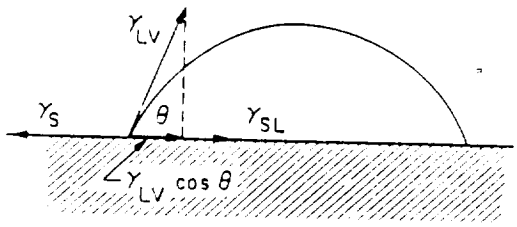

Figure 1. Surface tension forces acting at the perimeter of a sessile drop.

Where γ_S is the surface tension of the solid substrate,* γ_{SL}, the surface tension acting in the solid/liquid interface and γ the surface tension of the liquid in equilibrium with its vapour. At equilibrium one has, from Young's equation:

$$\gamma\cos\theta_o + \gamma_{SL} = \gamma_S \tag{9}$$

hence $F \to 0$ as $\cos\theta \to \cos\theta_o$.

The surface tension forces act at the perimeter of the drop. The total force/unit volume acting on a sessile drop of volume $V_o = 2\pi/3(R_o)^3$ is therefore:

$$\frac{2\pi r F(t)}{V_o} = \frac{2\pi r\ \gamma\cos\theta_o}{V_o}\left[\frac{\gamma_S - \gamma_{SL}}{\gamma\cos\theta_o} - \frac{\cos\theta}{\cos\theta_o}\right]$$

$$= \frac{3\ r\gamma\cos\theta_o}{R_o^3}\ [1 - \cos\theta/\cos\theta_o] \tag{10}$$

The maximum shear stress is therefore:

$$\tau_{max} = \frac{3r\gamma\cos\theta_o}{R_o^3}\ [1 - \cos\theta/\cos\theta_o]\cdot\delta \tag{11}$$

and the velocity of spreading:

$$\langle V\rangle = \frac{\gamma\cos\theta_o}{\eta}\ [1 - \cos\theta/\cos\theta_o]\ (r/R_o)\ (\delta/R_o)^2 \tag{12}$$

It remains to find a suitable expression for δ^2, the equivalent thickness of the drop. When the drop shape can be approximated by that of a spherical cap, it is possible to determine δ directly by means of Equation (6), since the volume of liquid ΔV that has left the domain of the original hemisphere can be calculated; the volumetric flow rate Q follows by differentiation of ΔV with respect to time. The exact equivalent width, remains, however, still to be determined.

* It is not necessary or possible to specify the surface tension of the solid explicitly, since the exact composition of the substrate surface is not known. Even though the present experiments are carried out on aluminum plates, the surface layer probably consists of hydrated aluminum oxide.

shape of a series of regularly shaped objects, differing only in size, are related to each other by the expression:

$$\Delta t_2 = R_2/R_1 \cdot \Delta t_1$$

where R_1 is a characteristic dimension of object 1, R_2 that of object 2; Δt_1 the time required for a certain change in the shape of object 1 and Δt_2, the time required for the same change a shape for object 2. Since the whole r/R_o vs t curve is shifted by R_2/R_1, this means also that from the shape of the r/R_o vs t curve no specific flow mechanism can be inferred.

Even though polymer melts are very non-Newtonian, the effect of a non-Newtonian viscosity has been neglected. This is justified in view of the small shear rates involved. Taking $<\delta> \approx \frac{1}{4}h$, one obtains from Eqn. (11) a value of the max shear stress, at $t = o$, of 225 dynes/cm^2. For a liquid with a viscosity of 10^3 poises, the smallest viscosity encountered in this work, the max. shear rate would be only ~ 0.2 sec^{-1}. If corrections for non-Newtonian flow are necessary, the equations for the flow of such a film, derived by Biermann [7], should be used.

Comparing the two expressions for the spreading velocity and the rate of penetration into a slit:

$$<v> = d(r/R_o)/dt = (\gamma/\eta R_o)\cos\theta_o\,(1 - \cos\theta/\cos\theta_o)\,f(\theta) \quad \text{(spreading)}$$

$$<v> = dl/dt = H/6\,(\gamma/\eta)\,\frac{\cos\theta}{l} \quad \text{(penetration)}$$

the question arises whether or not the time dependence of $\cos\theta$ measured in the drop spreading experiment can be used to calculate the rate of penetration. Because of the dissimilar geometries involved—penetration occurs between fixed boundaries, while in spreading there is always one free boundary—the two $\cos\theta$ functions cannot be used interchangeably. Nevertheless, the two cos θ functions have a similar shape as can be derived from further analysis of the penetration data, once γ/η is known.

Hence the assumption that cos θ is some inverse function of time, which leads to the extrapolation procedure suggested for the penetration data, is justified.

Two explicit empirical formulae for the time dependence of $\cos\theta$ have been suggested, the one by Newman [2]:

$$\cos\theta = \cos\theta_o[1 - ae^{-ct}] \tag{23}$$

and the other by Kwei, Schonhorn and Frisch [8]:

$$\frac{\cos\theta}{\cos\theta_o} = kt/(1 + kt) \tag{24}$$

flow requires high pressures, or long times, or both. Resin flow depends on viscosity, pressure gradient, and flow distance. Flow times for thermoplastic prepreg calendering are of the order of one second (20).

Adhesion of the polymer interface by diffusion, autohesion, is shown by Muzzy (21) to be relatively rapid, of the order of seconds. The process begins at the points of contact established during bulk compaction and proceeds simultaneously with polymer flow, which provides increased resin-resin interfacial contact.

Air flow out of gaps and voids is discussed in the next section. As pointed out in the August 27 memorandum, there is the potential for delamination, due to network elasticity, if the pressure is reduced when the matrix is still molten. To compensate for void formation due to crystallization shrinkage, pressure should be maintained until the composite is below T_g.

In summary, a review of the processes that occur during consolidation indicates that time intervals of several seconds are requires to complete the process. Calendering utilizes pressures of the order of 100 atm to cause through the thickness flow of polymers into thin woven fabrics. Roller pressure intervals may be as short as 0.01 seconds. Ultrasonic augmented pultrusion of powder coated towpreg has been accomplished with die residences times a short as 0.25 seconds. Both calendering and pultrusion utilize pressures that would be too high for ATP applications.

Current ATP work utilizes epoxies and APC-2 towpregs that are void free so that only tow gap consolidation need be achieved during the roughly one second of roller pressure. Thus, advanced composite materials for ATP also must be preformed into similar ribbon. To speed up the ATP process ways must be found to achieve tow gap consolidation in fractions of a second.

C. Heat Transfer

An analysis of the ATP heat transfer processing window was conducted by Ghasemi-Nejhad,et.al. (16). Two important features they identifed are that the outer surface of the towpreg cannot exceed the temperature at which degradation occurs during the brief heating period, and that the bottom surface of the towpreg must be above melt temperature to achieve adhesion at the interface. They concluded that the high heat transfer rates of lasers are not necessary, and that hot gas or infra-red heating is adequate to maintain the surface temperature. Unfortunately, they stopped at this point and did not address heating path length, melt temperature range, and

towpreg laying speed. Therefore a simple heat transfer model was developed to identify the role of these variables in defining the processing window.

The heat transfer process is illustrated in the following figure.In the model, linear temperature profiles are used to simplify calculations and to provide guidance as to the role of properties and dimensions.

The outer surface is assumed to be subjected to a constant temperature, T_o, over the heating length, L. T_o cannot exceed the resin degradation temperature for the short exposure times. At the beginning of the heating zone the towpreg is at temperature, T_c, and at the end of the zone it is at $(T_c + T_m)/2$, assuming a linear temperature profile within the towpreg. To provide tack for adhesion, the interface contact temperature must equal or exceed T_m at L where the roller applies pressure for consolidation. Along the interface the temperature increases from T_c to T_m so that the average interface temperature is $(T_c + T_m)/2$, assuming a linear rise in interface temperature along the distance L.

As the heater and roller move over the surface, heat is transferred into the tow in the heated zone. The heat acquired by the towpreg leaves with it at L.

The rate of heat conduction into the tow, while it is in the zone is

$$\dot{q} = \int_{A_o} K \frac{dT}{dx}\, da \qquad \text{where: } a = w\,dL \;,\; \frac{dT}{dx} = \frac{T_o - \frac{1}{2}(T_c + T_m)}{h}$$

$$q = WL\left(\frac{K}{h}\right)\left[T_o - \tfrac{1}{2}(T_c + T_m)\right]$$

where h is the towpreg thickness, W the towpreg band, or heating zone, width, K the through the thickness thermal conductivity, and A_o = WL.

The rate at which the acquired heat leaves the zone is

$$\Phi = A_t \rho C_p (T_L - T_c)\frac{dx}{d\theta} \qquad \text{where } T_L \doteq \frac{(T_o + T_m)}{2}$$

$$\Phi = Wh\rho C_p\left[\frac{(T_o + T_m)}{2} - T_c\right]U$$

where A_t = Wh and $U = \frac{dx}{d\theta}$ the laydown rate.

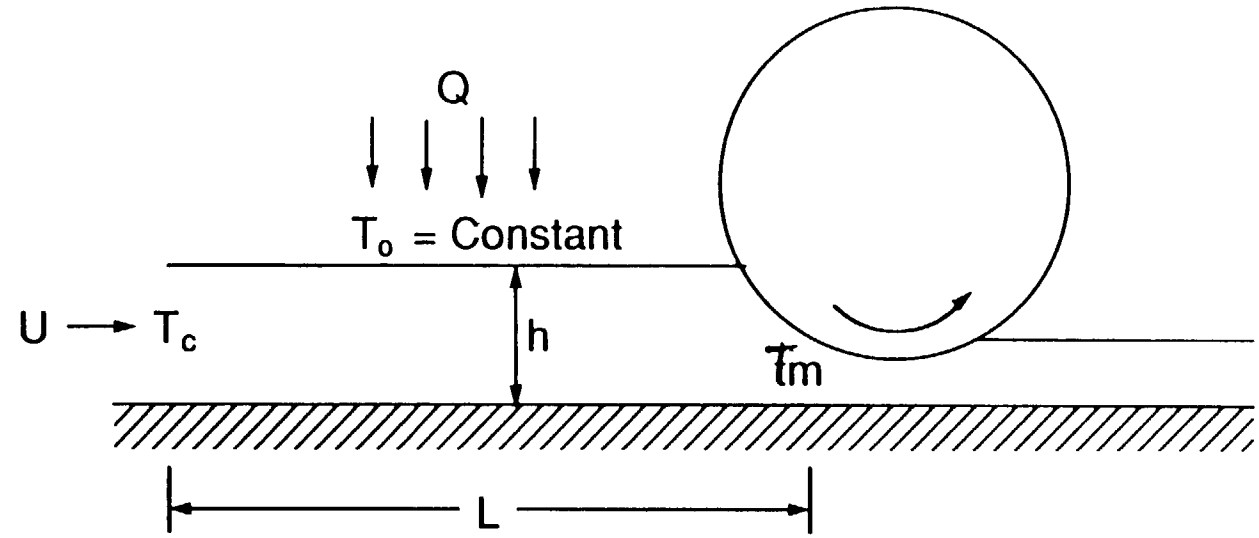

HEAT APPLIED AT TOP

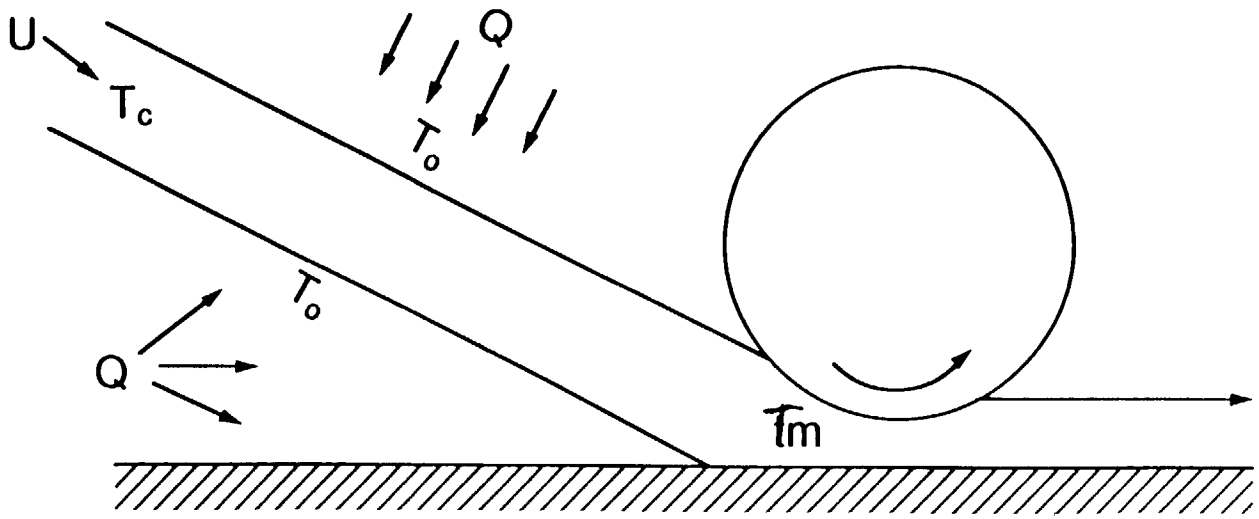

HEAT APPLIED TO TOP AND BOTTOM

ATP HEAT TRANSFER MODELS

For steady operation the energy entering the zone equals the energy leaving, so the above equations for Q are equal. The tow laying rate, U, is related to towpreg properties, system dimensions, and the temperatures and their differences by the expression

$$U = \frac{LK[T_o - (T_c + T_m)/2\}}{h^2 \rho C_p[(T_o + T_m)/2 - T_c]}$$

To check the accuracy of the model the same properties and dimensions as was used by Ghaseim-Nejhad,et.al.(16) in their check were used. Theyr are: $T_o = T_d = 550°C$, $T_m = 340°C$, $T_c = 100°C$, $K_{22} = K = 0.72$ W/m°C, ρ = 1,56o kg/m^3 , C_p = 1,425 W-sec/kg°C, h = 0.000125, and L = 2b = 0.002m

Substituting gives U = 0.040 m/sec. Interestingly, the computer model gave U = 0.05 m/sec(16). Thus, the linear profile model provides a conservative estimate of the heat transfer process.

If the towpreg is heated from the bottom during laydown the rate would be increased due to the increased transfer area.

As indicated by the above equation, the ATP thermal processing window dimensions are determined by three dimensiomless quantities:

L/h which is the ratio of the heating zone length to the towpreg thickness.

$Uh\rho C_p/K$ which is the ratio of the tow laying velocity, U, to the thermal penetration velocity, $K/h\rho C_p$.

$[T_o - (T_c+T_m)/2]/[(T_o+T_m)/2 - T_c]$ which is the ratio of the average temperature difference for heat transfer to the temperature rise of the towpreg.

The processing window boundaries are established by the range in magnitude of these variables, see following table.

The ATP process window model may be used to estimate the tape laying speed for a given system. To illustrate this, the maximum tape laying speed, for a typical set of resin properties and dimensions, are presented in the following figure for a range of melt temperatures and heater lengths. The process window is the area under the curves. The model indicates that adequate heat transfer can be achieved at lay down rates of 1 m/sec.

relationship applies for Reynolds numbers less than 2. For higher flow rates the drag coefficient may be introduced, however, as will be shown in the following example, this is not necessary.

> Consider a 10 micron air bubble, flowing through a resin having a viscosity of 100 poise, under an applied pressure gradient of 100 atm/cm. Substituting into the above equation gives a bubble velocity of 3.4×10^{-6}cm/sec. For a flow path of 1 cm the time required would be 2,900 seconds or 0.8 hours. The bubble Reynolds number is 10^{-6} for which the streamline laminar flow assumption is valid.

This calculation illustrates how slowly bubbles flow in the polymer melt. It confirms the need to avoid air entrapment during towpreg ribbon production and in the tow gaps during ATP. The flow obstruction technique used by Ancher (3) as well as the use of ultrasonics by Taylor (9) should be considered when designing dies for towpreg ribbon production. In addition, ultrasonics might be used with the ATP roller to increase resin flow into the tow gaps and thereby increase laydown speed.

Air flow through tow-tow channels in advance of the ATP roller may be estimated using the following correlation for high velocity compressible gas flow through a pipe (23).

$$W = (\pi/8)([(P_1^2 - P_2^2)gD^5M]/fLRT)^{1/2}$$

where W is the mass flow rate and $f = Re^{-0.2}$.

> For P_1= 100 atm, P_2 = 1 atm, L = 0.77 cm, D = 0.2 mm, T = 200°C, and a viscosity of 100 poise, substituting gives the weight rate of air flow to be 0.17 g/sec. The flow conduit is 0.2 mm in diameter so that the linear air flow rate would be 3,300 m/sec, which is above the velocity of sound. Thus, this equation does not apply. Flow at the open end of the conduit is sonic and controls the air flow rate in the tow-tow channel.

This calculation indicates that air escapes ahead of the roller at speeds up to the velocity of sound, which is 447 m/sec at 200°C. With roller speeds of 1 m/sec there will be ample time for the air in the tow gap to exhaust. Again, the issue is one of avoiding air entrapment in tow gaps and at the laydown interface.

VI. OBSERVATIONS AND RECOMMENDATIONS

This review of various aspects of advanced tow placement generally confirms discussions we have had in recent weeks and provides the background for our studies of towpreg custom ribbonizing for ATP. It also may serve to guide work on the customizing of towpreg for braiding.

Observations

Calendering and pultrusion provide several insights into ways to design dies and related equipment for producting ATP towpreg ribbon.

- The fact that calendering is accomplished at sheet speeds of 2 m/sec with applied pressure intervals of 0.01 seconds offers encouragement for possible achievement of high speed ATP.

- The flow obstruction technique used in calendering might be modified to reduce/avoid air entrapment at the die entrance.

- The Foster-Miller experience with through the thickness flow of LARC-TPI suggests that powder coated towpreg may provide a better approach to achieving high speed ribbon formation.

- Recent pultrusion research indicates the importance of temperature in reducing consolidation pressure for thermoplastics, and the value of using ultrsonic vibration of the die.

Current ATP studies are at slow laydown rates of about 0.01 m/sec. Heat transfer may not be the rate controlling factor in ATP on the fly consolidation. Calculations, using a simple linear temperature profile approach, suggest that adequate heat transfer can be achieved at laydown rates as high as 1 m/sec. And, air flow out of the tow gap is rapid. So, the slow ATP rates reported by researchers must be due to the slowness with which resin flows, and fibers move, into the tow gaps. Ultrasonic vibration of the roller and/or the tool might speed the process. This observation also points to the need to consider tows with other than rectangular cross sections.

The potential benefits of tack on demand for ATP on concave part surfaces should be explored. Thermoplastics and advanced thermosets offer this advantadge. Not having to handle tacky tow could reduce the internal tow

heating/cooling problems experienced in present robot heads. For example, when a tow is dropped, the cut hot tow is held in a clamp. If that tow is not restarted (unclamped and fed) within a minute or two it may gel and require shutdown and cleaning of the robot head mechanism.

It does not appear possible to produce ribbon on-line during ATP. Rather than attempt to develop towpreg dies for use on the robot, or on the floor near the robot, it seems more reasonable to incorporate towpreg ribbonizing with the carbon fiber production facility, as is presently done for sizing tow. That is, powder coat and die form (ribbonize) as the fiber tows are produced, with subsequent delivery of spools of the ATP towpreg ribbon to the part fabrictor for use in the ATP robot.

Recommendations

The following recommendations cover existing research and possible future investigations. Much of what is presented below is a rehash of things we have been discussing in recent weeks.

During the past months, while giving top priority to production of towpreg for weaving studies, several attempts were made to make ATP towpreg ribbon. Both PR 500 epoxy powder towpreg yarn and LARC-TPI thermoplastic powder towpreg yarn were passed over a hot grooved roller. The system was similar to the re-ribbonizing method used by Cincinnati Milcron to reduce, as received, ribbon width variations. These trials were unsuccessful.

The primary reason that the simple ribbon groove method did not work, even for epoxy towpreg, was the "hairiness" of dry powder coated towpreg. In the coating process, the dry tow bundle is pneumatically spread to achieve good penetration and distribution of particles throughout the fiber bundle. The spreading process, even though it uses fairly gentle air flow, results in loose and broken fibers at the towpreg surface. For weaving, twisting the tow helped somewhat to reduce surface "hair". Unfortunately, the simple groove die does not adequately adhere the "hair" to the towpreg ribbon.

Two approaches are being considered to adhere the loose surface fibers (hair) back onto the towpreg. One idea is to pass the hot towpreg through a cone shaped helical wire coil so that the loose fibers are wrapped around the tow prior to its entering the ribbon die. Another concept is to pass the hot towpreg over two cone rollers, one inverted with reference to the other, so

that loose fibers on all sides of the towpreg are hot pressed onto the tow surface before it enters the ribbon die.

The following figure illustrates the problem of tow gaps when rectangular ribbon is used for ATP. A potential solution is to use towpreg ribbon having a triangular cross section. As shown in the figure, triangular towpreg ribbon, when laid in alternating up/down sequence, has two potential advantages, which should serve to increase ATP towpreg laydown speed:

It provides tow overlap, which reqires minimum resin flow and fiber movement during consolidation, and

It provides a large tow-tow area, which should serve to improve adhesion and consolidation.

The shop is presently making towpreg ribbon dies that, it is hoped, can be used to make both rectangular and triangular cross section 12 k AS 4 thermoset and thermoplastic towpreg ribbon. The ribbon dimensions are shown in the folowing figure. Improvements on the present die design, if necessary, might incorporate ultrasonic vibration to augment consolidation and the use of flow obstruction to minmize air entrapment at the die entrance.

Use of towpreg having a triangular cross section will require being able to produce large quantities of it, as well as making robot head design modifications for its use in ATP. Once we have learned how to make triangular cross section towpreg ribbon, two technology transfer activities will be necessary:

Work with carbon fiber tow manufacturers to develop on-line triangular towpeg ribbon production, and

Work with the ATP equipment manufacturers to make appropriate design modifications in the laydown robot head.

During our discussions we also have considered towpreg ribbon having an ellipitical cross section. It would offer similar advantages to triangular towpreg and should be considered further as the dies may be simpler or easier to operate. Round cross section towpreg does not appear attractive since it would need to be flattened during consolidation.

We are beginning to study tow preg architecture for braiding applications. If it can be made with adequate flexibility, ellipitical towpreg may be attractive for braiding. As with weaving, braiding towpreg may not need

to be consolidated into void free ribbon. It may be enough to adhere the "hair" and to smooth the surface so that the tow-tow contact, which occurs during braiding does not present a problem. We should begin studies of the towpreg parameters required for braiding preform parts.

During the recent meeting with vistors from 3M Company, the discussion of resin transfer molding, RTM, identified micro-crack problems with tightly woven and stitched preforms. The problem may be at the contact points of bare fibers, which pose special resin penetration and wetting problems during RTM. It was observed from SEM photographs, that the high flow resins, like RP 500, form a thin, about one micron thick, sheath (manchon), over the carbon fibers during the brief heating period following powder deposition. If the preform were made with this resin sheathed fiber tow material, and if it was even stitched with it (using a 1 k towpreg yarn), there probably would not be bare fiber contact points to serve as micro-crack orgins. A study of towpreg architecture for <u>resin sheathed preform stitching thread (yarn)</u> may be worth pursuing.

Meanwhile work continues on improvements to the powder coating towpreg process.

RECTANGULAR CROSS SECTION

- 12K TOWPREG
- WIDTH RANGE

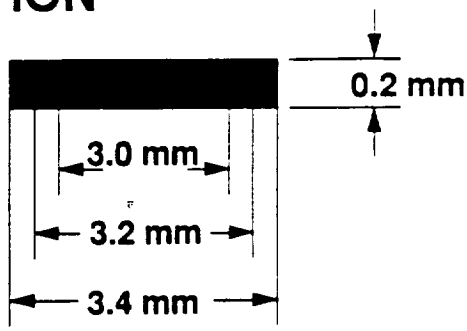

- TOW GAP RANGE

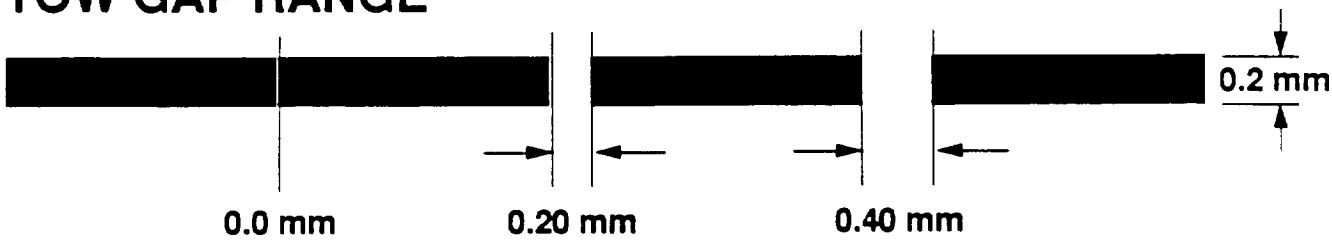

TRIANGULAR CROSS SECTION

- 12K TOWPREG
- WIDTH RANGE

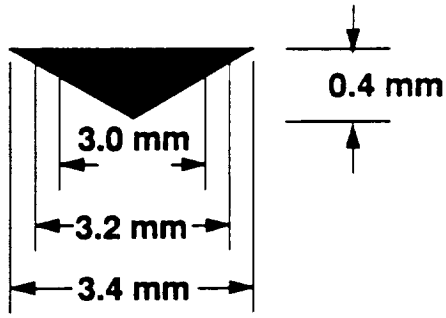

- TOW GAP RANGE

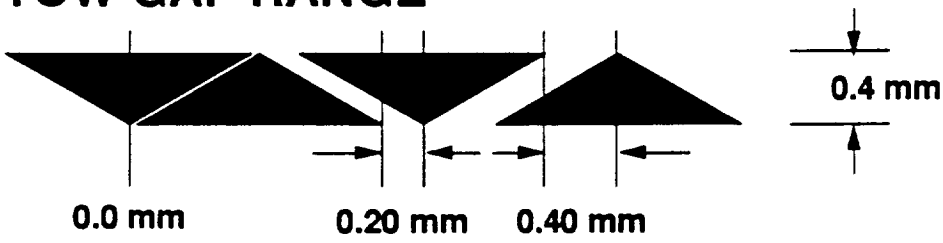

- TOW OVERLAP RANGE

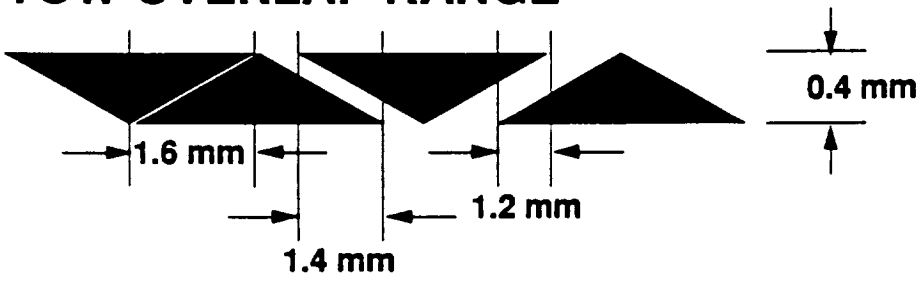

TOW PLACEMENT ARCHITECTURE

References

1. R.E. Gaskel, "The Calendering of Plastic Materials", J.Appl. Mech., Vol 17 pp334-336 (1950).

2. F.H. Ancher, "Calendering of Laminated Polymeric Materials", U.S. Patent No. 3,849,174, Nov. 19 (1974).

3. F.H. Ancher, "Calendering of Polymeric Materials", U.S. Patent No. 3,658,978, July 7,(1969).

4. A.A. Tseng, "Layflat Behavior and Temperature Variation in Calendering: A Review", J. Thermoplastic Composite Materials, Vol 4 pp123-139 (1991).

5. Foster-Miller,Inc. Progress Report, NASA Contract No. NAS 1-19095, July 22 (1991).

6. J.W. Seo and W.I. Lee, "A Model of the Resin Impregnation in Thermoplastic Composite," J.Composite Materials, Vol 25 pp1127-1142 (1991).

7. W.I. Lee and G.S. Springer, "Pultrusion of Thermoplastics," 36th International SAMPE Symposium Transactions, pp1309-1317, April (1991).

8. B.T. Astrom, P.H. Larsson and R.B. Pipes, "Experimental Investigation of a Thermoplastic Pultrusion process", 36th International SAMPE Symposium Transactions, pp1319-1331, April (1991).

9. S.R. Taylor and W.M. Thomas, "High Speed Pultrusion of Thermoplastic Composites", 22nd International SAMPE Technical Conference Thransactions, pp78-87, November (1990).

10. G.L. Batch, "Crosslinking Free Radical Kinetics and the Pultrusion Processing of Composites", PhD Thesis, University of Minnesota (D.C. Macosko advisor) (1989).

11. Y.R. Kim, S.P. McCarthy and J.P.Fanucci, "Compressibility and Relaxation of Fiber Reinforcements During Composite Processing", Polymer Composites, Vol 12, No 1, pp13-19 (1991).

12. J.P. Fanucci, S.C. Nolet, C. Koopernoes, and Y.R. Kim, "Measurement of Internal Die Pressure Distribution During Pultrusion of Thermoplastic Composite", 22nd International SAMPE Technical Conference Transactions, pp50-64, November (1990).

13. R.L. Anderson and C.G. Grant, "Advanced Fiber Placement of Composite Fuselage Structures", First NASA Advanced Composites Technology Conference, NASA Conference Publication 3104, Part 2, pp817-830 (1991).

14. D.O. Evans, M.M. Vaniglia and P.C. Hopkins, "Fiber Placement Process Study", 34th International SAMPE Symposium Transactions, pp1822-1833, (1989).

15. M.L. Enders and P.C. Hopkins, "Developments in the Fiber Placement process", 36th International SAMPE Symposium Transactions, pp778-790, April (1991).

16. M.N. Ghasemi-Nejhad, R.D. Cope and S.I. Guceri, "Thermal Analysis of in-situ Thermoplastic Composite Tape Laying", J. Thermoplastic Composite Materials, Vol 4, pp20-45, January (1991).

17. G. Ardichvili, "An Attempt at a Rational Determination of the Ambering of Calender Rolls", Kautschuk, Vol 14, pp23-28, (1938).

18. F. Brochard, "Spreading of Liquid Drops on Thin Cylinders: the 'Manchon/Droplet' Transition", J. Chem. Phys., Vol 84 no 8 pp 4664-4472 (1986).

19. H, Van Oene, Y.F. Chang and S. Newman, "The Rheology of Wetting by Polymer Melts", J. Adhesion, Vol 1, pp54-68 (1969).

20. S.S. Bafna and D.G. Baird,"Impregnation in Thermoplastic Prepregs: Model & Experiments", 36th International SAMPE Symposium Transactions,pp1708-1719, April (1991).

21. J.D. Muzzy,"Processing of Advanced Thermoplastic Composite", ASME Manufacturing International '88 Proceedings, Vol IV, The Manufacturing Science of Composite, T.G. Gutowski, editor, pp27-39 (1989).

22. K.J. Ahn, J.C. Serferis, J.O. Price and A.J. Berg, "Permeation Measurements Through Prepreg Laminates", SAMPE Journal, Vol 27, No 6, pp19-26 (1991).

23. J.H. Perry, ed., Chemical Engineer's Handbook, 4th Edition, p 5-24, McGraw-Hill (1963).